Co-funded by the

DISCO

Grant Agreement: 755443

DELIVERABLE D4.3

Model materials experiments: Final dissolution results

Dirk Bosbach (FZJ), Christelle Cachoir (SCK.CEN), Emmi Myllykylä (VTT), Christophe Jegout (CEA), Nives Rodriguez-Villagra (CIEMAT), Ian Farnan (UCAM), Claire Corkhill (USFD)

Date of issue of this report: **17/11/2021**

Report number of pages: 81 p

Start date of project: **01/06/2017**

Duration: 48 Months

Project co-funded by the European Commission under the Euratom Research and Training Programme on Nuclear Energy within the Horizon 2020 Framework Programme		
Dissemination Level		
PU	Public	X
PP	Restricted to other programme participants (including the Commission Services)	
RE	Restricted to a group specified by the partners of the Disco project	
CO	Confidential, only for partners of the Disco project	

Table of contents

1 Introduction

The efforts to improve fuel performance in nuclear power generation lead to an increased usage of a various new types of light-water reactor (LWR) fuels including Cr-, Al-, and Si-doped fuels [1-3]. While the improvement of in-reactor performance of these fuels has already been demonstrated, it is still uncertain, whether the corrosion/dissolution behaviour of such fuels in a deep geological repository is similar to conventional spent LWR-fuels. However, the chemical and structural complexity of spent nuclear fuels (SNF) and the associated high beta- and gamma radiation fields impede unravelling all the various concurring dissolution mechanisms from experiments with SNF. Thus within the EU-DisCo project (www.disco-h2020.eu), experiments on irradiated doped fuels are complemented with dissolution studies using systematically produced and carefully characterised UO_2-based model materials to understand the effects of the addition of Cr- or Al-oxide into the fuel matrix on SNF dissolution behaviour under repository relevant conditions. These model materials comprise (i) UO_2 reference materials, and (ii) Cr-/Al-doped UO_2, both, with and without alpha-emitting nuclides such as Pu-238, to address the effects of alpha-radiolysis on the oxidative dissolution of aged SNF after recession of the beta/gamma radiation field in the long-term. Single-effect studies on the dissolution behaviour of the model materials will provide complementary insights and supporting process understanding regarding the performance of modern doped fuels in the repository environment, which cannot be directly obtained from dissolution studies on SNF.

The main objectives of workpackage 4 are:

> (1) Understanding matrix corrosion of modern LWR fuels under deep geological repository relevant conditions
>
> (2) Systematic corrosion studies on Cr/Al/Gd-doped-UO_2-based and MOX model systems (prepared and characterized in WP2) complementary to SF corrosion studies in WP3
>
> (3) Special focus has been on the long-term (> 1,000 years) matrix corrosion by using alpha-doped model systems.

The experimental programme was intended to overcome the inherent complexity of spent fuel corrosion and to identify the separate effects of microstructure, doping level, surface area in support of the spent fuel corrosion studies in WP3. The results clearly allow for improving the predictive capability of SF corrosion models and reduction of associated uncertainties.

Since the formal start of WP4 in February 2018, a broad range of samples was studied in a range of experimental conditions. The outcome of these systematic studies is compiled in chapter 3. In general, a set of experimental conditions was defined in close communication with WP3 in order to allow for an easier comparison between the dissolution experiments performed in WP3 and WP4. Five different chemical compositions for the aqueous solution had been defined: (1) a bi-carbonate solution with H_2 (reducing, anoxic), (2) cementitious water with H_2 (YCWCa, reducing, anoxic), (3) synthetic COX water, (4) natural ground water (with (Fe(0)) and (5) a H_2O_2 solution (for accelerated dissolution experiments).

The dissolution behaviour of the model systems has been studied on respective pellets, which were prepared (and characterized) in WP2. One focus was on Cr-doped UO_2 pellets. The preparation of these materials in different groups provided a range samples which cover a range in dopant level and particle size. Since these parameters are not known for irradiated fuel pellets, the approach followed here ensured that the envelope of these parameters covers most likely those in “real” SNF.

This report comprises contributions from FZJ, SCK CEN, CIEMAT, CEA, VTT, Uni Cambridge as well Uni Sheffield. In the following, this report compiles the obtained dissolution rates and summarizes the results on dissolution experiments with model systems focusing on a description of the sample material, a detailed description of the actual leaching conditions and the used experimental setup as well as the accomplished results.

2 Overview of used samples (solids and aq. Phase)

2.1 SCK CEN

2.1.1 Overview of samples used

The UO_2 model materials were produced at SCK CEN for the experiments performed at SCK CEN and at VTT. The production method was optimized to reach 95 ± 1 % of the theoretical UO_2 density and to approach a grain size of 50 µm and a more or less homogeneous Cr distribution within the UO_2 matrix. Homogeneous α-doping was obtained by co-dissolving in nitric acid a given amount of certified depleted UO_2 and a smaller amount of an existing batch of ^{238}Pu /^{233}U doped UO_2 powder [4] to reach α-doping level representative for a fuel age of 10,000 years (~18 MBq/g UO_2). The solution of (Pu doped) uranyl nitrate is then precipitated as ADU ($(NH_4)_2U_2O_7$), oxidised to U_3O_8 and finally reduced to UO_2. A blend of 80% (Pu-)UO_2/ 20% U_3O_8 is then mixed with 1600 µg Cr_2O_3 powder per g UO_2 and 0.3 wt% zinc stearate (lubricant). Pellets are pressed around 550 MPa and sintered at - 410 kJ/mol at 1700°C for 8 to 24h in a flowing gas mixture of Ar- 4% H_2 and Ar- 0.5% O_2 [5].

Four model materials were achieved (Table 2.1.1.1): depleted UO_2 (UO_2), Cr-doped depleted UO_2 (Cr-UO_2), Pu-doped UO_2 (Pu-UO_2) and Pu-Cr-doped UO_2 (Pu-Cr-UO_2). All materials exhibit a rather homogeneous intergranular porosity (Figure 2.1.1.1). The Pu-Cr-UO_2 pellets (Figure 2.1.1.1d) also showed many intragranular pores, which possibly explains the lower density compared to the other model systems. The specifications of the model materials are given in Table 2.1.1.1. Although the Cr doping resulted in an increase of the average grain size of both Cr-UO_2 and Pu-Cr-UO_2 (Figure 2.1.1.1b- 1d), a 50-µm band of grains with diameter around 10 µm is present at the pellet periphery (Figure 2.1.1.2), as a result of Cr evaporation during the sintering process [6]. Additional analyses are still ongoing to determine the total Cr amount present in the pellet.

Table 2.1.1.1: Specifications of the UO_2 based materials used for the leaching experiments.

Type of model material	**UO_2**	**Cr-UO_2**	**Pu-UO_2**	**Pu-Cr-UO_2**
Pellet (ϕ / h-mm)	5.82 / 7.12	5.79 / 6.45	5.85 / 2.85	5.85 / 2.85
TD %[a]	96 ± 1	94.6 ± 1	93.8 ± 1	93.5 ± 1
Cr_2O_3 added (µg.g^{-1})	-	1600	-	1600
Pu (ppm/$UO_{2.00}$)	-	-	31.4	31.4
Average grain size (µm)[b]	10	38-48	14.5	26
Grain size periphery (µm)[b]	10	10	10	10
Lubricant-wt% (Zn stearate)	0.3	0.3	0.3	0.3

a: TD% is the percentage of the theoretical UO_2 density, measured by immersion technique.

b: grain size analyses were performed according to the line intercept method (ASTM Standard E112-13- [7]) with grain boundaries revealed by etching with HF + CrO_3 (UO_2, Cr-UO_2 samples) or by scanning electron microscopy with backscattered electron (a-doped samples).

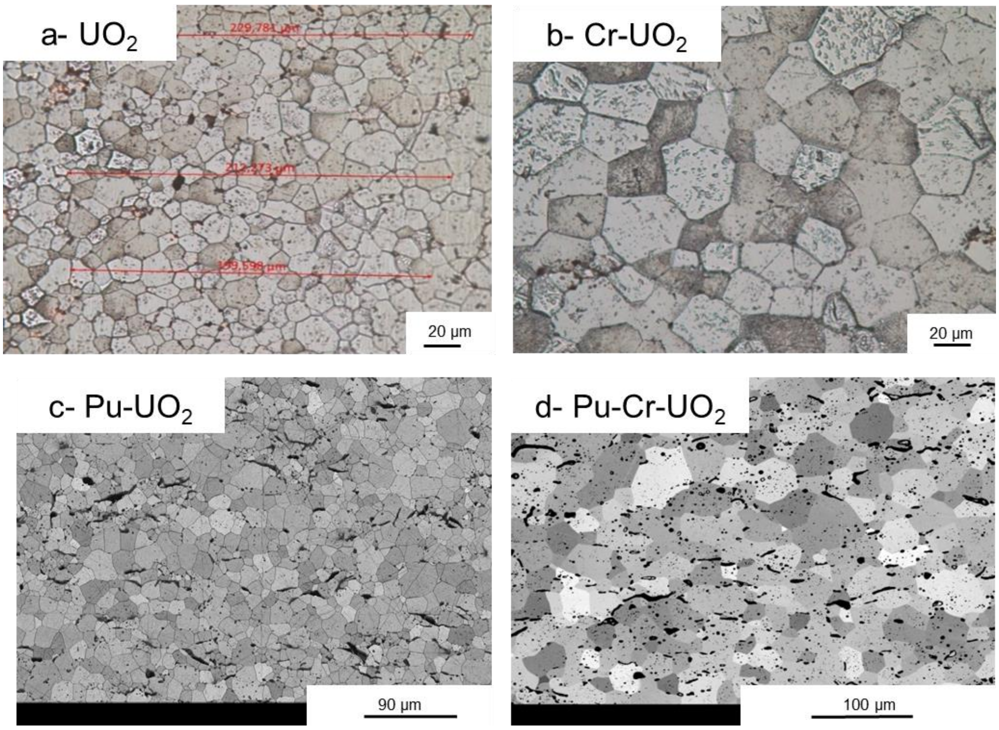

Figure 2.1.1.1: Average grain size of UO_2 based materials a- 10 µm for UO_2, b- 38-48 µm for Cr-UO_2, c-14.5 µm for Pu-UO_2, d- 26 µm for Pu-Cr-UO_2.

Figure 2.1.1.2: Pellet periphery of Cr-doped UO_2 with smaller grain size (band about 50 µm with grain size of 10 µm as highlighted by the white arrows).

2.1.2 Description of the different dissolution experiments

Static dissolution experiments were carried out with the four model materials, added as pellets: 'inactive tests' with UO_2 and Cr-UO_2 and 'active tests' with Pu-UO_2 and Pu-Cr-UO_2. The tests were done in two leaching solutions (Table 2.1.2.1): Young Cementitious Water at pH 13.5 (YCWCa) and in bicarbonate solution at pH 9. All experiments were performed in autoclaves with 10 bar H_2 gas in an Ar glove box (pO_2 below 10 ppm and pCO_2 below the detection limits) and at 20-25°C. A Pt/Pd catalyst was placed in the headspace of the autoclaves (not immersed in the solution) to scavenge the traces of atmospheric oxygen inside the autoclaves by reaction with the H_2 gas, without perturbation of the radiolytical reactions in the solution (Figure 2.1.2.1a).

The set-up consists of stainless-steel autoclaves with a PEEK insert of 50 ml (Figure 2.1.2.1b and 3c). The cover of the autoclaves is equipped with two outlet valves: one short inlet tube stopping immediately under the cover for gas inlet and one longer outlet tube near the bottom of the solution for the sampling of the solution. Gas pressure (H_2) is monitored during the experiment by a manometer. Each autoclave is filled with 30 ml of solution and one pellet of (doped) UO_2 (Table 2.1.1.1), corresponding to an initial ratio of UO_2 surface area to solution volume (SA/V) of 6 m^{-1} and 3 m^{-1} for the inactive and the active experiments, respectively. Prior to the leaching tests, the pellets were washed in 30 ml of 0.01 M NaCl in a PE bottle for a period of three to five weeks with a daily renewal the first week and a weekly renewal for the weeks thereafter [8]. One week before the end of the washing step the autoclaves were filled with 30 ml of the leaching solution (Table 2.1.2.1) in presence of the Pd/Pt catalyst with 5 bar H_2 pressure. When the U concentration in the washing solution stayed in the range of the U(IV) solubility ($10^{-8.5 \pm 1}$ M) [9], the pellets were transferred from the PE bottle to the autoclaves and the leaching experiment was started for a period up to 4 months. After 1, 3, 10, 30 (35), 72 and 155(156) days, an aliquot of 2ml was sampled without replenishment of solution and the autoclave was pressurised again up to 10 bar H_2 pressure.

At the end of the inactive experiments, the autoclave was dismantled and rinsed with 10 ml 1M HNO_3 to determine the fraction adsorbed on the walls of the autoclaves. The active experiments are still running and the dismantling was not yet decided at the time of this report.

The total U concentrations (without filtration) were measured during the washing and the leaching period while the soluble U concentrations (ultrafiltration < 3.5 nm) were only determined at pH 9 or pH 13.5. ^{238}U was measured by ICP-MS for the inactive experiments while ^{233}U and ^{238}Pu were measured by alpha-spectrometry for the active experiments. pH of the leachate was monitored over time and Cr and Zn (lubricant) concentrations were also quantified by ICP-MS time to time.

The inactive experiments were conducted from October 2019 to April 2020 after 156 days of leaching. The active experiments were started in June 2020 and performed for a period of 155 days in conditions similar as the inactive experiments. After 155 days of leaching, the active experiments were not dismantled in order to study the role of iron in our systems by comparison with experiments conducted at VTT in bicarbonate solution and with similar UO_2 model materials. The follow-up of the study was initiated in December 2020 outside of the Disco project and the experiments are still running. A possible dismantling is scheduled in the third quarter of 2021. A timeline for the experiments is shown in Figure 2.1.2.2.

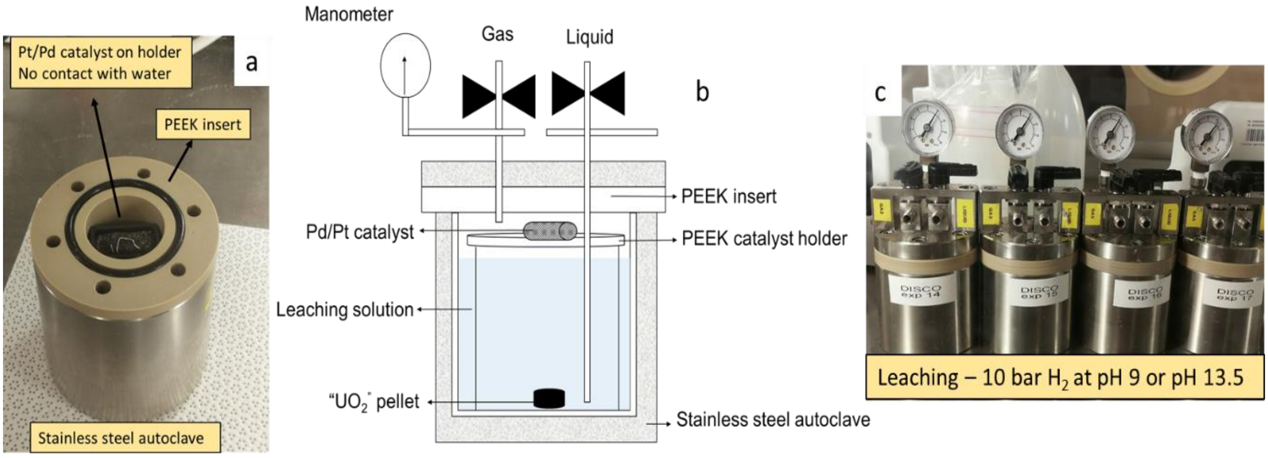

Figure 2.1.2.1: Experimental set-up a: inside cell, b- schematic drawing and c: autoclaves under 10 bar H_2 pressure.

Table 2.1.2.1: Measured initial composition of the leaching solutions at pH 13.5 and pH 9.

mol.L^{-1}	**Medium pH 13.5 (YCWCa)**	**Medium pH 9 (FIN)**
Na	1.28×10^{-1}	2.07×10^{-2}
K [a]	3.67×10^{-1}	2.33×10^{-5}
Ca [a]	4.43×10^{-4}	5.00×10^{-6}
C	5.08×10^{-4}	9.83×10^{-4}
SO_4^{2-} [a]	1.86×10^{-3}	5.21×10^{-6}
Si [a]	4.32×10^{-5}	3.71×10^{-5}
Cl	$< 8.45\times10^{-6}$	1.81×10^{-2}
U [a]	$< 8.40\times10^{-10}$	$< 8.40\times10^{-10}$
Cr [a]	4.93×10^{-8}	$< 1.35\times10^{-8}$
Zn [a]	2.29×10^{-7}	1.17×10^{-7}
Measured pH	13.6 ± 0.2	9.1 ± 0.2

a: these elements are not part of the composition, but they are measured either to compare both solutions (K, SO_4^{2-}, Si) or to define the background concentration (U, Cr, Zn).

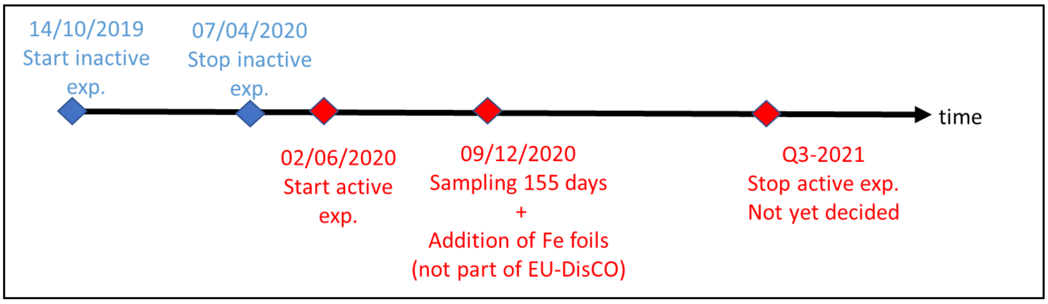

Figure 2.1.2.2: Timeline of the active and inactive experiments.

2.2 FZJ

2.2.1 Overview of samples used

In the framework of WP4 accelerated dissolution experiments were carried out in previously degassed bicarbonate solutions ($NaHCO_3$, 10 mmol/L) representing simplified groundwater, using hydrogen peroxide (H_2O_2, 2.25 mmol/L) to mimic the oxidative radiolytic dissolution of UO_2. To achieve anoxic conditions the solutions were flushed with argon during the complete experimental run time.

The UO_2 model materials with and without Cr doping for the dissolution experiments were synthesised in the framework of WP2. Additionally, commercially available Cr-doped pellets (AREVA) were used for these experiments.

Table 2.2.1.1: UO_2 pellets used for dissolution experiments and their properties. The last column shows the initial dissolution rate determined for the first 24 h of the experiment (see 3.1.2).

Sampl.e.	doping Cr_2O_3 / wt ppm	doping method	oxygen pot. / kJ/mol O_2	T.D. / %	grain size / µm	height / mm	diameter / mm	geom. surf. / mm^2	initial dissolution rate / mol/sec*m^2
SL-DC-19-2	pure UO2	-	-510	93.50	12	1.38	8.36	146.03	1.7922E-06
SL-DC-19-3	pure UO2	-	-510	94.00	12	1.51	8.52	154.44	1.6949E-06
SL-DC-19-4	pure UO2	-	-510	94.60	12	1.48	8.49	152.70	1.6189E-06
SL-DC-19-5	pure UO2	-	-510	95.00	12	1.54	8.64	159.06	1.3978E-06
SL-DC-35-1	pure UO2	-	-420	96.48	12	1.24	8.46	145.38	1.1639E-06
SL-DC 18-1	1000	CPM	-510	95.85	12	1.55	8.30	148.50	1.0643E-06
SL-DC-18-5	1000	CPM	-510	97.61	12	1.36	8.48	149.19	7.7766E-07
SL-DC-22-7	1000	WCM	-510	98.75	19	1.38	8.45	148.79	6.9764E-07
SL-DC-33-1	1000	CPM	-420	97.01	20	1.19	8.53	146.18	6.4937E-07
SL-DC 33-2	1000	CPM	-420	97.02	20	1.26	8.50	147.14	1.2287E-06
SL-DC 36-1	1000	WCM	-420	97.02	24	1.32	8.45	147.20	1.5435E-06
SL-DC 47-2	1500	WCM	-420	98.50	38	1.58	8.30	149.41	1.6586E-06
SL-DC 47-6	1500	WCM	-420	98.50	38	1.60	8.33	150.87	1.3891E-06
SL-DC 47-7	1500	WCM	-420	98.50	38	1.50	8.32	147.94	1.5781E-06
SL-DC 47-9	1500	WCM	-420	98.50	38	1.40	8.32	145.33	1.8291E-06
SL-DC 37-2	2500	WCM	-420	98.35	69	1.16	8.38	140.85	5.5499E-07
SL-DC 23-2	0.5 % Nd	CPM	-510	98.19	ND	1.61	8.33	151.13	2.1741E-07
SL-DC 24-1	1 % Nd	CPM	-510	98.55	ND	1.58	8.33	150.34	1.1108E-07
SL-DC 24-2	1 % Nd	CPM	-510	98.55	ND	1.28	8.30	141.59	1.3013E-07
AREVA 1	1500	?	?	96.20	37	1.74	9.20	183.24	1.4837E-06
AREVA 2	950 + 1.3 % Nd	?	?	94.20	10	1.86	9.26	188.80	1.6478E-07

Doping Cr_2O_3 = amount of initial Cr_2O_2 doping given in wt. ppm; Doping method: CPM = co-precipitation method, WCM wet coating method; Oxygen pot. = oxygen potential during sinter process; T.D. = theoretical density; geom. surf. = geometrical surface.

All pellets produced in the framework of WP2 were sintered for 10 h at 1700°C. A compilation of the samples and their properties is shown in Table 2.2.1.1. The pellets used for the dissolution experiments have a diameter of approximately 8.5 mm and a thickness of approximately 1.5 mm, except the commercially available pellet purchased from AREVA (approx. 9.2 mm diameter, approx.1.8 mm height). One site of the pellet was polished mirror like, whereas the other side was only grinded by a 1200 sandpaper.

2.2.2 Description of the dissolution experiments

The experimental setup incl. a schematic view on the experimental vessels for the accelerated dissolution experiments developed at FZJ is shown in Figure 2.2.2.1. A detailed explanation of this experimental setup is described in DisCo deliverable 4.2 [10].

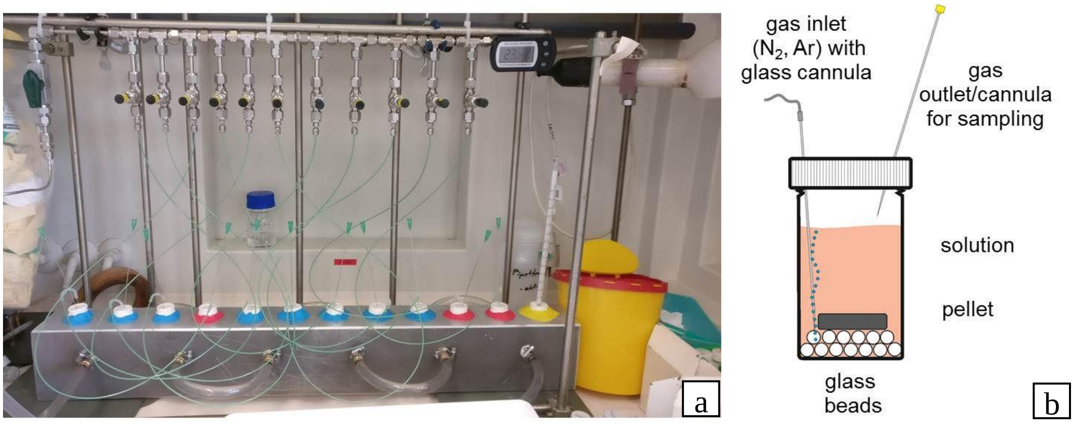

Figure 2.2.2.1: (a) Experimental setup of the dissolution experiments. (b) Schematic drawing of the experimental vessels for the accelerated dissolution experiments.

The driving force for the UO_2 dissolution in this kind of accelerated dissolution experiment is the oxidative potential of H_2O_2 which is proportional to its concentration in solution. The $NaHCO_3$ in the solution represents the bicarbonate contained in groundwater. Additionally, it inhibits the precipitation of U(VI) phases and therefore ensures a reliable measurement of the uranium concentration in the solution. The $NaHCO_3$ does not intervene directly in the oxidation process, but - with oxidative dissolution - complexes the U (VI) and thus influences the kinetics / driving force, so that the dissolution rate increases with the bicarbonate content [11]. The end of the dissolution process is marked by the accomplishment of a constant uranium concentration in the solution. This plateau is not due to the limit of U(VI) solubility, but due to the complete consumption of H_2O_2 in the solution.

Due to the previously discovered surface passivation effect when repeatedly employing the same pellets in the dissolution tests, only results from dissolution experiments using pristine pellets were considered for determining the dissolution rates [8, 12]. During the dissolution experiments, solutions were systematically sampled and the H_2O_2 (UV-Vis) and the uranium (ICP-MS) concentrations were determined.

2.3 VTT

VTT conducted 200 days static leaching experiments with Cr-doped UO_2 materials fabricated by SCK-CEN during the DisCo project (see Table 2.1.1.1). Materials included Cr doped UO_2 pellets with and without α-doping with ^{238}Pu, and similar UO_2 materials without Cr as reference materials. The α-doping of ^{238}Pu in pellets correspond to an α-dose of approximately 10 000 year old SNF. These materials were leached under anaerobic conditions in reference FIN water and in natural groundwater, ONK-KR15, sampled at disposal level in ONKALO at the Olkiluoto site.

Prior to experiments with Cr doped materials, VTT conducted 200 days leaching experiments with existing UO_2 materials with 5% or 10% ^{233}U alpha doping, simulating the alpha dose of 10,000 years old and 3,000 years old SNF, respectively. These static leaching experiments were run in OL-KR6 groundwater under anaerobic conditions of Ar glove box.

Pre-leaching of the Cr-doped pellet series (Table 2.3.1) was conducted according to a similar procedure used by SCK-CEN to remove the oxidised surface layer, which might have formed during delivery. The mass of a single pellet was about 0.78 g, including some variation between different pellets. In a 4 weeks long pre-leaching procedure the whole solution volume, 30 ml of 0.01 M NaCl, was first changed daily during first weeks and then biweekly and weekly. The uranium concentration $10^{-8.5 \pm 1}$ M was gained in the end of the 4 weeks leaching period.

Table 2.3.1:

Samples.	**Bicarbonate water (FIN)**	**Natural water (ONK-KR15)**
UO_2	1 pellet	2 pellets
Pu-UO_2	1 pellet	2 pellets
Cr-UO_2	1 pellet	2 pellets
Pu-Cr-UO_2	1 pellet	2 pellets
Blank test with iron	1 experiment	1 experiment
blank test	1 experiment	1 experiment
blank with ^{233}U spike	1 experiment	

The existing samples, ^{233}U alpha doped UO_2 fragments (see Table 2.3.2 and Figure 2.3.1), had been stored under anaerobic glove box conditions for 4 years. There are parallel samples (2-0 and 1-0, 1-5 and 2-5, 1-10 and 2-10) for 1 g samples and only one sample per doping level with higher mass (~3g). The previous dissolution experiments were carried out under saline groundwater and thus, the samples required preparation before experiments by pre-leaching twice with bicarbonate solution before start of the actual experiments in natural groundwater.

The purpose of pre-leaching was to remove salts possibly precipitated during the storage period. After pre-washing in bicarbonate solution, the UO_2 fragments were rinsed twice with 2 ml of MQ-water, and were allowed to dry for a short moment, before weighting them into a clean saucer.

Table 2.3.2: Compositions for 0 % , 5% and 10 % ^{233}U doped pellets inlcuding the sample masses.

UO_2 phase	[^{233}U] (%)	[^{235}U] (%)	[^{238}U] (%)	$^{235}U/^{238}U$	Samples (g)
Un-doped	0	2.82	97.18	0.029	1, 1, 3 g
5% ^{233}U-doped 15.7 MBq/g	5.0	4.5	90.5	0.050	1, 1, 3 g
10% ^{233}U-doped 31.4 MBq/g	10.0	4.5	85.5	0.053	1, 1, 2.5 g

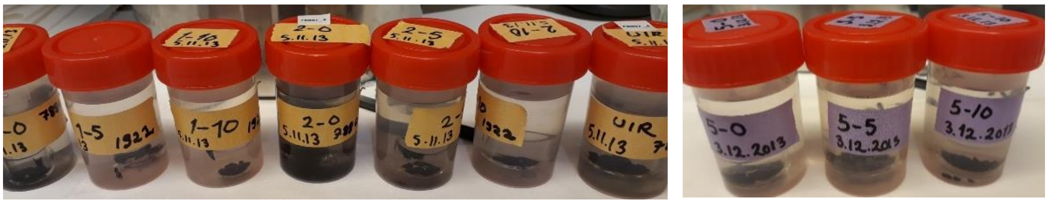

Figure 2.3.1: The old samples, ^{233}U alpha doped UO_2 fragments placed is glass saucers inside the test vessels during the bicarbonate pre-leaching without iron.

ONK-KR15 groundwater was selected for the leaching experiments of new Cr and/or Pu-doped UO_2 materials fabricated in the DisCo project. ONK-KR15 stands for the ONKALO characterization drill core at the depth of -399 m. This groundwater represents groundwater conditions at the disposal level. It has less sulphate and carbonate (0.16 mM) in comparison to OL-KR6 (2.5 mM HCO_3^-), but relatively low salinity compared to saline waters (see Table 2.3.3). ONK-KR15 water resembles the composition of saline OL-KR5 used previously in REDUPP experiments, but ONK-KR15 was selected instead due to unavailability of OL-KR5. It represents groundwater water, which has not been mixed with any other water types. These kind of low carbonate and saline groundwater conditions prevails in disposal sites in Finland and Sweden. Thus, it is relevant to gain information on the possible effect of low carbonate in comparison to bicarbonate (1 to 2 mM) concentrations used in many reference waters in the DisCo project.

The experiments with ^{233}U-doped UO_2 were conducted only in brackish OL-KR6, because it showed slight solubility increasing effect with 10% alpha doping in previous experiments [13, 14]. Brackish, high carbonate water does not represent the current groundwater conditions at the disposal level (app. - 400 m). However, this kind of conditions might occur for example in the postglacial situation, if the groundwater layers will be strongly mixed at Olkiluoto site.

Table 2.3.3: Compositions for natural groundwaters OL-KR6 (brackish) and ONK-KR15 (saline) used in DisCo dissolution experiments. Two columns for OL-KR6 show the slight temporal variation and ONK-KR15 are given as average values from data collected from 2011 to 2018.

	OL-KR6 (2013)	**OL-KR6 (2016)**	**ONK-KR15 (2011-2018)**
pH	7.6	7.6	8.0
Ammonium, NH_4 (mg/l)	0.31	0.29	0.025
Bicarbonate, HCO_3 (mg/l)	159	153	9.7
Bromide, Br (mg/l)	12	11	46
Calcium, Ca (mg/l)	540	530	1242
Chloride, Cl (mg/l)	3340	3340	6162
Dissolved inorg carbon (mg/l)	27	31	1.8
Fluoride, F (mg/l)		0.4	1.6
Iron, Fe (total) (mg/l)	0.36	0.28	0.01
Iron, Fe^{2+} (mg/l)		0.28	0.015
Magnesium, Mg (mg/l)	151	151	33
Nitrate, NO_3 (mg/l)	0.4	0.4	<0.04
Nitrite, NO_2 (mg/l)	0.2	0.2	<0.02
Nitrogen, N(Total) (mg/l)	0.36		0.077
Non Purgeable Organic Carbon	4.6	5.1	3.5
Phosphate, PO_4 (mg/l)		0.2	0.2
Potassium, K (mg/l)	18	18	10
Silicate, SiO_2 (mg/l)	11	12	6.3
Sodium, Na (mg/l)	1460	1460	2392
Strontium, Sr (mg/l)	5.5	5.8	10.2
Sulphate, SO_4 (mg/l)	404	406	0.33
Sulphide, $S_2{}^{-}$ (mg/l)		0.02	0.05
Sulphur, S (total) (mg/l)	130	130	0.6
Total dissolved solids (mg/l)	6101	6088	9913
Carbonate alkalinity, HCl	0.05	0.05	<0.05
Total acidity, NaOH uptake	0.18	0.16	0.05
Total alkalinity, HCl uptake	2.6	2.5	0.16

Both ground waters contained natural uranium when sampled. OL-KR5 contained 1.2 µg/L (≈ 5 x 10^{-9} mol/L) and ONK-KR15 0.015 µg/L (≈ 6.5 x 10-11 mol/L^{238}U. Prior to the leaching experiments natural U concentration was decreased to 10^{-10} mol/L) level by precipitating U on iron foil added into the solution. OL-KR5 was also filtered (0.45 µm) before addition to experiments.

The experimental system for dissolution tests is described in Figure 2.3.2, showing the test vessel with an iron strip leaning to the vessel wall, and an UO_2 pellet lying on the bottom of the vessel. The fragmented samples containing ^{233}U were placed into a glass saucer, which functions as a holder for the fragments. The iron foil maintains reducing conditions, producing some H_2. It also mimics the cast iron insert of the copper canister that will be present next to SNF in the repository.

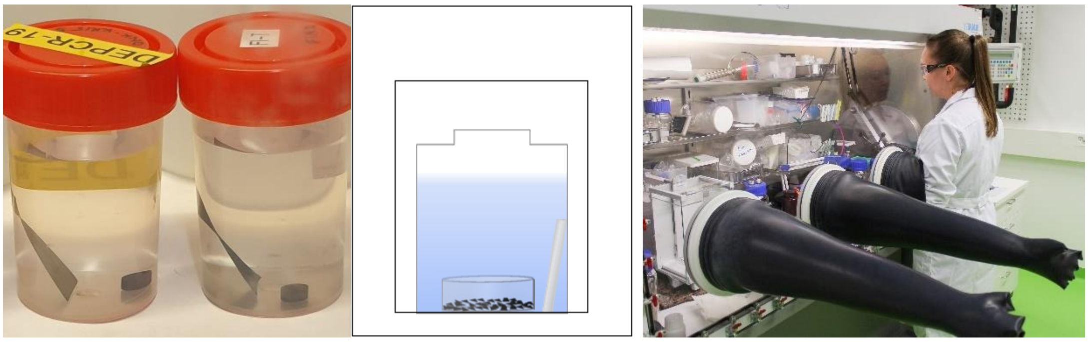

Figure 2.3.2: Image of the plastic vessel (V=60 ml) with pellet sample (left) and schematic image of UO_2 fragments are placed in the glass saucer and the iron strip is leaning on the vessel wall in leaching media (middle). All the experiments were conducted inside the anaerobic glove box under Ar atmosphere (right).

In the experiments with existing ^{233}U-doped fragments and Cr-doped series in FIN reference water, the leaching solution was spiked with ^{235}U, to follow the precipitation and adsorption or U beside the release of uranium from the solid phase. Prior to the spike of ^{235}U-rich solution, 168 µl of 0.01 M NaOH were added to neutralize the acid content of the spike. Next, the solution spike $^{235}U/^{238}U$ ~10/1 was added to give an initial total U concentration of $3.4 \bullet 10^{-9}$ mol/L and the solution was stirred with the tip of the pipette before addition of solid UO_2 and closure.

In all experiments, the evolution of the ^{238}U concentration was followed by sector field ICP-MS (Element 2 by ThermoScientific). In the case of natural groundwater other elements like Fe, Cr, Ba, Mn were also analysed. From the experiment with added tracer ^{235}U spike, the change of the isotopic ratio was followed, to estimate release versus sorption/precipitation on surfaces. Water conditions were also followed by measuring pH of the leaching solution few times during the experiments. The prevailing redox conditions were also evaluated by measuring the Eh at the end of the experiments.

2.4 CIEMAT

CIEMAT contribution, in the context of WP2 and WP4 of the DisCo project, focused on the dopants effect on UO_2 matrix leaching resistance through experiments in different representative aqueous systems. The experimental campaign included preparatory work, characterization of raw materials and samples and testing of experimental set-ups. An attempt to replicate Gd and Cr-, Cr/Al-doped UO_2 fuel was made to synthetize doped novel samples in a similar way as in commercial UO_2 fuel manufacturing processes (UO_2-0.06 $^{w}/_{o}$ Cr_2O_3, UO_2-0.05 $^{w}/_{o}$ Cr_2O_3-0.02 $^{w}/_{o}$ Al_2O_3 and UO_2-4.5 $^{w}/_{o}$ Gd_2O_3). Samples produced were tested to experimentally investigate the influence of H_2 (g) on the matrix dissolution rate of doped UO_2. Different characterization techniques were used for surface analysis (Raman spectroscopy, laser diffraction analyser, SEM, BET and XRD) and for aqueous composition (ICP-MS).

2.4.1 Samples preparation from CIEMAT

For the fabrication and characterization of model materials to study the fuel matrix corrosion behaviour under repository conditions, CIEMAT had prepared a series of sintered pellets.

Fabrication procedure

After a pre-characterization process of the raw materials to ensure proper particle size distribution, and to define suitable dopant blending ratios, the methodology applied for fabrication of UO_2 doped with 0.06 $^{w}/_{o}$ Cr_2O_3, 0.05 $^{w}/_{o}$ Cr_2O_3-0.02 $^{w}/_{o}$ Al_2O_3, and 4.5 $^{w}/_{o}$ Gd_2O_3 compacts was conventional “dry route” consisting of mechanical dry blending of ceramic powders (together with the binder EBS, Ethyl Bis Stearamide, $C_{38}H_{76}N_2O_2$), to ensure suitable homogenization. The starting powders were UO_2, Cr_2O_3, Al_2O_3 and Gd_2O_3, the first one provided by ENUSA (Empresa Nacional del Uranio S.A., Spain) and the others by Alfa-Aesar. The methodology implies cold-compacting into 25 tons uniaxial press (700 MPa) to obtain green pellets, calcination at three temperature steps, and sintering in reducing atmosphere for 4 h at 1675 °C in an alumina tubular furnace. During sintering, the binder is vaporized from green pellets, resulting in densification. The controlled atmosphere in the furnace used to sinter the pellets acts to prevent oxidation at these high temperatures. After cooling, pellets were polished and isothermally annealed at around 80-90% of the sintering temperature in 4.7%H_2/N_2, to reveal the grain structure and morphology. In Figure 2.4.1.1 a diagram of the powder metallurgical process is shown.

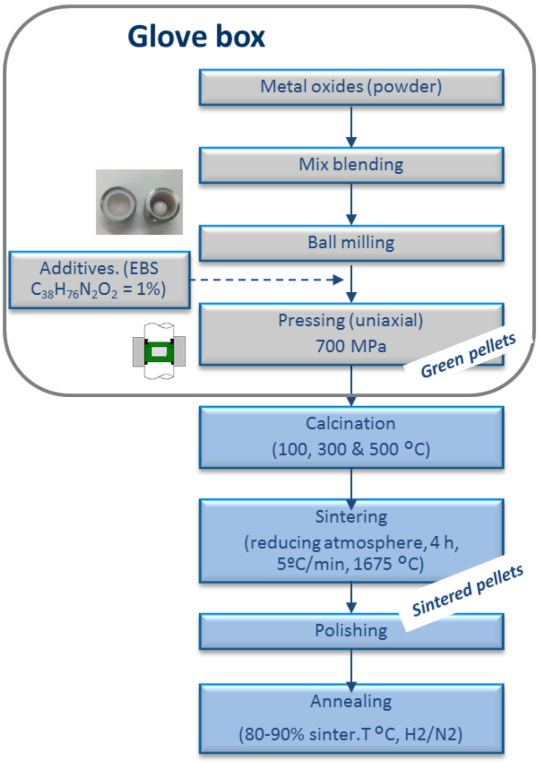

2.4.1.1: Fabrication flow diagram of conventional “dry route” used in CIEMAT for pellet production.

In order to confirm the final stoichiometry of doped pellets, a detailed characterization was carried out by XRD and Raman spectroscopy. SEM analyses were performed to identify the microstructure, porosity and grain size distribution, calculated by the linear intercept method [15]. Specific surface area was determined by BET method [16] and the density was measured by both geometric and Archimedes methods. All of them are summarized in Table 2.4.1.1.

Table 2.4.1.1 Solid characterization techniques (CIEMAT).

Techniques	Parameter	Equipment
BET	N_2-BET Surface Area	ASAP 2020 Micromeritics ISO 12800E
XRD	Crystalline structure	D8 ADVANCE Eco (Bruker) - ICD
Raman spectroscopy	Structural / speciation	HORIBA LabRam HR Evolution
OM / SEM	Surface morphology/grain size Lineal intercept method (Heyn)	Hitachi SV6600 15 kV ASTM E 112-96 UNE-EN ISO 643:2012
Laser diffraction	Particle size	Malvern 2600 series
Archimedean test	Density	Sartorious kit

Pellet characterization

An overview of the dimensions and characteristics of the sintered fuel pellets is given in Table 2.4.1.2. For all the doped discs, the sample's average grain size showed an increase with respect to undoped UO_2 typical grain size, except for the Gd_2O_3 doped samples, which remained unchanged [17, 18]. The grain size of Cr-doped UO_2 samples is in agreement with previously published data [19, 20] for the selected weight ratios of Cr/U. Figure 2.4.1.2 shows the grain structure of sintered pellets. Matrix homogeneity was observed in all samples, meaning that dopants are well solubilized. The lattice parameter of each sample (Table 2.4.1.2) was calculated from XRD by using the unit cell refinement process provided by the software TOPAS (Bruker Analytical X-Ray Systems), taking the Fm-3m space group.

Table 2.4.1.2: Results on doped UO_2 pellet characterization.

SAMPLE	UO_2 – 0.06 ${}^{w}/_{o}$ Cr_2O_3	UO_2 – 0.05 ${}^{w}/_{o}$ Cr_2O_3 -0.02 ${}^{w}/_{o}$ Al_2O_3	UO_2 – 4.5 ${}^{w}/_{o}$ Gd_2O_3
SSA (m^2/g)	0.63 ± 0.02	0.25 ± 0.01	0.63 ± 0.02
Grain size (μm)	10.16 ± 1.17	9.87 ± 1.02	0.5 ± 0.08
Density ($g{\cdot}cm^{-3}$)	9.83 ± 0.07	9.80 ± 0.43	9.81 ± 0.11
Lattice parameter (nm)	0.547113 (7)	0.547198 (5)	Phase #1 $(Gd_{0.004}U_{0.996})O_2$ 0.54705(6) Phase #2 $(Gd_{0.05}U_{0.95})O_2$ 0.5463(2) Phase #3 $(Gd_{0.12}U_{0.88})O_2$ 0.5450(3)

SEM examination (Figure 2.4.1.2) of the grain growth revealed that the U mixed oxides containing Cr and Cr-Al show a homogeneous microstructure of dopants in solid solution.

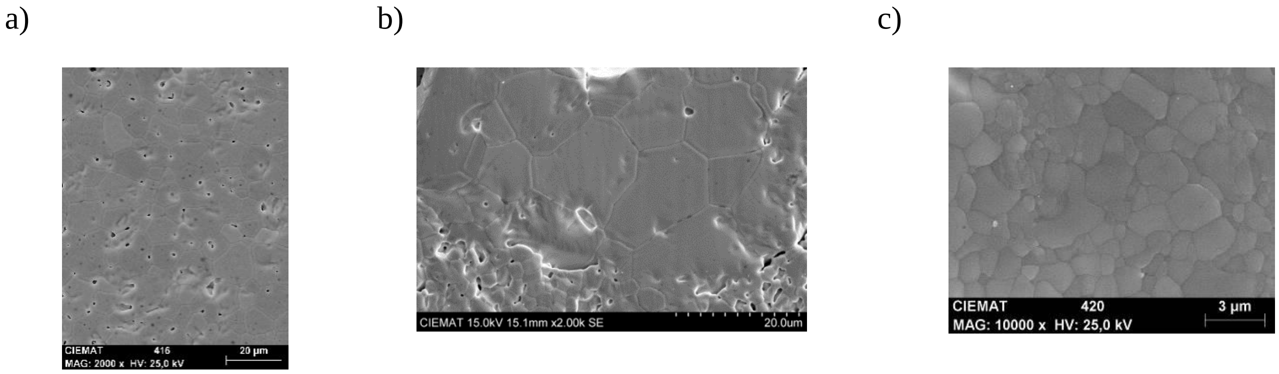

Figure 2.4.1.2: SEM images and microstructure of prepared doped UO_2 samples a) UO_2 -0.06 ${}^{w}/_{o}$ Cr_2O_3; b) UO_2 -0.05 ${}^{w}/_{o}$ Cr_2O_3 -0.02 ${}^{w}/_{o}$ Al_2O_3 and c) UO_2 -4.5 ${}^{w}/_{o}$ Gd_2O_3.

Figure 2.4.1.3 corresponds to the diffraction patterns obtained from the UO_2 -0.06 $w/_o$ Cr_2O_3; UO_2 -0.05 $w/_o$ Cr_2O_3 -0.02 $w/_o$ Al_2O_3 and UO_2 -4.5 $w/_o$ Gd_2O_3 pellets. It is well-known that the crystal structure of UO_2 is cubic, fluorite-type, so the lattice is characterized by only one lattice parameter (*a*). Diffraction peaks of all prepared samples were acquired under the same conditions, and the *a* value of the lattice parameters was obtained from each one by using the unit cell refinement method, applying the corresponding error corrections. From the diffraction peaks of each sample, it can be seen that dopants are well dissolved in the UO_2 grains. XRD diffraction patterns of Cr and Cr/Al doped UO_2 samples show a slight decrease of the lattice parameter with respect to undoped UO_2, which demonstrates that dopants have entered in the UO_2 fluorite structure. The XRD of UO_2-Gd_2O_3 samples showed that Gd is in solid solution in the urania lattice; however, the peaks shift to higher angles than pure UO_2 evidenced the expected decrease in lattice parameter.

Diffractograms contain the same set of peaks consistent with FCC. By using the unit cell refinement method and assuming Vegard ´s law-like behaviour, three different lattice parameters corresponding to different FCC solid solutions of $(U_{1-x}Gd_x)O_2$ with different Gd content were observed, with markedly different Gd content ranging from 0.4% to 12%, giving an average composition of 4.5% (Table 2.4.1.2). A lattice contraction with Gd content is shown as expected causing a higher densification. XRD data of gadolinium sample is in agreement with literature where it is found a phase close to the grain boundaries with higher concentration of Gd_2O_3.

Figure 2.4.1.4 illustrates Raman spectra acquired for the initial samples. The plot represents the averaged spectra from 10 individual spectra recorded at various locations of each disc. No oxidation on doped-UO_2 in the form of UO_{2+x} was observed in preleached samples by XRD and Raman.

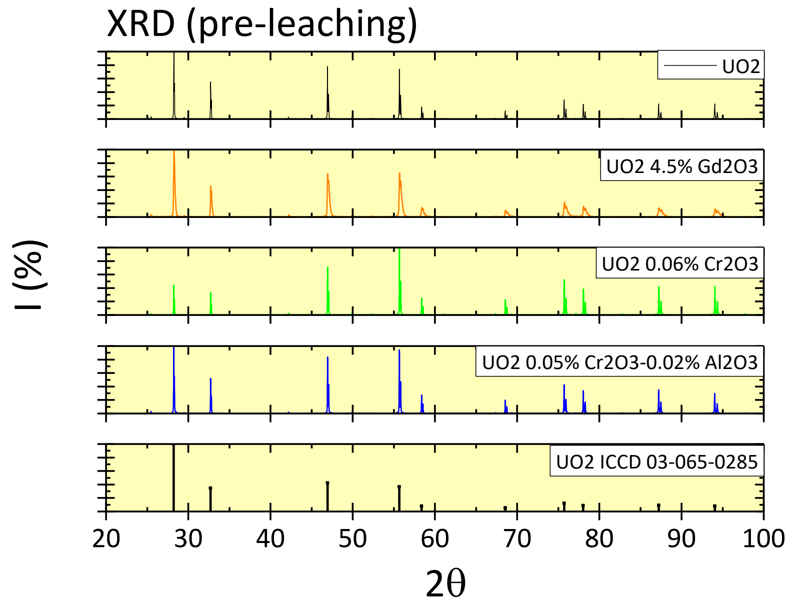

Figure 2.4.1.3: XRD patterns of fabricated solid samples UO_2 -0.06 $^{w}/_{o}$ Cr_2O_3, UO_2 -0.05 $^{w}/_{o}$ Cr_2O_3 -0.02 $^{w}/_{o}$ Al_2O_3 and UO_2 -4.5 $^{w}/_{o}$ Gd_2O_3, together with UO_2 ICDD reference data.

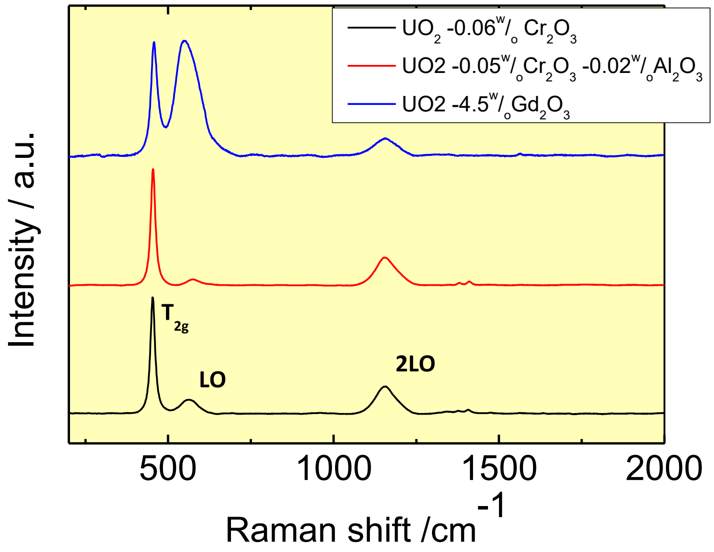

Figure 2.4.1.4: Raman spectra of fresh doped UO_2 pellets.

Regarding Raman spectroscopy results, Figure 2.4.1.4 shows the sum of ten spectra per pellet, as all of them have been acquired in the same conditions. Comparing these spectra, and based on the profile analysis (curve fitting) of peaks, three main bands were identified, whose wavenumbers have been calculated from the second derivative analysis [21-23].

- The band at 445 cm^{-1} is assigned to the T_{2g} (vibration of the U-O bond in the UO_2 matrix).
- The band at 575 cm^{-1} is due to the L-O phonon and is associated with the close to perfect fluorite lattice.
- The band at ~1145 cm^{-1} is assigned to a phonon vibration of the lattice, which gives places to the 2LO band (the first overtone of this phonon vibration).

When doped samples are measured, two additional Raman features appear:

- The band at 540 cm^{-1} is assigned to the creation of oxygen vacancy (O_v) clusters. This band is related to defects in the lattice caused by the introduction of the dopant.

The two main bands associated with the fluorite lattice experiment the following changes [17]:

- At 445 cm^{-1} decrease in intensity and peak shift in the order: UO_2 -0.05 ${}^{w}/_{o}$ Cr_2O_3 -0.02 ${}^{w}/_{o}$ Al_2O_3 > UO_2 -4.5 ${}^{w}/_{o}$ Gd_2O_3 > UO_2 -0.06 ${}^{w}/_{o}$ Cr_2O_3.
- At 1145 cm^{-1} decrease in intensity as follows: UO_2 -4.5 ${}^{w}/_{o}$ Gd_2O_3 > UO_2 -0.05 ${}^{w}/_{o}$ Cr_2O_3 -0.02 w/o Al_2O_3 > UO_2 -0.06 ${}^{w}/_{o}$ Cr_2O_3.

Specific features from each Raman spectrum can be extracted for the samples in order to be compared with those with leached ones (Table 2.4.1.3). The analysis of the normalized areas has been performed taking the T_{2g} band as a reference. The normalized area of the LO band showed an increase with the Cr concentration [17]. This band is especially intense in the Gd doped sample, according to the higher solubility of Gd in UO_2. On the other hand, the 2LO band remains almost constant for Cr- and Cr/Al-doped UO_2, attending to data but is substantially reduced for the Gd-doped UO_2.

Table 2.4.1.3: List of the different vibrational modes featured in the Raman spectrum of as-prepared doped UO_2 solid samples.

	UO_2 -0.06 $^{w}/_{o}$ Cr_2O_3	**UO_2 -0.05 $^{w}/_{o}$ Cr_2O_3 -0.02 $^{w}/_{o}$ Al_2O_3**	**UO_2 -4.5 $^{w}/_{o}$ Gd_2O_3**
		Frequencies (cm^{-1})	
ν T_{2g}	445.20333 ± 0.64827	441.5 ± 0.615	443.05286 ± 1.19572
ν LO	567.03667 ± 2.28693	562.15667 ± 1.91732	525.98857 ± 2.95688
ν 2LO	1146.01 ± 1.24102	1142.00556 ± 1.66723	1144.40714 ± 0.83908
		Normalized areas	
A LO/T_{2g}	0.15057 ± 0.03207	0.10307 ± 0.03288	3.45387 ± 0.44057
A 2LO/T_{2g}	1.00918 ± 0.13753	1.06733 ± 0.20441	0.46476 ± 0.0698

To quantify total Cr, Al, Gd and U in samples accurately, digestion of a fragment of each type of doped-UO_2 was performed in a mixture of acids (HCl, HNO_3 and HF) using a microwave digestion system (Figure 2.4.1.5) (Milestone ETHOS One) with pressurized closed vessel (Teflon) and analysed with ICP-MS.

Figure 2.4.1.5: Microwave digestion system with pressurized closed vessel.

The results in % are given in Table 2.4.1.4. After acid digestion, total dopant recovered from these samples was lower than expected from the initial quantity added. The empirical errors associated with the methodology (fabrication and digestion) summed up to the potential "volatilization" of Cr_2O_3 could explain these low values obtained from microwave digestion procedure. EPMA (Electron Microprobe Analysis) have been used by other authors [24] for quantitative data on elemental fraction in pellets, supporting the fact of some Cr volatilization from the solid phase at high temperatures (from 1300 °C) and even low oxygen pressure conditions. The Cr "evaporation" was attributed to the dissociation of Cr_2O_3 into Cr(g) and oxygen, depending on the atmosphere composition [24-26]. Digestion percentages in Table 2.4.1.4 should be used with caution when interpreting data from this analysis and should not be considered to extract a final conclusion.

Table 2.4.1.4: Analytical results and relative fractions of doping obtained by ICP-MS for doped-UO_2 samples prepared in the present study.

	Al	**Cr**	**Gd**	**U**	**Al_2O_3**	**Cr_2O_3**	**Gd_2O_3**	**UO_2**
Composition	**µg/l**				**%**			
UO_2 -0.06 $^w/_o$ Cr_2O_3		5.91E+02 ± 159		3.98E+06 ± $3\cdot10^4$		0.017		91
UO_2 -0.05 $^w/_o$ Cr_2O_3 – 0.02 $^w/_o$ Al_2O_3	4 ±3.6	1.18E+02 ±205		3.61E+06 ± $7\cdot10^4$	0.0002	0.004		90
UO_2 -4.5 $^w/_o$ Gd_2O_3			4.05E+04 ± $1\cdot10^3$	3.07E+06 ± $8\cdot10^4$			1.2	88

Aqueous solution chemistry

Three test media were proposed as leachants:

- PC: $NaClO_4$ 0.02M, as a blank media tests pH 7 – 7.6 to buffer ionic strength,
- BC: bicarbonate water (0.019 M $NaHCO_3$- 0.001M NaCl) pH 8 - 9 as highly carbonated media compared to those expected under repository conditions, and
- YCW: young cementitious water (YCW-6) pH ~13.5 to assess the stability of doped-UO_2 in the highly alkaline chemical environment. The YCW leachant were prepared adjusting SCK CEN methodology [27].

All of them were carefully prepared by the addition of pure chemical reagents to boiled and cooled MilliQ water and bubbling He gas to minimize the presence of dissolved O_2 and minimize the effects of atmospheric CO_2. Solutions were stored under Ar atmosphere in a glove box for one month. After that, they were filtered by means of a PVDF membrane with a pore size of 0.22 µm, except for the high pH solution, for which a PTFE membrane was used.

Details of analytical element concentrations of prepared aqueous leachants are shown in Table 2.4.1.5. Uranium Limit Of Quantification (LOQ) for all solutions, defined as the smallest concentration that can be quantitated with acceptable accuracy under certain conditions, was quantified as follows: LOQ = 10 x standard deviation of matrix blank measured by ICP-MS, and the intrinsic uncertainty ±15%. LOQ for the rest of the elements of interest (Cr, Al, Gd) were calculated by the same method, and are also shown in Table 3.1.4.1. The elemental composition, redox and pH were monitored *ex situ* in the anoxic atmosphere glovebox. U concentration was around 10^{-10} mol·l^{-1} ($NaClO_4$), 10^{-9} mol·l^{-1} (BC) and ranged between 10^{-9} - 10^{-8} mol·l^{-1} (YCW). Fe concentration was around 10^{-8} – 10^{-7} mol·l^{-1}.

*Fel! Hittar inte referenskälla.**: Aqueous media composition.***

	$NaClO_4$ 0.02M	**$NaHCO_3$-(0.019 M) NaCl (0.001M)**	
Conc / mol·l $^{-1}$	**PC**	**BC**	**YCW-6**
Na	$2.18\cdot10^{-2}$	$2.1\cdot10^{-2}$	$1.3\cdot10^{-1}$
Mg	$2.07\cdot10^{-6}$	$1.48\cdot10^{-6}$	<LOQ
Al	$3.61\cdot10^{-10}$	$3.55\cdot10^{-9}$	$4\cdot10^{-9}$
K	$2.80\cdot10^{-4}$	$1.40\cdot10^{-4}$	$3\cdot10^{-1}$
Ca	$2.89\cdot10^{-6}$	$5.6\cdot10^{-6}$	$1.7\ 10^{-4}$
Cr	$1.9\cdot10^{-9}$	$4\cdot10^{-9}$	$9.2\cdot10^{-8}$
Mn	$7.0\cdot10^{-9}$	$1.9\cdot10^{-8}$	$3\cdot10^{-8}$
Fe	$3.4\cdot10^{-8}$	$9\cdot10^{-8}$	$4.2\cdot10^{-7}$
Co	$3.9\cdot10^{-10}$	$1.43\cdot10^{-9}$	<LOQ
Ni	$<1.7\cdot10^{-9}$	$<1.7\cdot10^{-9}$	<LOQ
Cu	$2.3\cdot10^{-9}$	$1.2\cdot 10^{-8}$	$9.7\cdot10^{-8}$
Cs	$1.9\cdot10^{-10}$	$1.38\cdot10^{-9}$	$2.3\cdot10^{-10}$
Ba	$9.9\cdot10^{-9}$	$1.8\cdot10^{-8}$	$1.9\cdot10^{-8}$
Ce	$7.1\cdot10^{-12}$	$1\cdot10^{-10}$	<LOQ
Gd	$9\cdot10^{-12}$	$8\cdot10^{-11}$	<LOQ
Pb	$5.7\cdot10^{-10}$	$5.3\cdot10^{-9}$	$1.5\cdot10^{-8}$
Th	$<4.3\cdot10^{-12}$	$<4.3\cdot10^{-12}$	<LOQ
U	$1.2\cdot10^{-10}$	$3.6\cdot10^{-9}$	<LOQ
Cl^-	$1.0\cdot10^{-4}$	$1.1\cdot10^{-3}$	$1.5\cdot10^{-8}$
SO_4^{2-}	-	$3.3\cdot10^{-5}$	$1.9\cdot10^{-3}$
pH	7.2±0.1	8.9±0.1	13.5±0.1
LOQ (U)	10^{-10}	10^{-9}	10^{-9}
LOQ (Cr)	$8\cdot10^{-9}$	$3\cdot10^{-8}$	$5\cdot10^{-7}$
LOQ (Al)	10^{-9}	10^{-9}	10^{-7}
LOQ (Gd)	$7\cdot10^{-11}$	$6\cdot10^{-10}$	10^{-11}

2.4.2 Dissolution experiments

Experimental set-up

PEEK-lined 316 stainless steel autoclaves (total volume 380 ml; Figure 2.4.2.1) were equipped with a PEEK vessel and three valves in the lid (quick-fit type) to allow injecting/releasing gas into the reactor and sampling of solutions during the experiment (Figure 2.4.2.1). O-ring seals were made of Viton®. The pressure vessels are designed to achieve maximum temperatures of 250°C. Sampling of the aqueous phase was carried out via a polyurethane tube. Prior to use, unirradiated fuel discs of approximately 0.9 g were first annealed at 1000 °C in reducing conditions and washed twice with 1 mM bicarbonate water and twice with pure MilliQ water (resistivity r=18.2 $M\Omega \cdot cm^{-1}$), generally to remove U(VI) from the surface, and then the solid samples were stored in an Ar glove box.

CIEMAT has performed nine leach experiments on three types of fresh fuel disc (previously described), at the bottom of the reactor except for BC and YCW system, in which sample discs were suspended by a Pt wire. In parallel, blank tests containing only leaching solution were run under the same conditions to check for possible cross-contamination.

The doped UO_2 samples were exposed to 300 ml of three synthetic groundwaters (PC, BC and YCW) for 136 (in PC), 168 (in BC) and 379 days (in YCW), respectively, under anoxic/reducing conditions of 7-8 bar 4.7%H_2-N_2 gas ($pH_2 = 0.37 \pm 1$ bar). Autoclaves were installed in an Ar glove box at room temperature (22 ± 3 °C). Oxygen concentration in the glove box was measured to be 1000 ppm along all the tests, as a consequence of an undetected failure of the oxygen sensor. Subsamples of ~ 3.5 ml aqueous phase were collected through a sampling valve without opening the reactor, due to the overpressure inside the reactor. Samples of the leachate were taken at regular time intervals, without renewal of the aqueous solution, i.e. in static mode. After each sampling, the autoclave was refilled with 4.7%N_2/H_2 up to 8 bar to reach the initial conditions. The aliquots were filtered using ~ 1.5 ml for microfiltration (0.22 μm) and ~ 1.5 ml for ultrafiltration (Amicon Ultra-4 3k Millipore 1 - 2 nm).

Unfiltered and microfiltered aliquots of solutions were diluted and acidified with 10% HNO_3 solution. Samples were analysed by ICP-MS using an iCAP Qc (Thermo Fisher Sci instrument). The limit of detection of ICP-MS was in the range of ppt ($pg \cdot g^{-1}$) and the LOQ in the ppb range ($ng \cdot g^{-1}$). Uncertainty of the elemental concentration measured by this technique is around 15%.

Measurements of pH have been performed during the entire experiment using a pH Glass Electrode (Metrohm) and pH-meter 905 Titrando (Metrohm). The pH electrode was calibrated with commercial pH buffer solutions (4, 7, 9). Redox potential was measured with an Ag/AgCl Combined Pt-ring Electrode (Metrohm).

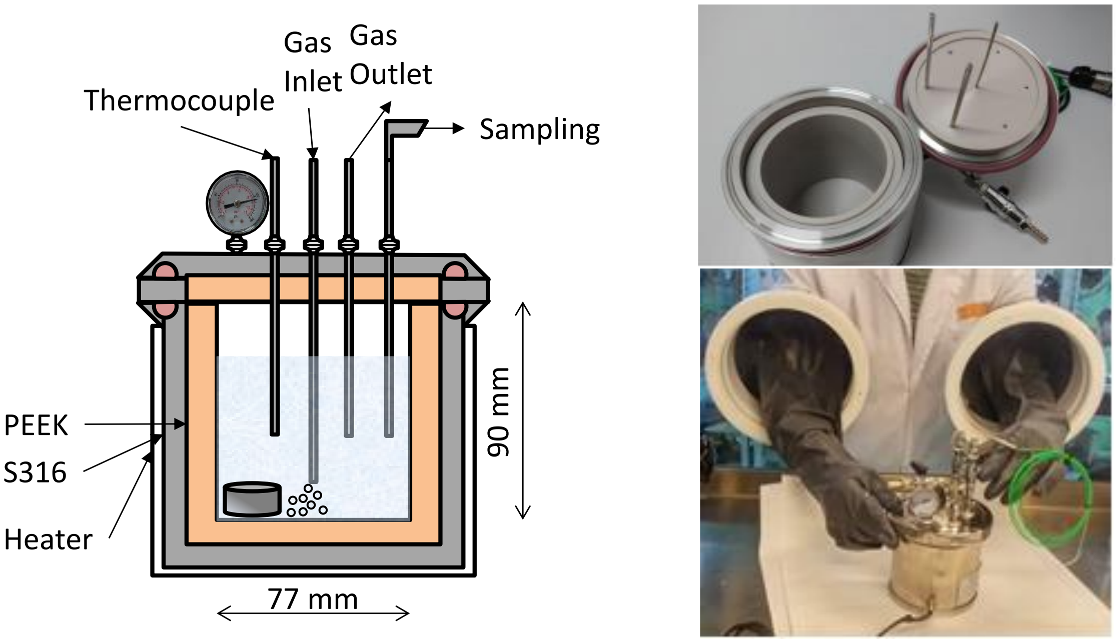

Fel! Hittar inte referenskälla.: ***Image of PEEK-lined stainless steel thermostatized autoclaves at CIEMAT radioactive facilities.***

Element release

Uranium, chromium, aluminium and gadolinium concentrations in the leachate solutions were measured by ICP-MS and their evolution are plotted in Figure 3.1.4.1a, Figure 3.1.4.2a, Figure 3.1.4.3a (U); Figure 3.1.4.5a and Figure 3.1.4.6a (Cr); Figure 3.1.4.8a (Al) and Figure 3.1.4.10a (Gd).

The normalised dissolution rates of U (R_L(U) in g·$(m^2 \cdot d)^{-1}$ as a function of time were calculated as follows:

$$R_L(X)\left(g\cdot(m^2\cdot d)^{-1}\right) = \frac{[X](mol\cdot l^{-1})}{f_x \cdot \left(\dfrac{SA(m^2)}{V_t(l)}\right)\cdot t(d)}$$

Where *[X]* is dissolved element concentration (mol·l^{-1}); *fx* is the theoretical fraction of element X in the solid sample; *SA* is the geometric surface area in $m^2 \cdot g^{-1}$ (without roughness factor correction $\lambda = SA_{tot}/SA_{BET}$); *Vt* is the remaining volume at time *t* in days. The normalized dissolution rate (R_L) was plotted as a function of time as shown in in Figure 3.1.4.1b, Figure 3.1.4.2b, Figure 3.1.4.3b for U; Figure 3.1.4.5b and Figure 3.1.4.6b for Cr; Figure 3.1.4.8b for Al and Figure 3.1.4.10b for Gd.

Generally, in the following Figures, filled symbols represent microfiltered (or not-filtered) aqueous samples and empty symbols are ultrafiltered.

2.5 UFSD

2.5.1 Samples prepared by USFD

Cr- doped and undoped UO_2 samples have been prepared via a nitrate synthesis route using uranium (VI) nitrate hexahydrate in solution (0.3 mol.L^{-1}) and chromium (III) nitrate nonahydrate in solution (1.6 mol.L^{-1}) ($Cr(NO_3)_3.9H_2O$ 99.99 %, Sigma Aldrich). Analysis of the supernatants by ICP-OES showed successful Co-precipitation of U and Cr both at 99.9%. Resultant precipitates were calcined to oxide at 750 ˚C for 4 hours under a reducing (N_2 – 5% H_2) atmosphere and characterised by SEM and XRD. The Cr content was determined by complete dissolution of ~ 20mg of powder in 2M HNO_3 and analysing the solutions by ICP-MS. The matrix Cr content was also measured by EPMA. Pressed pellets were sintered at 1700 ˚C for 8 hours under a reducing (N_2 – 5% H_2) atmosphere and ground using SiC paper, polished to 1 µm using diamond suspension and thermally etched at 1500 °C in a reducing atmosphere (N_2 – 5% H_2). The average grainsize, analysed by SEM, and density, measured both geometrically and by the Archimedes method, were determined before use in dissolution experiments. Samples have also been characterised by Raman spectroscopy and Vertical Scanning Interferometry (before and after dissolution), and by Cr K-edge, U $M_{4,5}$ edge and U L_3-edge X-ray Absorption Spectroscopy to determine Cr and U oxidation state and local coordination, and EPMA to determine the concentration of Cr within the matrix.

2.5.2 Dissolution experiments

Experiments were carried out on both Cr-doped and undoped UO_2 in ovens at 25°C, 40°C and 60°C ± 2°C. Duplicate polished and annealed monolith samples (from 0 to 2400 nominal ppm Cr) were submerged in 50 mL simulant ground water solution (1 mM $NaHCO_3$ + 19 mM NaCl) and an aliquot (2 mL) removed at each time point. Fresh solution, heated to the appropriate temperature, was replaced in order to maintain the same SA/V ratio and the solutions agitated to avoid elemental build up. Aliquots of solution were taken at day 1, 3, 7, 14, 21 and 28 days, then bi-weekly for the duration of the experiment (except when Covid-19 laboratory closures would not allow any sampling – during this time, the ovens remained switched on). The mass and pH were also monitored throughout the experiment with no significant change in either. Concentrations of U in solution, after filtration through a 0.22 µm filter, were measured by ICP-MS for experiments performed at all three temperatures. The normalised mass loss of U ($N_L(U)$) was determined, where the mass loss (concentration) was normalised by the mass fraction of U and sample geometric surface area. It was not possible to detect Cr at any stage throughout the experiments. At the termination of the experiment, which was determined when $N_L(U)$ measurements indicated that solution saturation of U had occurred, monoliths were removed from solution for post-dissolution characterisation by SEM, XRD and for selected samples, by Raman spectroscopy.

2.6 UCAM - Mixed oxide simulants

U, Th mixed oxide pellets (and endmembers as reference materials) have been prepared and characterised for leach tests in an anoxic glovebox. An annealing treatment in a furnace integrated into the glovebox was carried out at 1200˚C in 5% H_2/N_2 before the dissolution test. Static oxidative dissolution tests were then carried out in polypropylene vessels, under an argon atmosphere without the samples leaving the glovebox. The leaching solution was deareated, simulant Callovian-Oxfordian ground water, with 1.3×10^{-4} M H_2O_2 added initially. The endmember and mixed oxide pellets were pre-washed and then leached for 15 days. Washouts of the leaching vessels were obtained by an acid rinse (2M HNO_3 (aq)) at the end of the experiment.

Uranium concentrations were obtained by inductively-coupled plasma mass-spectrometry and converted to U releases, NL_U, using the following equation:

$$NL_U = \frac{m_U}{x_{solid \times S}} \qquad (1)$$

with m_U the mass of dissolved uranium (g), x_{solid} the fraction of uranium in the solid and S the surface area of the pellet (m^2). Surface area was calculated by combining the pellet geometry with a three-dimensional scanning electron microscopy technique that gave the ‘true to projected’ or equivalent surface area of the pellets as 1.25.

3 Update of dissolution experiments

3.1 Cr/Al/Gd doped UO_2 model systems

3.1.1 Results from SCK CEN

3.1.1.1 pH and redox potential

pH and redox potentials of the leaching solution are measured at sampling time in the sampling bottle. Therefore, the change of pressure to which the samples are exposed when they are taken from the autoclaves to the glove box at much lower pressure may have disturbed the solution and then may have impact the measured values, especially the redox potentials.

In the YCWCa-L whatever the type of materials, the pH of the solution remains constant close to 13.5 ± 0.1. In the FIN solution, the pH of the leaching solution is more fluctuating and in the range of 9.9 ± 0.5 and 9.5 ± 0.5 to, respectively for UO_2/Pu-UO_2 and Cr-UO_2 and Pu-Cr-UO_2 which is slightly higher than the target value of 9.1 (Table 2.1.2.1).

At the opposite, the redox potential in FIN and YCWCa-L behaves similarly with a decrease from -100 to -350/-450 $mV_{/SHE}$ in the solutions of the inactive experiments, while it is more oxidizing and fluctuating between -100 and +100 $mV_{/SHE}$ in the active experiments. Although the measured values are maybe not fully representative of the Eh prevailing inside the autoclaves, these suggest that the Pt/Pd catalyst coupled to the H_2 pressure would allow a good scavenging of atmospheric oxygen (inactive experiments) without counteract the oxidising species from the radiolysis (active experiments).

3.1.1.2 Uranium concentration

Figure 3.1.1.5.1 shows the total U concentration as a function of time for the different model materials at pH 13.5 (Figure 3.1.1.5.1 a) and at pH 9 (Figure 3.1.1.5.1 b). Table 3.1.1.2.1 and Table 3.1.1.2.2 give the measured total and soluble U concentrations as a function of time for the inactive and active experiments, respectively.

pH 13.5

For the inactive experiments (Figure 3.1.1.5.1 a-red symbols) after a high initial U release, up to 1.6×10^{-7} for UO_2 and 2.2×10^{-8} $mol.L^{-1}$ for Cr-UO_2, the U concentration slightly decreased. After 155 days, the U concentration stabilised around 8.2×10^{-8} for UO_2 and 1.4×10^{-8} $mol.L^{-1}$ for Cr-UO_2. The presence of Cr thus reduced by a factor 6-7 the U concentration over the entire test duration. The measured U concentration up to $3x10^{-8}$ $mol.L^{-1}$ suggested the release U(VI) in spite of the washing step before the leaching experiments.

For the active experiments (Figure 3.1.1.5.1 a-green symbols) a high initial U release of 1.7 $\times10^{-7}$ for Pu-UO_2 and 1.0×10^{-7} $mol.L^{-1}$ for Pu-Cr-UO_2 is also observed with no clear influence of Cr up to 10 days. Afterwards, while the U concentration remained around 1.0×10^{-7} $mol.L^{-1}$ for Pu-Cr-UO_2, the U concentration for Pu-UO_2 increased. After 35 days, the U concentration is about 5 times higher than for the Pu-Cr-UO_2, and remains stable close to 5.2 × 10^{-7} $mol.L^{-1}$ (Figure 3.1.1.5.1 a- green symbols). This suggests that, at pH 13.5, the Cr doping lowers the U concentration also in presence of alpha field.

In most cases, the U concentration in the ultrafiltered samples represents more than 90% of the total U concentration (Table 3.1.1.2.1 and Table 3.1.1.2.2), the difference corresponding to the uncertainty of measurement techniques. However, the U-colloids (= difference between total and soluble U concentrations) are increasing after 155 days in the UO_2 system without a-field, possibly as precursors of a U-phase formation.

pH 9

For the inactive experiments, a high initial U release of 1.8 × 10^{-7} for UO_2 and 2.2 × 10^{-8} $mol.L^{-1}$ for Cr- UO_2 was measured (Figure 3.1.1.5.1 b blue-symbols). Then, the U concentration considerably decreased with time to stabilize after 30 days around 2 × 10^{-9} $mol.L^{-1}$ for both systems. This suggests a possible control of the U in solution by UO_2. The higher ratio of colloidal U / total U (Table 3.1.1.2.1) supports the possible over-saturation with a U secondary phase, but the concentration of colloidal U remains small (about 10^{-9} M). During the first 10 days of leaching, the presence of Cr seems to reduce the U release, similarly as at pH 13.5 (Figure 3.1.1.5.1 a- blue symbols), but this effect disappears with time. After 72 and 155 days the U concentration showed a slight increase, more for UO_2 than for Cr-UO_2. This suggests again a reducing effect of the Cr. As the experiments were stopped after 155 days, we cannot verify if this trend continues afterwards.

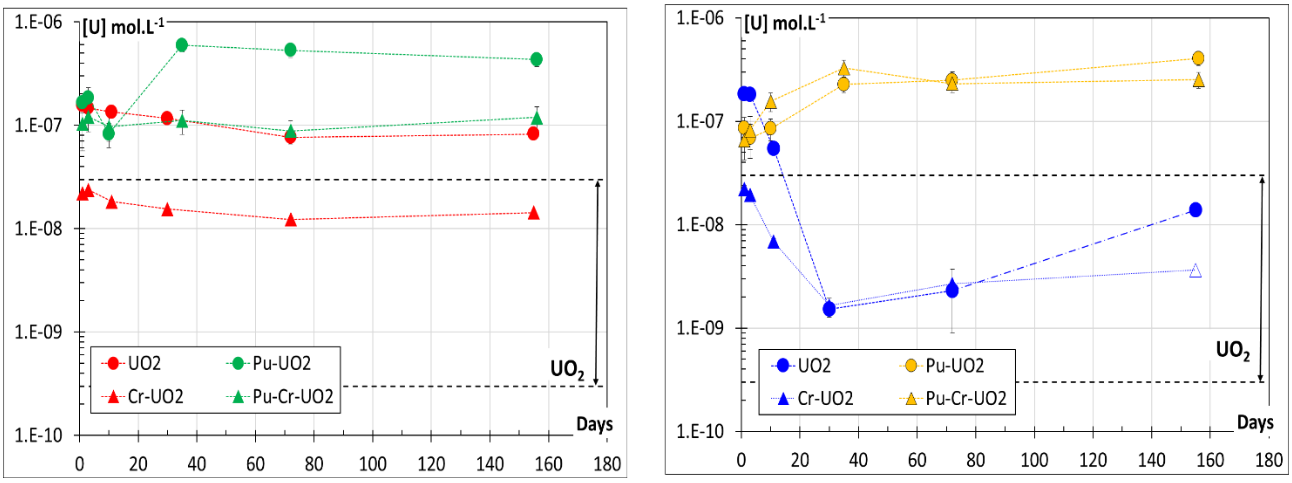
a (pH 13.5) **b (pH 9)**

Figure 3.1.1.5.1: Total U concentrations as a function of time with 10 bar H_2 - a: at pH 13.5 for inactive experiments (red symbols) and active experiments (green symbols): at pH 9 for inactive experiments (blue symbols-empty symbol ≤ detection limit) and active experiments (yellow symbols). On both graphs, the black dotted lines represent the U(IV) solubility range [28].

For the active experiments, the initial U concentration is high again (9 -7 x 10^{-8} $mol.L^{-1}$- Figure 3.1.1.5.1 b- yellow symbols). After this initial release, the U concentration slightly increases and tends to stabilise around 3 × 10^{-7} $mol.L^{-1}$ after 35 days (Figure 3.1.1.5.1 b- yellow symbols). There is no pronounced Cr effect. The presence of U colloids in active experiments at pH 9 is also rather limited and remains within the uncertainties of the alpha-spectrometry (Table 3.1.1.2.2).

Table 3.1.1.2.1: U concentration (mol.L^{-1}) as function of time in the experiments with UO_2 and Cr-UO_2 pellets at pH 13.5 and at pH 9. $[U]_T$= Total, not filtered U concentration and $[U]_s$= soluble, ultrafiltered U concentration (< 3.5 nm).

	pH 13.5				pH 9			
	UO_2		Cr-UO_2		UO_2		Cr-UO_2	
	$[U]_T$	$[U]_s$	$[U]_T$	$[U]_s$	$[U]_T$	$[U]_s$	$[U]_T$	$[U]_s$
Days	$\times 10^{-8}$ mol.L^{-1}				$\times 10^{-8}$ mol.L^{-1}			
1	15.6 ± 1.6	15.3 ± 1.6	2.2 ± 0.2	2.2 ± 0.2	18.4 ± 1.9	16.0 ± 1.6	2.2 ± 0.2	2.2 ± 0.2
3	14.7 ± 1.5	14.2 ± 1.4	2.4 ± 0.2	2.3 ± 0.2	18.1 ± 1.8	16.3 ± 1.7	1.9 ± 1.9	1.7 ± 0.2
11	13.4 ± 1.3	11.9 ± 1.2	1.8 ± 0.2	1.7 ± 0.2	5.4 ± 0.6	5.2 ± 0.5	0.7 ± 0.07	0.6 ± 0.06
30	11.6 ± 1.2	11.0 ± 1.1	1.6 ± 0.2	1.5 ± 0.2	0.2 ± 0.5	0.1 ± 0.4	0.2 ± 0.05	0.1± 0.04
72	7.7 ± 0.8	6.8 ± 0.7	1.2 ± 0.1	1.0 ± 0.1	0.2 ± 0.03	< 0.06	0.3 ± 0.03	< 0.06
155	8.2. ± 0.8	4.3 ± 0.4	1.4 ± 0.1	0.5 ± 0.3	1.4 ± 0.1	< 0.4	< 0.4	< 0.4

Table 3.1.1.2.2: U concentration (mol.L^{-1}) as function of time in the experiments with Pu-UO_2 and Pu-Cr-UO_2 pellets at pH 13.5 and in at pH 9. $[U]_T$= Total, not filtered U concentration and $[U]_s$=soluble, ultrafiltered U concentration (< 3.5 nm).

	pH 13.5				pH 9			
	Pu-UO_2		Pu- Cr-UO_2		Pu-UO_2		Pu- Cr-UO_2	
	$[U]_T$	$[U]_s$	$[U]_T$	$[U]_s$	$[U]_T$	$[U]_s$	$[U]_T$	$[U]_s$
Days	$\times 10^{-8}$ mol.L^{-1}				$\times 10^{-8}$ mol.L^{-1}			
1	16.6 ± 3.6	13.8 ± 3.9	10.3 4.7	8.4 ± 3	8.6 ± 2.3	8.8 ± 2.9	6.7 ± 2.3	8.8 ± 2.9
3	18.5 ±4.5	8.9 ± 3	12.1±3.4	11.4 ± 3	6.9 ± 2.4	5.4 ± 2	8.2 ± 2.9	5.4 ± 2.5
11	8.3 ± 2.2	10.2 ± 2.4	9.7 ± 2.6	8.4 ± 2.5	8.4 ± 2	11.7 ± 2.9	15.5 ± 3.2	18.7 ± 3.9
35	59.5 ± 8.3	57.4 ± 8.4	11.1 ± 3	11.2 ±2.5	22.7 ± 3.8	20.2 ± 3.9	32.7 ± 6.2	29.9 ± 5.4
72	53.1 ± 7.8	53.4 ± 8.4	8.8 ± 2.2	9.9 ± 3	24.9 ± 5	23.6 ± 4.9	23 ± 4	25 ± 4.9
156	43.3 ± 6.4	46.5 ± 6.4	11.9 ± 3	10.6 ±2.6	40.5 ± 5.8	34.8 ± 5.4	25.3 ±4.4	25 ± 4.4

3.1.1.3 Plutonium concentration

A complete overview of the not filtered and ultrafiltered Pu concentrations is reported in Table 3.1.1.3.1 and the not filtered Pu concentrations are illustrated in Figure 3.1.1.3.1 with the associated U concentrations, for the active tests in the two reference solutions.

pH 13.5

The total Pu concentrations are in the range of 1 to 50 x10^{-14} mol.L^{-1} and appear also slightly lower in presence of Cr, similarly to U (section 4.2). The Pu concentrations are lower than the Pu(IV) solubility [28], and also two orders of magnitude lower than the expected Pu concentrations representative for a congruent dissolution (i.e. Pu dissolving at the same rate as U after normalization w.r.t. the fraction of the Pu in the doped UO_2) , as represented by the orange dotted rectangular on Figure 3.1.1.3.1a.

In most of the cases, the ultrafiltered Pu concentrations are close to or below the detection limits for both the Cr and not Cr doped systems. Considering the difference between the not filtered and the ultrafiltered concentrations, this suggests either a strong sorption of Pu on the filters or the presence of Pu colloids, but this appears less likely considering the low Pu concentrations.

pH 9

For both Pu-UO$_2$ and Pu-Cr-UO$_2$ systems, the total Pu concentrations are fluctuating around to 3 x 10^{-14} mol.L^{-1}, suggesting no Cr effect on Pu release. Similarly to pH 13.5, the measured Pu concentrations are also two orders of magnitude too low to be representative for congruent dissolution (orange dotted rectangular on Figure 3.1.1.3.1b). and the ultrafiltered Pu concentrations are close to or below the detection limit. Regarding the large difference between the not filtered and ultrafiltered concentrations, the high sorption of Pu on the filters or the Pu colloids are thus put forwarded.

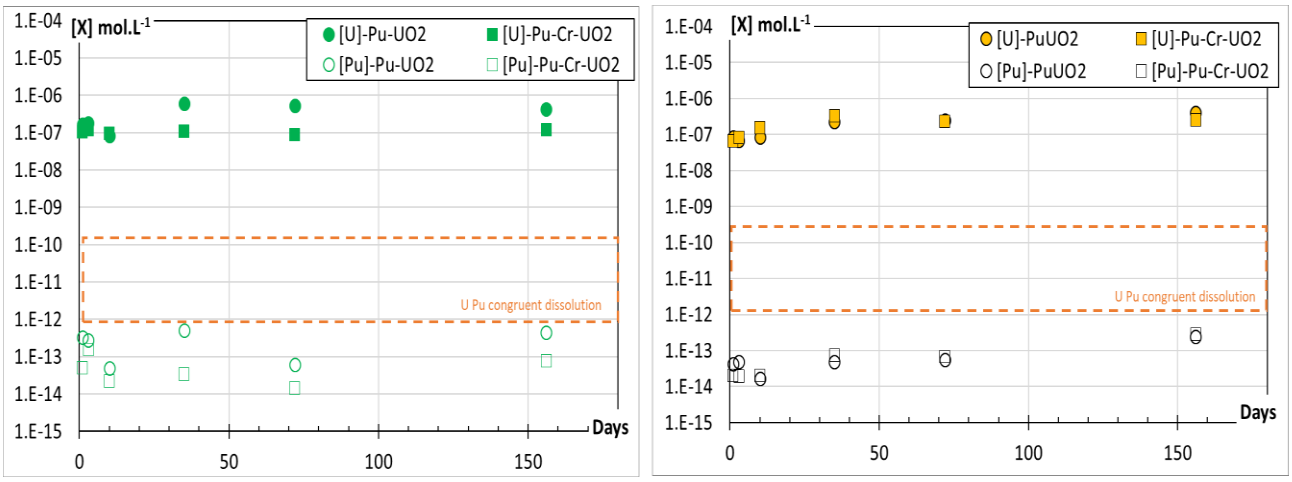
a (pH 13.5)

b (pH9)

Figure 3.1.1.3.1: Total Pu and U concentrations as function of time with 10 bar H_2 - a: at pH 13.5 for Pu-UO$_2$ experiments (Pu empty green point symbols and U filled green point symbols) and Cr-Pu-UO$_2$ experiments (Pu empty green square symbol and U empty green square symbol); b: at pH 9 for or Pu-UO$_2$ experiments (Pu empty black point symbols and U filled yellow point symbols) and Cr-Pu-UO$_2$ experiments (Pu empty black square symbol and U empty yellow square symbol). On both graphs, the orange dotted ~rectangular represents the Pu concentration domain of U, Pu congruent dissolution.

Table 3.1.1.3.1: Pu concentration (mol.L^{-1}) as function of time in the experiments with Pu-UO$_2$ and Pu-Cr-UO$_2$ pellets at pH 13.5 and in at pH 9. [Pu]$_T$=Total, not filtered Pu concentration and [Pu]$_s$=soluble, ultrafiltered Pu concentration (< 3.5 nm).

	pH 13.5				pH 9			
	Pu-UO$_2$		Pu- Cr-UO$_2$		Pu-UO$_2$		Pu- Cr-UO$_2$	
	[Pu]$_T$	[Pu]$_s$	[Pu]$_T$	[Pu]$_s$	[Pu]$_T$	[Pu]$_s$	[Pu]$_T$	[Pu]$_s$
Days	× 10^{-14} mol.L^{-1}				× 10^{-14} mol.L^{-1}			
1	32 ± 5	0.4 ± 0.3	5.1 ± 1.1	< 0.5	4.3 ± 0.9	< 0.5	2.1 ± 0.7	< 0.5
3	28 ±3	0.5 ±0.2	16 ±2.4	< 0.5	4.9 ± 1	< 0.3	1.9 ± 0.6	< 0.3
11	5 ± 0.9	0.5 ± 0.3	2.2 ± 0.6	< 0.2	1.7 ± 0.6	0.6 ± 0.06	2 ± 0.5	1 ± 0.3
35	52 ± 6	1.4± 0.5	3.5 ± 0.7	< 0.3	5±= 0.9	0.7± 0.06	7.6 ± 1.2	< 0.3
72	6 ± 1	< 0.3	1.4± 0.5	< 1.4	5.5 ± 1.3	0.5 ± 0.06	6.8 ± 1.1	0.8 ± 0.05
156	45 ± 5	2 ± 0.5	7.8 ± 1.3	< 0.3	24.3 ± 2.9	2.9 ± 0.3	28.9 ± 3.1	5.6 ± 0.9

3.1.1.4 Cr concentration

An overview of the not filtered Cr concentrations are reported in Table 3.1.1.4.1 and shown as function of time in Figure 3.1.1.4.1 for the inactive and active systems. In most cases, the Cr concentrations are close to the detection limit of the ICP-MS (between 1 to 8 x10^{-8} mol.L^{-1}), also close to the background concentrations of the reference solution (Table 2.1.2.1 and the red and blue dotted lines in Figure 3.1.1.4.1) and not so different that the Cr concentrations measured in not doped Cr system and leached in the same solution (red and blue rectangulars in Figure 3.1.1.4.1), especially at pH 9. At pH 13.5, we can notice a small increase of the initial Cr release.

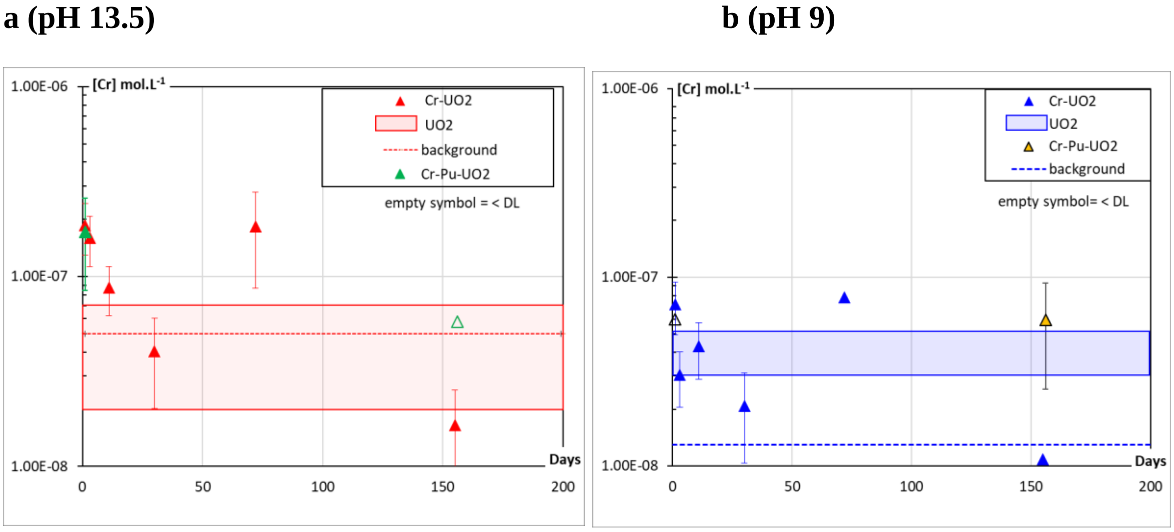

a (pH 13.5) **b (pH 9)**

Figure 3.1.1.4.1: Cr concentration (mol.L^{-1}) as function of time with 10 bar H_2 - a: at pH 13.5 for inactive experiments (red symbols) and active experiments (green symbols); b: at pH 9 for inactive experiments (blue symbols) and active experiments (yellow symbols). On both graphs, the red and blue rectangulars represent the concentration in the experiments performed in similar conditions in the UO_2 system. The dotted lines correspond to the background Cr concentration in the reference solutions and the empty symbols represent concentration below the detection limit (DL).

For both pHs, no effect of the alpha-field is observed on Cr release. This observation suggests rather a pH effect on Cr release than an influence of the redox conditions, reflecting the dominant Cr species as a function of pH : $Cr(OH)_3$ and $Cr(OH)_4^-$ at pH 9 and pH 13.5, respectively.

Table 3.1.1.4.1: Cr concentration (mol.L^{-1}) as function of time in the active and inactive experiments at pH 13.5 and at pH 9. $[Cr]_T$= total, not filtered Cr concentration.

	pH 13.5				pH 9			
	$[Cr]_T \times 10^{-8}$ mol.L^{-1}				$[Cr]_T \times 10^{-8}$ mol.L^{-1}			
	UO_2	Cr-UO_2	Pu-UO_2	Cr-Pu-UO_2	UO_2	Cr-UO_2	Pu-UO_2	Cr-Pu-UO_2
Days								
1	6.5 ± 1.1	18.6 ± 5.6	na	17.1 ± 8.7	na	7.2 ± 2.2	na	< 6
3	na	16 ± 4.7	na	na	na	3 ± 0.9	na	na
11	na	8.7 ± 2.5	na	na	na	4.3 ± 1.4	na	na
30(35)	5.1 ± 2.4	4 ± 2	na	na	3.5± 1.9	2.1 ± 1	na	na
72	< 8.8	18.3 ± 1	na	na	< 9	< 7.8	na	na
155 (156)	2 ± 1	1.6 ± 0.9	na	< 5.8	2.2± 1.1	1.1± 0.6	na	5.9 ± 3.4

na= not analysed

3.1.1.5 Zn concentration

As Zn-stearate is used as lubricant in the production of the inactive and active UO_2 based models, the Zn concentrations were measured in the different leaching systems as function of time. An overview of the not filtered Zn concentrations is reported in Table 3.1.1.5. for the different active and inactive systems leached in the two reference solutions. For all systems and for both pHs, the Zn concentration is almost equivalent and 10 times higher than the Zn concentration in the reference solutions (Table 2.1.2.1), suggesting that the Zn was maybe not fully volatilized during the sintering process, and then released during the leaching experiments. However, no interaction of Zn with U and Cr is expected.

Table 3.1.1.5.1: Zn concentration (mol.L^{-1}) as function of time in the active and inactive experiments at pH 13.5 and in at pH 9. [Zn]$_T$= Total, not filtered Zn concentration.

	pH 13.5				pH 9			
	$[Zn]_T \times 10^{-6}$ mol.L^{-1}				**$[Zn]_T \times 10^{-6}$ mol.L^{-1}**			
	UO_2	Cr-UO_2	Pu-UO_2	Cr-Pu-UO_2	UO_2	Cr-UO_2	Pu-UO_2	Cr-Pu-UO_2
Days								
1	5.9 ± 0.6	2.9 ± 0.3	na	3.1 ± 0.3	2.5 ± 0.2	2.6 ± 0.3	na	1.8 ± 0.2
3	na	na	na	na	na	na	na	na
11	na	na	na	na	na	na	na	na
30(35)	4.9 ± 0.5	2 ± 0.2	na	na	1.9 ± 0.2	2.2 ± 0.2	na	na
72	3.9 ± 0.4	3.4 ± 0.3	na	na	2.3 ± 0.2	2.5 ± 0.2	na	na
155 (156)	1.8 ± 0.2	1.4 ± 0.1	na	3.1 ± 0.3	1.1 ± 0.1	0.9 ±0.09	na	1.3 ± 0.1

na= not analysed

3.1.1.6 Surface analyses of the samples

The surfaces of the leached inactive samples (Figure 3.1.1.6.1c-d) were analysed by SEM and compared to not leached inactive samples (Figure 3.1.1.6.1a-b). It is important to note that the surface of the pellet was analysed without any specific preparation (grinding/polishing or cross sectional cutting) before the analysis.

While Secondary Electron (SE) pictures are taken to highlight the topography of the samples, Back Scattered Electron (BSE) pictures will provide valuable information of sample composition and crystal orientation.

On the figures (Figure 3.1.1.6.1a and b), we observe a clear separation of the grains as well as deep grain boundaries. No differences in characteristics of grain surface and grain boundaries were visible 1- between UO_2 and Cr-UO_2 systems and 2-over the entire pellet surface for the Cr-doped UO_2. These observations are in agreement with the fact that, although the grain size in the bulk of the pellet is larger for the Cr-UO_2, the external surface of the pellets have a similar grain size for both types of materials taking into account the Cr-depletion in the outmost layer of the Cr-doped pellet (Figure 2.1.1.2).

The leaching process does not create any significant effect on grain boundary appearance (Figure 3.1.1.6.1c, d), only an acicular structure can be observed at the surface of some grains of the Cr-UO_2 leached at pH 9 (Figure 3.1.1.6.1d). This structure could be ascribed to the presence of U_4O_9 at the surface of the UO_2 grains. As the U concentration shows a similar behaviour for UO_2 and Cr-UO_2 materials leached at pH 9 (Figure 3.1.1.2.1b, blue curves), we can also assume that such a structure would be present at the surface of the UO_2 leached at pH 9.

The analyses of the leached surface of the active experiments are not reported in this report. In December 2020 (Figure 2.1.2.2), it was decided to continue these experiments to study of the impact of Fe foil addition on the U concentrations in the active systems, to allow comparison with the experiments performed at VTT (see section Discussion). This study is performed outside of the DisCo project.

A (UO_2 – not leached) **b (Cr-UO_2 –not leached)**

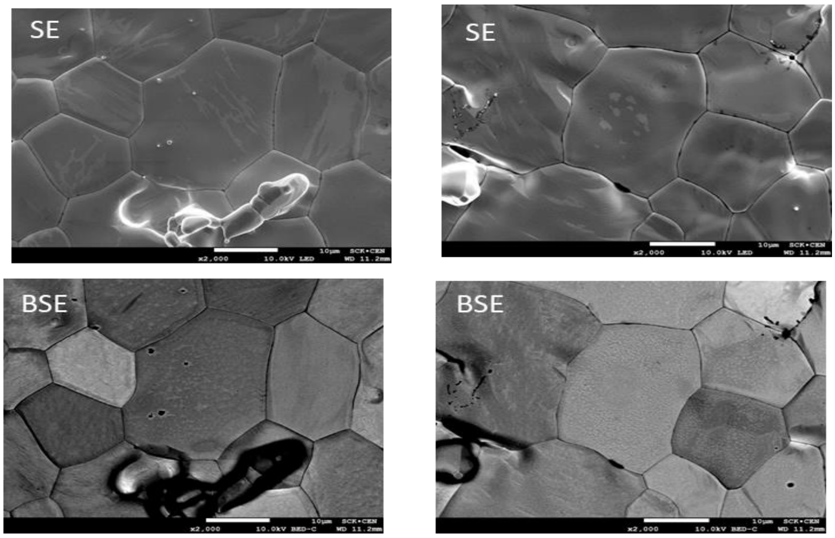

c (Cr-UO_2 – pH 13.5) **d (Cr-UO_2 – pH 9)**

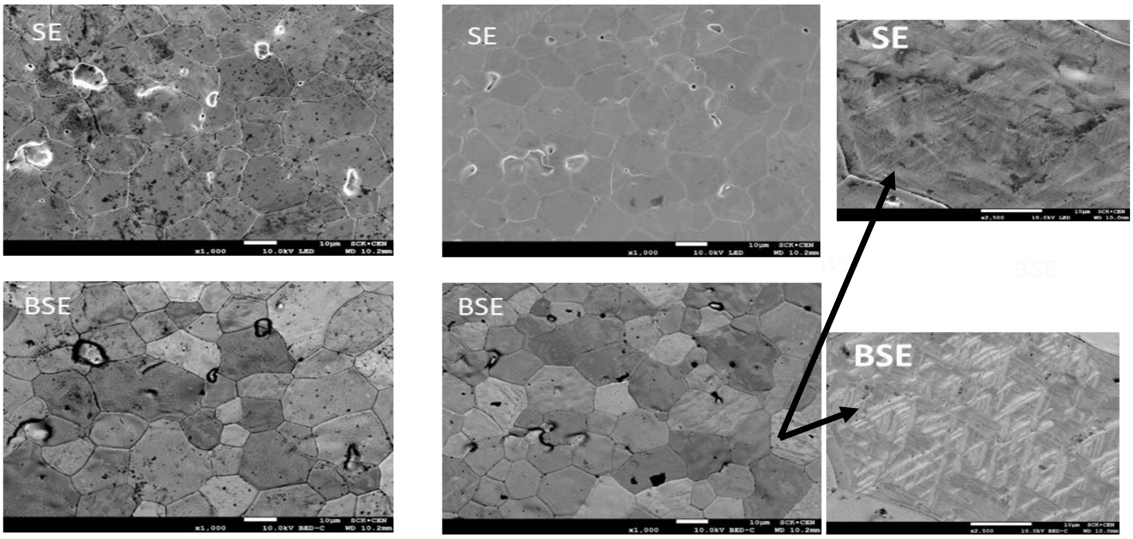

Figure 3.1.1.6.1: SEM images of : a UO_2 not leached, b: Cr-UO_2 not leached, c: Cr-UO_2 leached at pH 13.5, d: Cr-UO_2 leached at pH 9 with acicular structure (possibly = U_4O_9) on Cr-UO_2 grain surface.

3.1.1.7 Dissolution rate

Based on U concentrations (Figure 3.1.1.2.1) and the geometrical surface of the leached pellet (no roughness factor applied), we have estimated the dissolution rate for the different UO_2 model systems in the different leaching conditions (equation 1).

$$rate\ (mg.m^{-2}.d^{-1}) = \frac{[U].V(sol.)}{S_{pellet}.time} \qquad \text{eq.(1)}$$

With [U] in $mg.L^{-1}$, V in L, S_{pellet} in m^2 and time in day

Inactive systems

A fast initial dissolution rate between 0 and 1 day of leaching has been determined at 6.2 ± 0.6 (pH 13.5) and 7.2 ±0.7 $mg.m^{-2}.d^{-1}$ (pH 9) for depleted UO_2 and 0.9 ± 0.1 $mg.m^{-2}.d^{-1}$ (pH 13.5 and pH 9) for Cr-doped $UO_{2,}$, respectively (Table 3.1.1.7.1). These values suggest a lowering effect of Cr on the remaining U (VI) from oxidized layer. The nature of the leaching solution does not play any role on this initial release.

After this short initial period, no further dissolution can be measured as the net U release is close to zero (either constant or decreasing U concentrations) for all experiments.

After the acid rinsing of the autoclaves at the end of the experiments, the amount of U adsorbed on the walls of the autoclaves was equivalent for all experiments and UO_2 based models. This adsorbed amount appears more or less independent on the experimental conditions and of same order of magnitude as the initial release of U. We assume that the cell walls are saturated as soon as the experiments have started and not influencing the further U release in solution.

Active systems

A fast initial dissolution rate between 0 and 1 day, has also been determined at 11.5 ± 2.5 $mg.m^{-2}.d^{-1}$ (pH 13.5) and 5.8 ±1.5 $mg.m^{-2}.d^{-1}$ (pH 9) for Pu-UO_2 and at 7.1 ± 3.2 $mg.m^{-2}.d^{-1}$ (pH 13.5) and 4.4 ± 1.2 $mg.m^{-2}.d^{-1}$ (pH 9) for Pu-Cr-doped $UO_{2,}$ (Table 3.1.1.7.1). The dissolution rates are higher in presence of an alpha-field with little or no effect of the Cr, suggesting that nor H_2 nor Cr doping is enough to completely counteract the radiolytical oxidation in the Pu doped systems.

After this short initial period, two different trends are observed for the Cr doped UO_2 depending on the pH. While at pH 13.5, the U release stopped immediately after the initial release, the dissolution continued up to about 35 days at pH 9.

Table 3.1.1.7.1: Initial dissolution rate (mg.m^{-2}.d^{-1}) for the different UO_2 model systems at pH 13.5 and pH 9.

Initial rate (mg.m^{-2}.d^{-1})	**UO_2**	**Cr-UO_2**	**Pu-UO_2**	**Pu-Cr-UO_2**
pH 13.5	6.2 ± 0.6	0.9 ± 0.1	11.5 ± 2.5	7.1 ± 3.2
pH 9	7.2 ± 0.7	0.9 ± 0.1	5.8 ± 1.5	4.4 ± 1.6

3.1.2 Results from FZJ

The accelerated dissolution experiments conducted in the frame of WP4 were performed using pure, Cr_2O_3 and Nd_2O_3 doped UO_2 pellets, as well as commercially available Cr_2O_3 and Cr_2O_3 plus Nd_2O_3 doped UO2 pellets. It has to be noted that the Nd-doped pellets were not produced within the frame of the DisCo-project.

Figure 3.1.2.1 shows the uranium concentration in solution normalised to the geometrical surface area during the first 300 hours of dissolution experiments using pellets with different composition. Red circles represent experiments with pure UO_2, squares represent experiments with pellets doped by co-precipitation method, diamonds experiments using pellets doped with wet coating method and triangles experiments using commercially available pellets. The blue colour indicates that the samples used for the experiments were Cr_2O_3 doped, green symbols represent Nd_2O_3 doping. The yellow stars in Figure 3.1.2.1, right, represent the H_2O_2 concentration in solution of a blank experiment.

It is visible, that the plateau which marks the end of the dissolution experiment is reached after approximately 100 h for all experiments. For most experiments this also marks the time when the H_2O_2 concentration is below 0.3 mmol/L and most of the hydrogen peroxide is used by oxidation of UO_2 or is decomposed. It is remarkable that the lowest uranium concentration in the solution was detected in experiments with the highest H_2O_2 concentration in solution at that instant of time. A comparison with a blank experiment (yellow stars in Figure 3.1.2.1, right) shows a distinctly higher H_2O_2 consumption for experiments with UO_2 pellets. Experiments performed with pure or Cr_2O_3 doped UO_2 pellets currently do not provide sufficient justification that can explain this behaviour. Possibly, parts of the sample were not completely wetted during the experiment. However obviously all experiments with Nd_2O_3 bearing UO_2 pellets show a significantly lower uranium concentration.

In the context of this work, the experiments with Cr_2O_3 doped UO_2 show no significant difference in the solution behaviour of uranium to the experiments conducted with pure UO_2 pellets. The comprehensible changes in the microstructure caused by Cr_2O_3 doping (see table 2.2.1.1) do not seem to have any significant influence on the dissolution behaviour of the UO_2 matrix. The surface normalised uranium concentration after accomplishment of the plateau is between 0.08 and 0.26 µmol/L/mm^2. The initial dissolution rates for the experiments performed with pellets with and without Cr_2O_3 doping are between $5.55*10^{-7}$ and $1.83*10^{-6}$ mol/sec·m^2. The mean of the initial dissolution rate of these experiments is $1.24*10^{-6} \pm 4.1*10^{-7}$ mol/sec·m^2 (RSD = 32.6 %). Initial dissolution rates determined for the commercially available pellets are in good accordance with the values determined for pellets produced within WP2.

The surface normalised uranium concentrations for experiments with Nd doped UO_2 pellets after accomplishment of the plateau is between 0.029 and 0.015 µmol/L/mm^2. The initial dissolution rates for the experiments performed with pellets with Nd_2O_3 doping are between 1.11 and 2.17*10^{-7} mol/sec·m^2 (mean 1.56*10^{-7}± 4.04*10^{-8} mol/sec·m^2, RSD = 25.9 %). Although the experiments on Nd_2O_3 bearing UO_2 pellets were not performed within the framework of the DisCo project, the results are of importance for the activities in WP5.

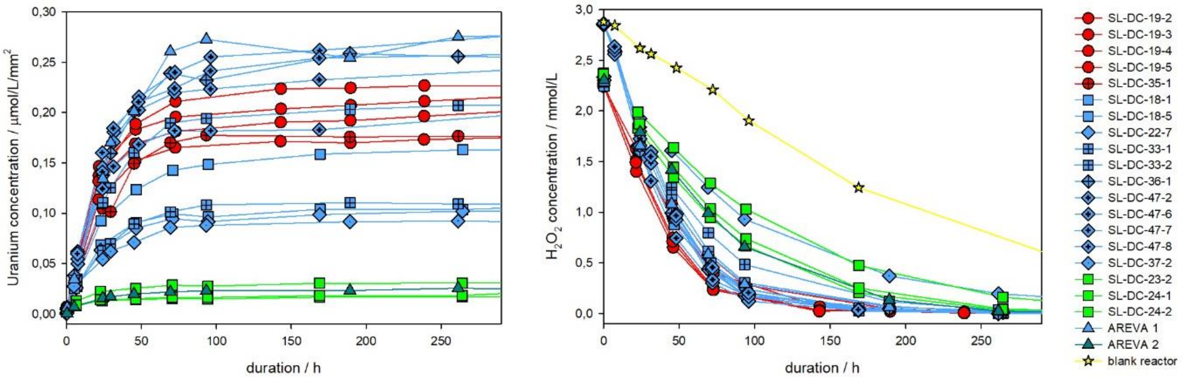

Figure 3.1.2.1: Left: uranium concentration in solution normalised to the geometrical pellet surface versus experimental duration. Right: H_2O_2 concentration in solution. The properties of the samples are listed in table 1. Symbol code: circles = pure UO_2 samples, squares = samples doped via co-precipitation method, diamonds = samples doped via wet coating method, triangles = commercially available samples, star = blank reactor (only H_2O_2). Colour code: red = pure UO_2, blue = Cr_2O_3 doped, green = Nd_2O_3 doped.

3.1.3 Results from VTT

Results of the leaching experiments with Cr-UO_2 and Cr-Pu-UO_2 pellets in natural groundwater ONK-KR15 in comparison to materials without Cr doping are presented in Figure 3.1.3.1. Results show that neither the Cr doping or Pu doping seemed to affect the uranium solubility under anoxic and reducing conditions created by Ar atmosphere and iron foil. In all experiments, the ^{238}U concentrations levels were down close to 2x10^{-11} mol/L after 150 days leaching.

The results of parallel leaching experiment with Cr-UO_2 and Cr-Pu-UO_2 pellets in FIN reference water are presented in Figure 3.1.3.2. The behaviour of total uranium concentration (^{235}U-^{238}U) is similar to natural groundwater showing a decrease from initial concentrations close to 1x10^{-9} mol/L to a 1x10^{-11} mol/L level after 150 days. In the case of FIN reference water, concentrations seemed to fall even slightly below 1x10^{-11} mol/L. There is one exception in 150 days sampling in which Cr-Pu-UO_2 pellet seems to show higher concentrations, that can be an artefact, a piece of solid or colloid material in sampling, which has dissolved as the sample was acidified under aerobic conditions. These results differ from the ones gained by SCK CEN in FIN water in their autoclave experiments, in which the effect of Pu doping was clearly observed. The effect of the Fe foil to U behaviour has to be studied in more detail to explain the observed difference.

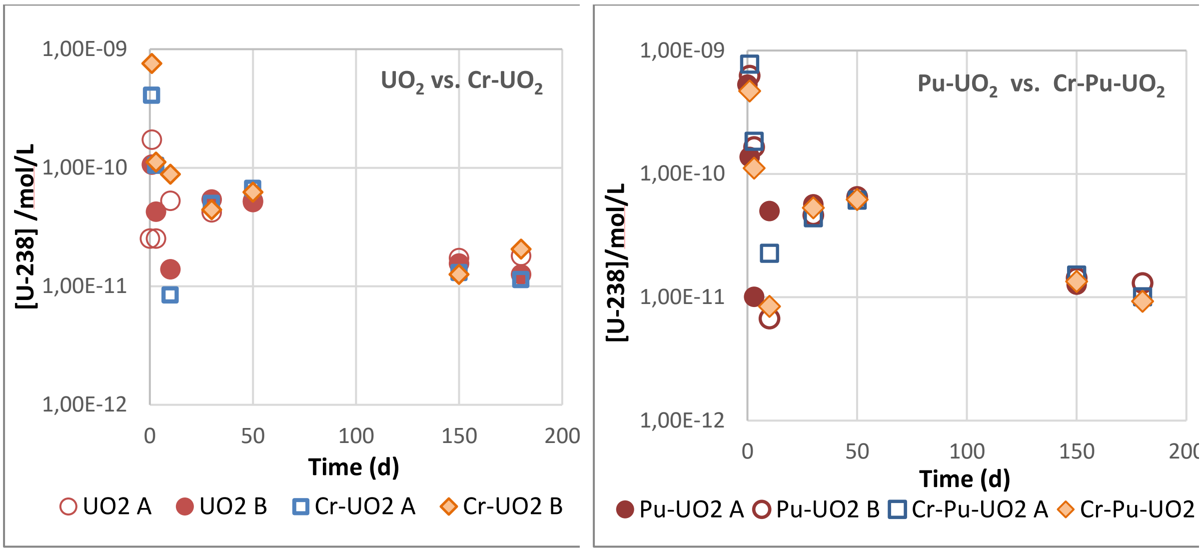

Figure 3.1.3.1: Evolution of ^{238}U concentrations in leaching experiments with UO_2, Pu-UO_2, Cr-UO_2, Cr-Pu-UO_2 pellets in natural groundwater ONK-KR15 under anaerobic and reducing conditions.

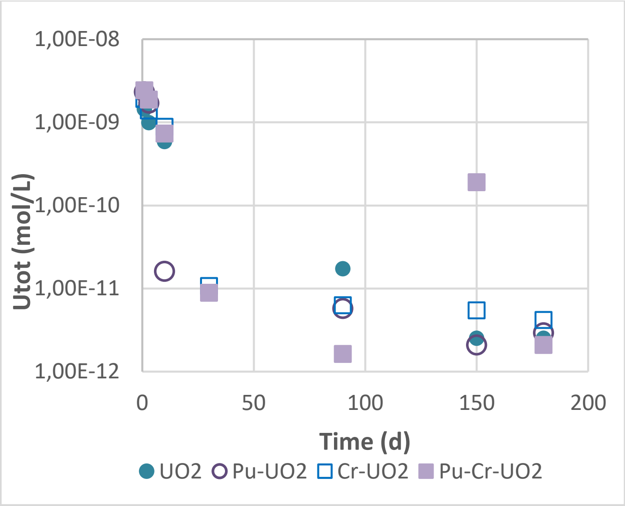

Figure 3.1.3.2: Evolution of ^{238}U concentrations in leaching experiments with UO_2, Pu-UO_2, Cr-UO_2, Cr-Pu-UO_2 pellets in FIN reference wate under anaerobic and reducing conditions.

Figure 3.1.3.3 shows the behaviour of pH during the leaching experiments with Cr/Pu -doped pellets. In natural groundwater the pH remained much more stable, whereas in FIN water the pH tends to slightly increase from 9.1 towards 10 during 180 days.

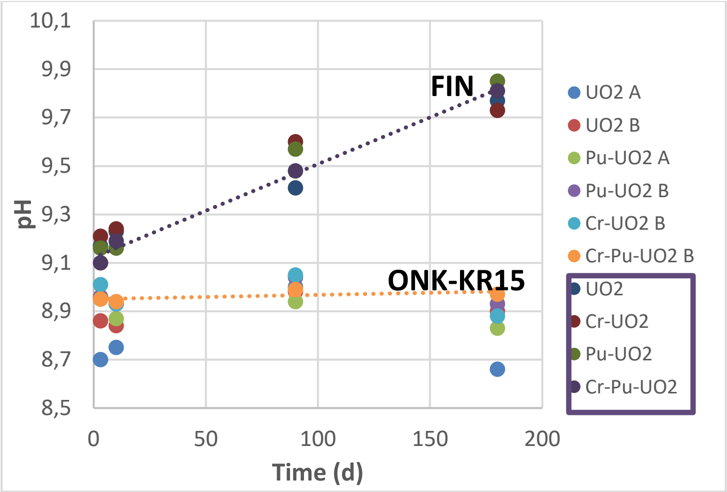

Figure 3.1.3.3: Evolution of pH in experimental series with Cr and Pu doped UO$_2$ and similar reference materials (UO$_2$ and Pu-UO$_2$) in ONK-KR15 natural ground water and in FIN reference water.

The blank experiment with iron foil and spike for the experimental series with ^{233}U-doped UO$_2$ materials showed a decrease of isotopic ratio in a similar manner to the experiments themselves; see Figure 3.1.3.4 (left). This indicates that the iron foil or the vessel surfaces might play a role for precipitation or adsorption of uranium phases and that it would favour the lighter isotope ^{235}U in these reactions. Thus more blanks with and without iron foil with added ^{235}U spike were run in parallel with the Cr/Pu doped UO$_2$ series in FIN water. These results revealed that the iron foil played a bigger role in this isotope fractionation on the surfaces, but the isotope ratio changed a bit also in a blank having only PP walls as adsorption place, see Figure 3.1.3.4 (right). In literature, uranium fractionation is known to take place by abiotic reductive precipitation [29], this can be assumed to be the reason for the observed behaviour in the blank experiments.

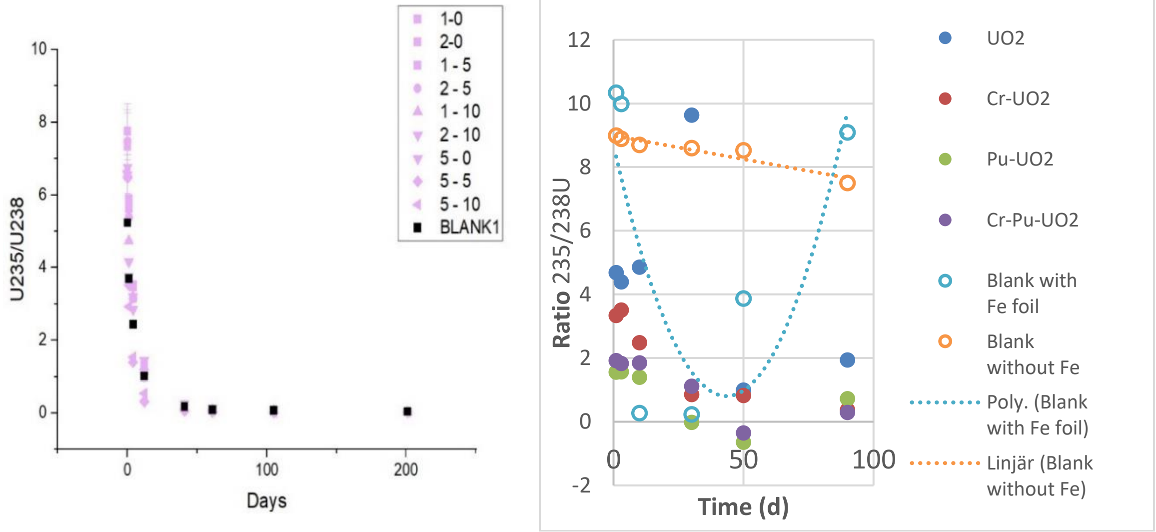

Figure 3.1.3.4: Evolution of ^{235}U/^{238}U isotopic ratio in experiments and blank experiments. The plot on the left shows the change in ^{233}U doped UO$_2$ series and corresponding blank with tracer and iron foil. The plot on the right represents the results from Cr-and Pu-doped pellets and blanks with spike with and without Fe foil.

3.1.4 Results from CIEMAT

The evolution of the elemental concentrations and normalised dissolution rates for each of the elements analysed in this work are presented and discussed in the following subsections.

Uranium

Figure 3.1.4.1a, Figure 3.1.4.2a and Figure 3.1.4.3a illustrates the solution analysis of dissolved U vs time for dissolution of UO_2-0.06 $^w/_o$ Cr_2O_3, UO_2-0.05 $^w/_o$ Cr_2O_3-0.02 $^w/_o$ Al_2O_3 and UO_2 -4.5 $^w/_o$ Gd_2O_3, respectively. Based on the first series of tests, H_2 atmosphere (pH_2 = 0.37±1bar) was not capable to maintain the system in reducing conditions, as it is suggested from concentration results. The U concentration in the solutions reach plateau levels in PC and YCW for both materials, whereas this effect is hardly observed in BC. In any case, no substantial differences were found between filtered/not-filtered and ultrafiltered samples.

Independent of the redox conditions, U concentrations at pH = 7.2 (PC) solution of $\sim 10^{-9}$ $mol \cdot l^{-1}$ in the time frame of investigation (136 days), were close to the quantification limit (10^{-10} $mol \cdot l^{-1}$) indicating an extremely low matrix dissolution rate. Moreover, those concentration values in PC are quite close to the solubility limit of 10^{-9} $mol \cdot l^{-1}$ [30] in absence of complexing agents.

At pH = 8.9 (BC), higher final U concentrations are quantified when compared to those at pH 7.2 ($\sim 10^{-6}$ $mol \cdot l^{-1}$ for Cr-doped UO_2 and $\sim 10^{-7}$ $mol \cdot l^{-1}$ for Cr/Al-doped UO_2). The trend of U concentration in solution shows that there is a slight increase in dissolution with time for the Cr-doped UO_2 in BC with seems to reach a plateau. The presence of H_2 was expected to provide reducing conditions and decreases the obtained uranium concentrations (at least two orders of magnitude lower than in oxidizing conditions). High concentration values are close to that found under oxidizing environment, so it could be caused by slight oxidation/dissolution of U(IV) to U(VI) on the pellet surface, promoted by the presence of a complexing agent (HCO_3^-). Under this assumption, the aqueous species of uranium in hexavalent state would occur as carbonate complexes more dominantly than hydroxy-complexes. Nevertheless, as it was suggested by Bosbach et al. in [10], more examinations for longer time periods are required.

At pH = 13.5 (YCW), U concentrations are similar to those in the tests in BC, despite the highest HCO_3^-/CO_3^{2-} concentration measured in YCW (0.45 M). Ollila [31] pointed out the redox sensitivity of the U solubility at strongly alkaline pH like cement pore water conditions and with medium/low carbonate content; in these conditions the solubility remains lower than in groundwater with a high carbonate content. Results suggest that the measured Eh (YCW) in these experiments (Table 3.1.4.1), in the range of -9 to -40 mV, could be enough to increase the U concentrations over the expected values ($\sim 10^{-9}$M) [32] while in BC the Eh has been found to be higher (70 – 138 mV).

It is expected that dissolution rates obtained with a matrix doped with Gd_2O_3 will be more resistant to oxidation; however, similar trends were observed in the samples tested being the U concentration values in BC somewhat lower than in YCW. No distinctive trends were observed for the dissolution rates in the aqueous media, concluding that there is unremarkably contribution of Gd-doped UO_2 to U concentration as a function of chemical environment (pH).

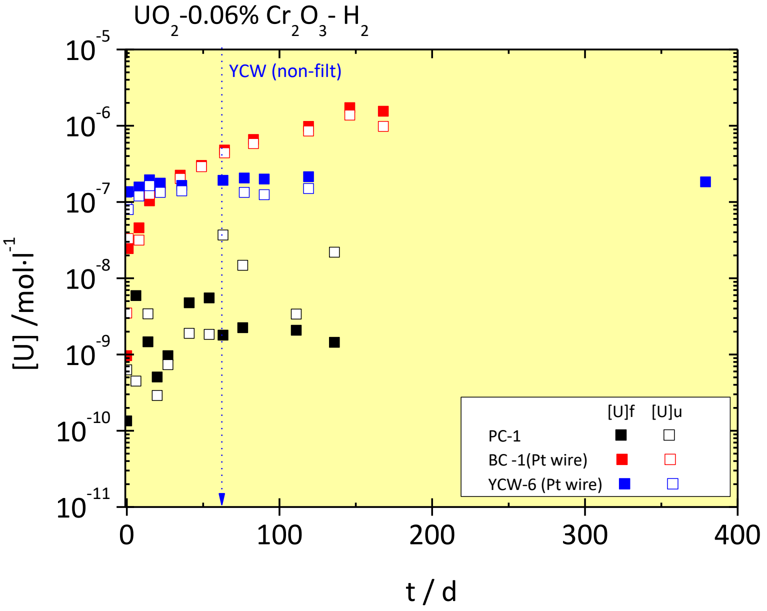

a)

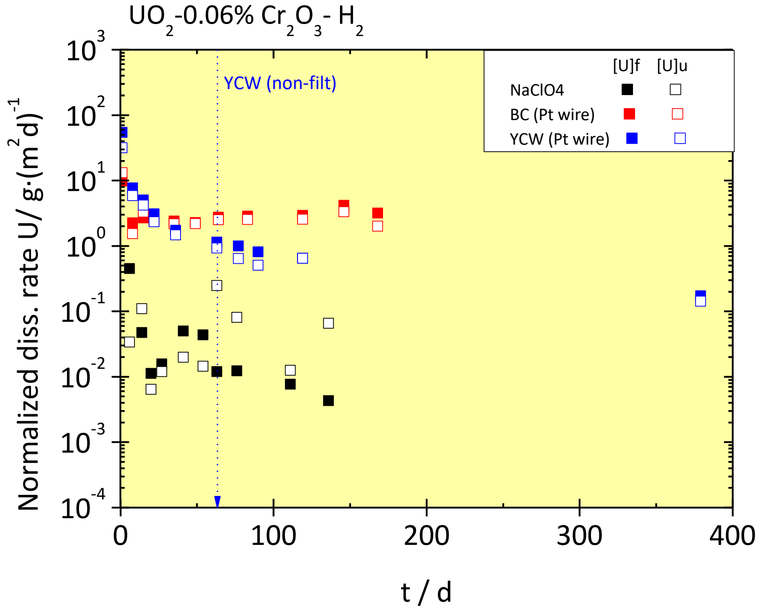

b)

Fel! Hittar inte referenskälla.Fel! Hittar inte referenskälla.: ***U concentration measured (a) and Normalized dissolution rate (b) in the aqueous phase vs time. Experiments carried out with UO_2-0.06 $^w/_o$ Cr_2O_3 in 0.02M $NaClO_4$ (pH =7.2), 0.019 M $NaHCO_3$ (pH = 8.9) and YCW-6 (pH = 13.5) in autoclave experiments (pH_2 = 0.37 ± 1 bar) at 22 ± 3 °C.***

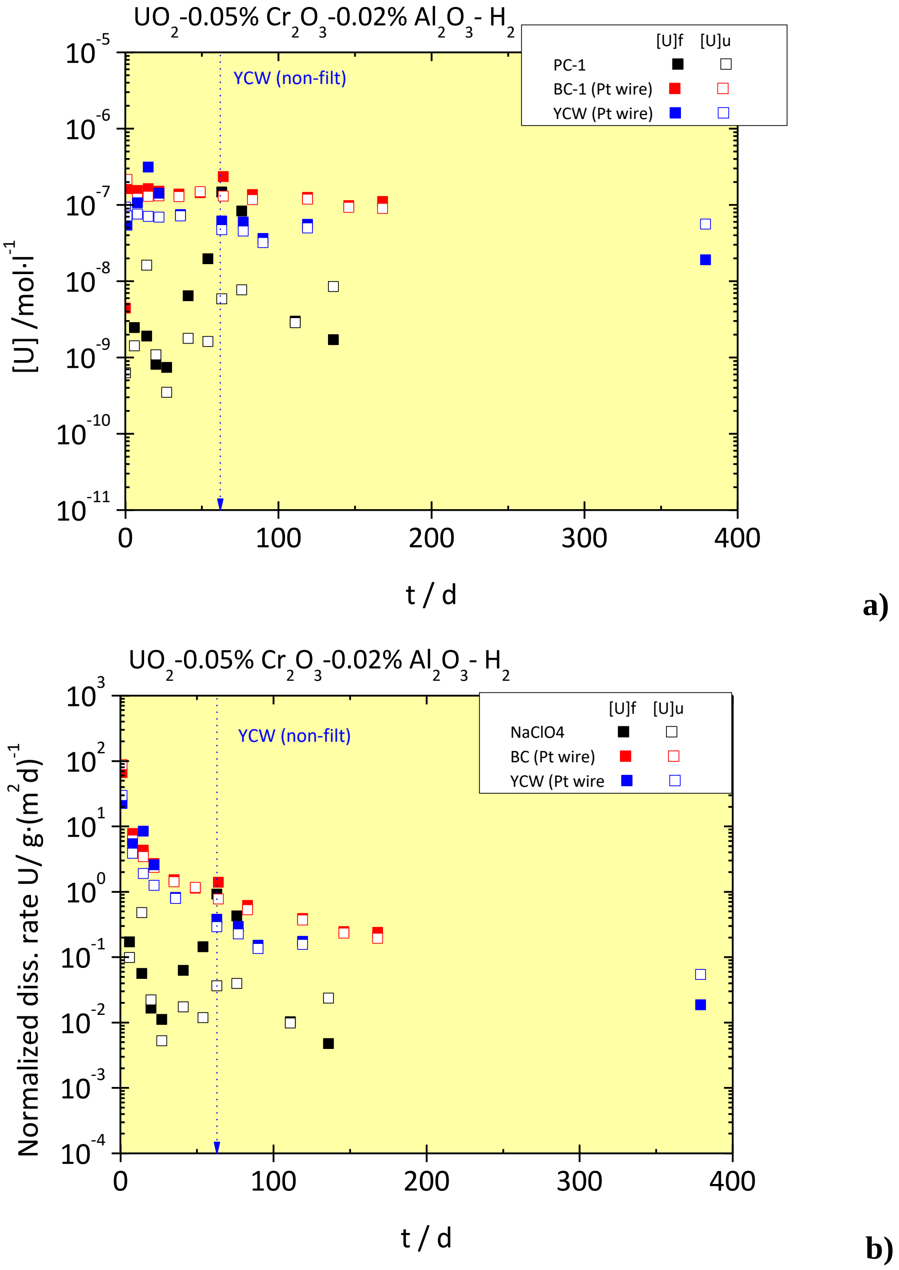

Figure 3.1.4.2: U concentration measured (a) and Normalized dissolution rate (b) in the aqueous phase vs time. Experiments carried out with UO_2-0.05 $^w/_o$ Cr_2O_3-0.02 $^w/_o$ Al_2O_3 in 0.02M $NaClO_4$ (pH =7.2), 0.019 M $NaHCO_3$ (pH = 8.9) and YCW-6 (pH = 13.5) in autoclave experiments (pH_2 = 0.37 ± 1 bar) at 22 ± 3 °C.

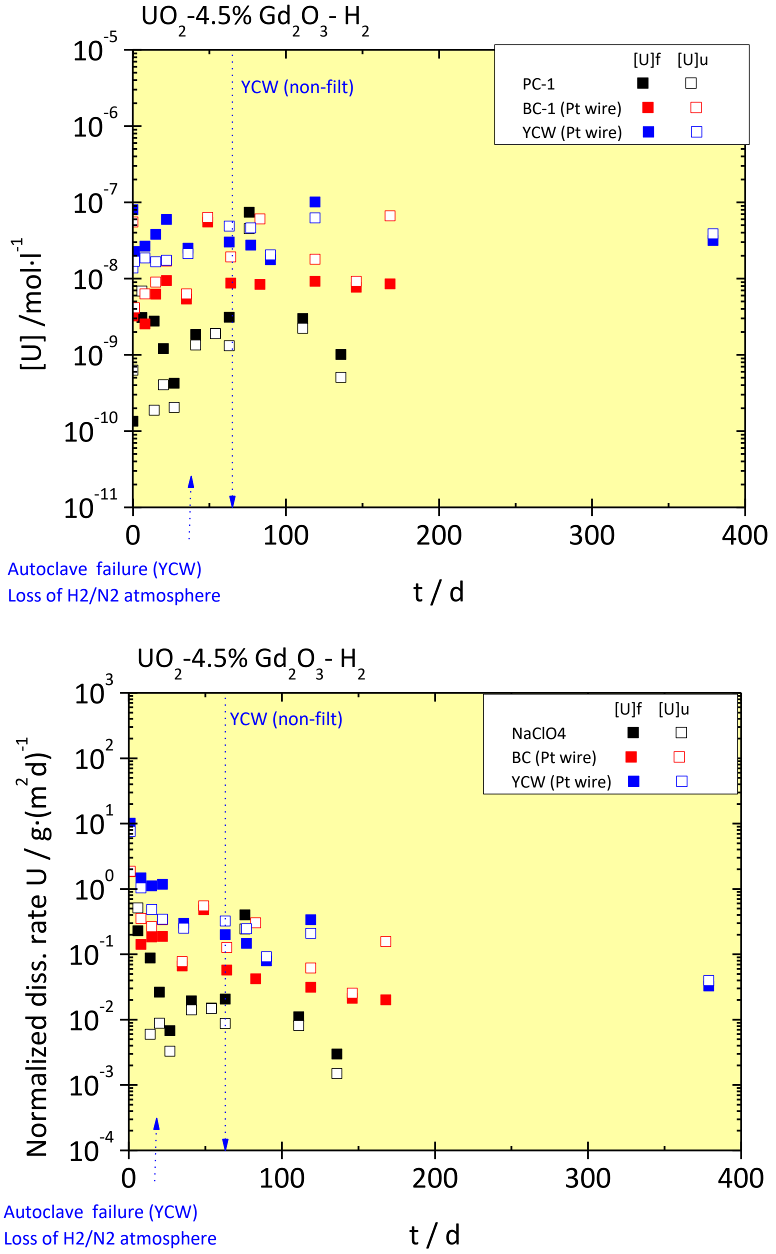

a)

b)

Figure 3.1.4.3: U concentration measured (a) and Normalized dissolution rate (b) in the aqueous phase vs time. Experiments carried out with UO_2-4.5 w/o Gd_2O_3 in 0.02M $NaClO_4$ (pH =7.2), 0.019 M $NaHCO_3$ (pH = 8.9) and YCW-6 (pH = 13.5) in autoclave experiments (pH2 = 0.37 ± 1 bar) at 22 ± 3 °C.

In general, the normalized dissolution rate profile decreased vs time, as shown in Figure 3.1.4.1b, Figure 3.1.4.2b and Figure 3.1.4.3b. The dissolution release of U is faster at the beginning of the experiment in YCW and in BC. The presence of H_2 was expected to provide reducing conditions and decreases the obtained U dissolution rates (at least two orders of magnitude lower than in oxidizing conditions). The initial higher release of uranium quantified, close to that found under oxidizing environment, suggests a potential remaining dissolved oxygen in the water or even a slight pre-oxidation/dissolution of U(IV) to U(VI) on the pellet surface, promoted by the presence of complexing agent (HCO_3^-). The second dissolution stage, slower and long-term, is attributed to matrix dissolution in the case of U.

In PC solution (pH=7.2), the initial/final dissolution rates were found to be 0.4 to $4\cdot10^{-3}$ $g\cdot(m^2d)^{-1}$ for Cr-doped UO_2 pellet, 0.2 to $5\cdot10^{-3}$ $g\cdot(m^2d)^{-1}$ for the Cr/Al-doped UO_2 and 0.2 to $7\cdot10^{-3}$ $g\cdot(m^2d)^{-1}$ for Gd-doped UO_2. Taking into account the low geometric surface area, the final U dissolution rates for the shown pellets are quite similar; showing that dopants (Cr, Cr/Al and Gd) have no significant effect on the dissolution rates of these UO_2-based materials in a neutral pH medium.

In BC solution (pH=8.9), normalised dissolution rates were noticeably higher, as a consequence of the bicarbonate. In this media the dissolution rates were found to be 9.7 to 3.2 $g\cdot(m^2d)^{-1}$ for Cr-doped UO_2 pellet, 66.2 to 0.2 $g\cdot(m^2d)^{-1}$ for the Cr/Al-doped UO_2 and 1.8 to $2\cdot10^{-2}$ $g\cdot(m^2d)^{-1}$ for Gd-doped UO_2. The obtained data are far from those obtained in [33] for unirradiated UO_2 in flow through reactors using $[HCO_3^-]$ 10^{-3}M. The mentioned authors reported a dissolution rate of U of $2\cdot10^{-3}$ $g\cdot(m^2d)^{-1}$. According to Ollila, at 10^{-3} M of free HCO_3^-, the major complex formation with carbonate would be the $UO_2(CO_3)_3^{4-}$ [32]. Nguyen et al. [34] report rates results from flow-through dissolution tests of UO_2 pellets (calculated using geometric surface area and roughness factor of 3) in solutions of 20 mM HCO_3^- (pH=11) with fixed partial pressure of oxygen (0.02 atm) of around $4\cdot10^{-3}$ $g\cdot(m^2d)^{-1}$. Other researchers have found the same results, a significant decrease in the dissolution rate using different Gd doping UO_2 under aqueous carbonate/bicarbonate solutions.

In YCW solution (pH=13.5), normalised dissolution rates were close to those calculated in BC, even though the bicarbonate concentration was higher than other values used in literature. In this media the initial/final dissolution rates were found to be $5\cdot10^{1}$ to $2\cdot10^{-1}$ $g\cdot(m^2d)^{-1}$ for the Cr-doped UO_2 pellet, $2\cdot10^{1}$ to $2\cdot10^{-2}$ $g\cdot(m^2d)^{-1}$ for the Cr/Al-doped UO_2, and $1\cdot10^{1}$ to $1.8\cdot10^{-1}$ $g\cdot(m^2d)^{-1}$ for Gd-doped UO_2.

Overall, the results obtained from these static dissolution tests for the three media considered are far from those expected in reducing systems. Actually, they are not in consonance with literature data, when dissolution rates were calculated using geometric SSA with no roughness factor, which consider grain boundary accessibility, thus the geometric choice underestimates real surface area. Taking into account the aforementioned discussion, dissolution rates are overestimated by 3 orders of magnitude. It is well known that that the SSA of the matrix will play a critical role on the final reaction rates [35].

The main outcomes of the U concentration and $R_L(U)$ at the end of each experiment are summarized in Figure 3.1.4.4a and Figure 3.1.4.4b respectively, as a function of pH. The highest values were observed in presence of BC medium and high pH/carbonates concentration, which confirms the tendency of bicarbonate complexing agents to solubilise U.

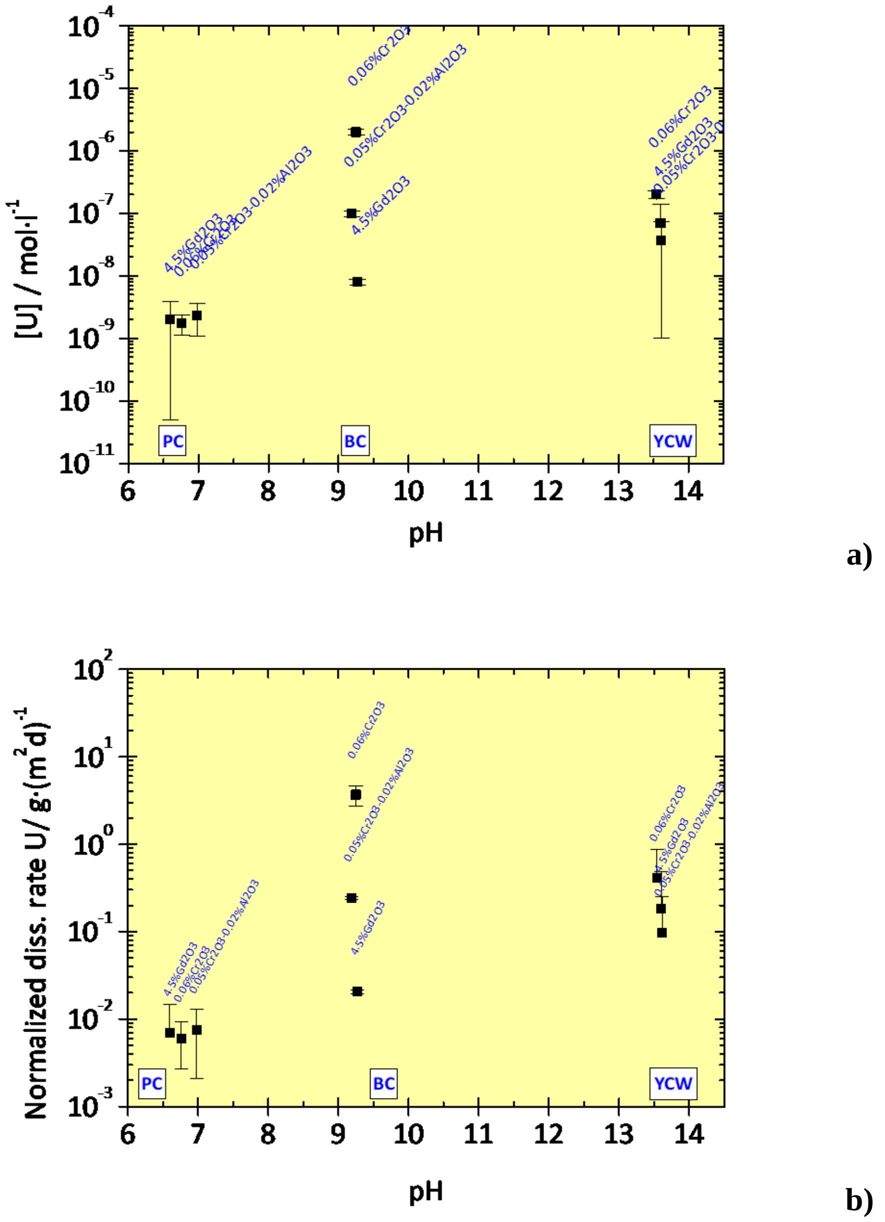

Figure 3.1.4.4: Summary of final U data observed for concentration measured (a) and Normalized dissolution rate (b) in the aqueous phase vs time in PC, BC and YCW as a function of pH.

Chromium

Chromium is a redox-sensitive element, which means that its solubility behaviour in aqueous media is mainly affected by redox potential and pH. Thermodynamically, Cr(VI) could only be present at relatively high pH. At low pH, the high redox potential of the Cr(VI)/Cr(III) couple promotes Cr(III) stabilization. In contrast, under alkaline conditions the redox potential is reduced, which point out a stabilization of Cr(VI). Consequently, thermodynamically, Cr(VI) could only exist at relatively high pH (>9) [36]. Cr released (see Figure 3.1.4.5a and Figure 3.1.4.6a of UO_2-0.06 $^w/_o$ Cr_2O_3 and UO_2-0.05 $^w/_o$ Cr_2O_3-0.02 $^w/_o$

Al_2O_3, correspondingly) is in the solubility range (~$2\cdot10^{-8}$M) and below the LOQ in the three leachants considered (Table 2.4.1.5) of $8\cdot10^{-9}$ mol·l^{-1} in PC, $3\cdot10^{-8}$ mol·l^{-1} in BC and $5\cdot10^{-7}$ mol·l^{-1} in YCW. At high pH, where the concentrations were found in the range 10^{-7} - 10^{-6} mol·l^{-1} and knowing that the measured Eh was near zero, one may think about potential oxidation of Cr(III) to Cr(VI) in order to be solubilised as chromate, feasible in both aerobic and middle anoxic environments [37].

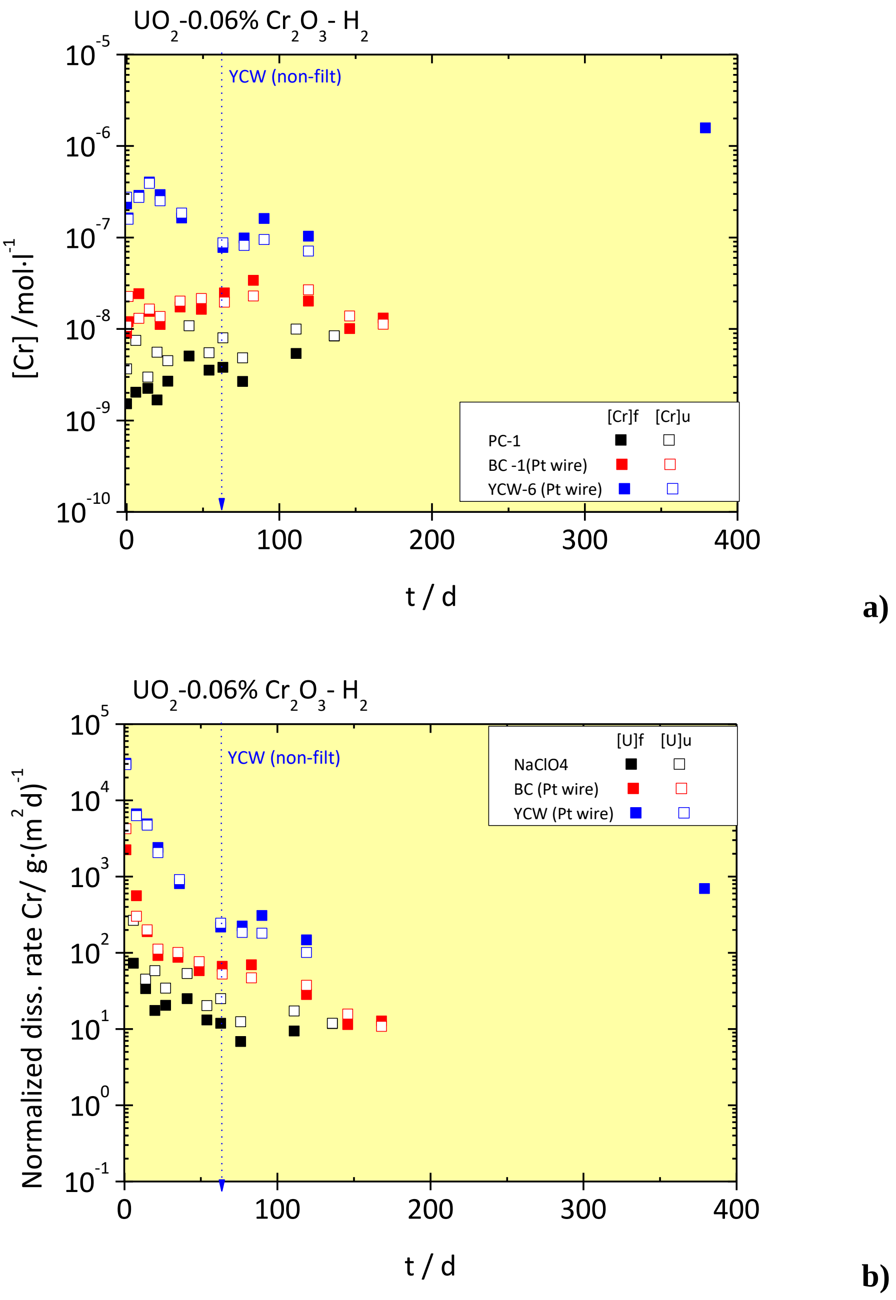

Figure 3.1.4.5: Cr concentration measured (a) and Normalized dissolution rate (b) in the aqueous phase vs time. Experiments carried out with UO_2-0.06 w/o Cr_2O_3 in 0.02M $NaClO_4$ (pH =7.2), 0.019 M $NaHCO_3$ (pH = 8.9) and YCW-6 (pH = 13.5) in autoclave experiments (pH2 = 0.37 ± 1 bar) at 22 ± 3 °C.

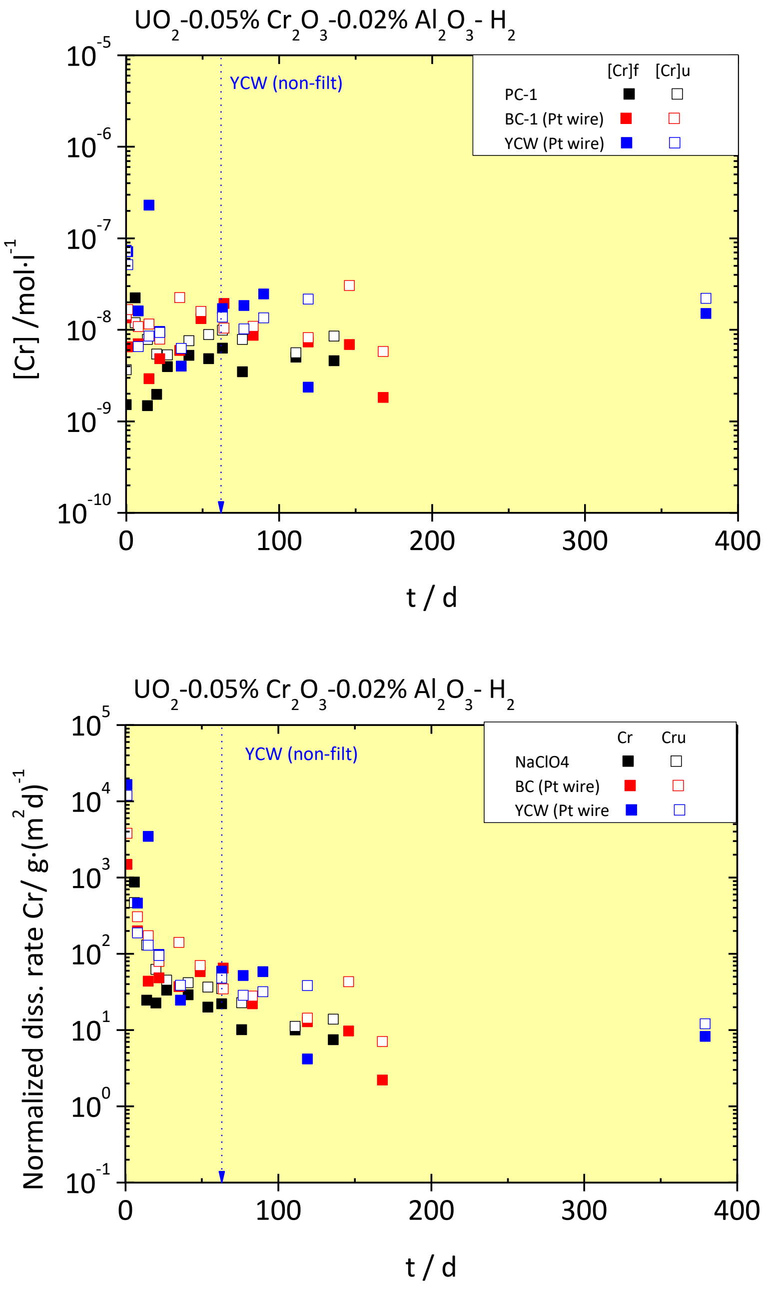

a)

b)

Figure 3.1.4.6: Cr concentration measured (a) and Normalized dissolution rate (b) in the aqueous phase vs time. Experiments carried out with UO$_2$-0.05 w/o Cr$_2$O$_3$-0.02 w/o Al$_2$O$_3$ in 0.02M NaClO$_4$ (pH = 7.2), 0.019 M NaHCO$_3$ (pH = 8.9) and YCW-6 (pH = 13.5) in autoclave experiments (pH2 = 0.37 ± 1 bar) at 22 ± 3 °C.

Figure 3.1.4.7 shows the Cr/U ratio in solution for the two pellets containing Cr and in the three leachants. These values were several orders of magnitude far than that in the solid pellets. In the timeframe of leaching, the Cr/U congruence ratios for all the doped UO$_2$ fuel samples ranged from $6 \cdot 10^{-3}$ to 9. Taking into account the experimental uncertainty and the LOQ (Cr), it can be concluded that the concentration of Cr is higher than expected from a congruent corrosion of the doped UO$_2$ pellets, especially in the PC system. The preferential leaching is probably due to the fact that Cr is released as a function of pH, being the low solubility in the range of 8 to 10. This means that non congruent dissolution of the material occurred. The results of the analysis of the rinse solutions of the leaching vessels were also included, and relatively high Cr concentrations were found also in the rinse. These values could be attributed to some Cr sorption on the vessel walls and could indicate the occurrence of a higher degree of Cr mobilization from the samples. It must be indicated that the values plotted in Figure for the rinse ratio (Cr/U) are concentrations in 300 ml of 2M nitric acid, which is in the same volume than the nominal amount of leachant.

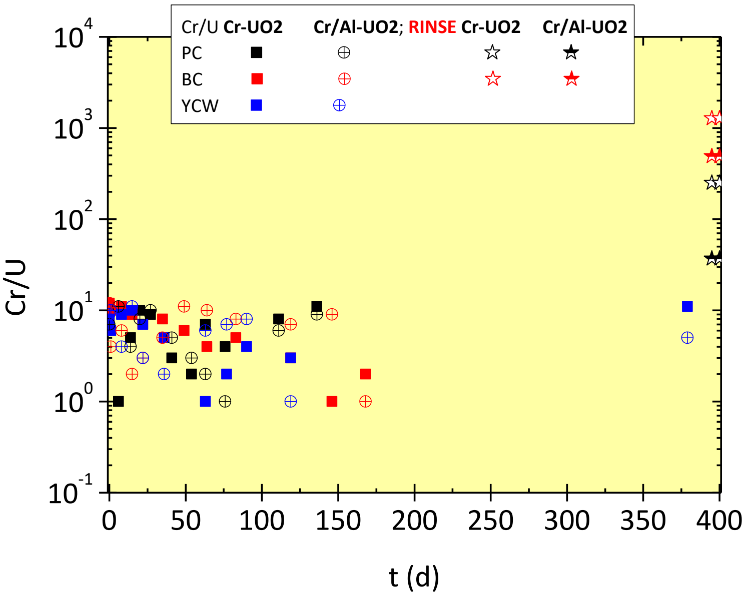

Figure 3.1.4.7: Cr/U concentration ratio in the aqueous phase vs time. Experiments carried out with UO_2-0.06wt% Cr_2O_3 and UO_2-0.05 w/o Cr_2O_3-0.02 w/o Al_2O_3 in 0.02M $NaClO_4$ (pH =7.2), 0.019 M $NaHCO_3$ (pH = 8.9) and YCW-6 (pH = 13.5) in autoclave experiments (pH2 = 0.37 ± 1 bar) at 22 ± 3 °C. Rinse ratio is represented as stars for PC and BC.

Aluminium

Data of Al quantified in solution are in accordance with expected values owing to the fact that Al concentrations in the solid samples UO_2-0.05 $^{w}/_{o}$ Cr_2O_3-0.02 $^{w}/_{o}$ Al_2O_3 are quite low, summed up that it is almost insoluble in water (at pH between 6 and 8, the Al solubility is 10^{-8}-10^{-7}M). However, the data are consistent with the hypothesis proposed in the literature in alkaline solutions, i.e. Al is slightly soluble in alkaline solution (higher than 11). In YCW conditions, Al would be solubilized, probably in the form of $Al(OH)_3$ (am) or negatively charged $Al(OH)_4^-$ [38], which in turn can interact with anionic species in the system (hydroxyl, sulphates, carbonates or even silicates as impurities coming from glass containers during leachant preparation) [39].

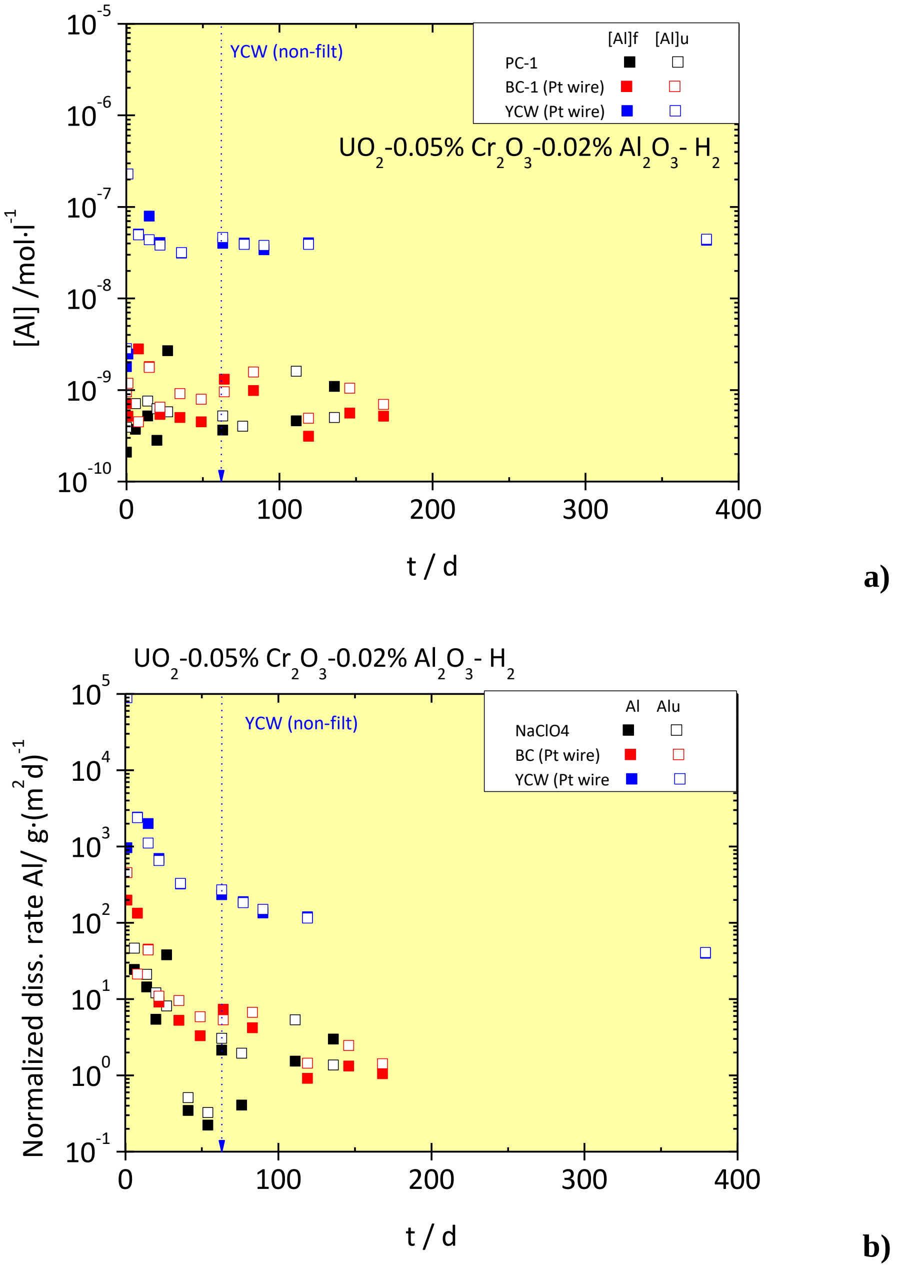

Figure 3.1.4.8: Al concentration measured (a) and Normalized dissolution rate (b) in the aqueous phase vs time. Experiments carried out with UO2-0.05 w/o Cr2O3-0.02 w/o Al2O3 in 0.02M NaClO4 (pH = 7.2), 0.019 M NaHCO3 (pH = 8.9) and YCW-6 (pH = 13.5) in autoclave experiments (pH2 = 0.37 ± 1 bar) at 22 ± 3 °C.

The Al/U ratios in solution indicate a congruent dissolution in YCW near to 1, and below this value in PC and BC probably due to the concentration values close to the LOQ. However, considering the higher Al/U values calculated from the rinse in BC, it can be assumed that all the Al dissolved in this aqueous phase is sorbed on the PEEK vessel walls.

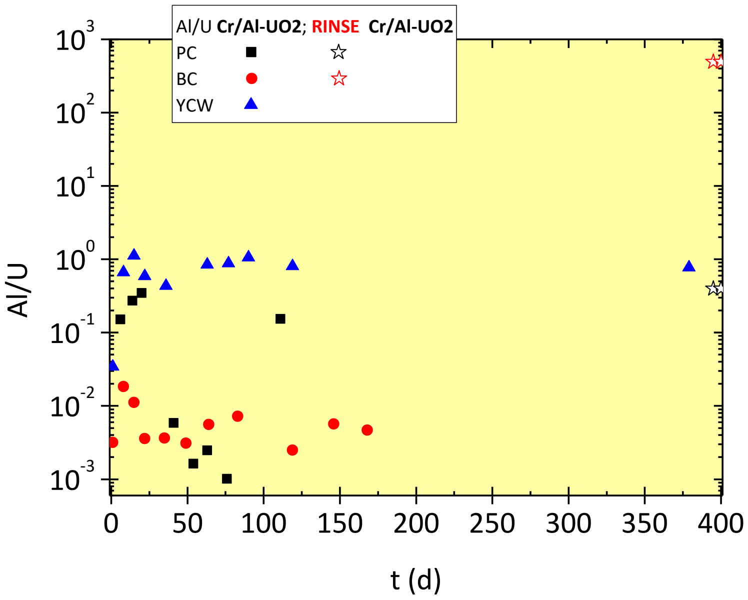

Figure 3.1.4.9: Al/U concentration ratio in the aqueous phase vs time. Experiments carried out with UO_2-0.06 w/o Cr_2O_3 and UO2-0.05 w/o Cr_2O_3-0.02 w/o Al_2O_3 in 0.02M $NaClO_4$ (pH = 7.2), 0.019 M $NaHCO_3$ (pH = 8.9) and YCW-6 (pH = 13.5) in autoclave experiments (pH2 = 0.37 ± 1 bar) at 22 ± 3 °C. Rinse ratio is represented as stars for PC and BC.

Gadolinium

Gadolinium is moderately soluble in strong mineral acids but it has very low solubility in water and alkaline pH. In Figure 3.1.4.10a and Figure 3.1.4.10b, the measured concentration evolution and normalized dissolution rates with UO_2-4.5 $^{w}/_{o}$ Gd_2O_3 in 0.02M $NaClO_4$ (pH = 7.2), 0.019 M $NaHCO_3$ (pH = 8.9) and YCW-6 (pH = 13.5) are shown. Due to the presence of Gd(III), it is suggested that trivalent rare-earth dopants (RE(III)), may prevent the UO_2 oxidation[40, 41], and then, affecting the UO_2 oxidation resistance.

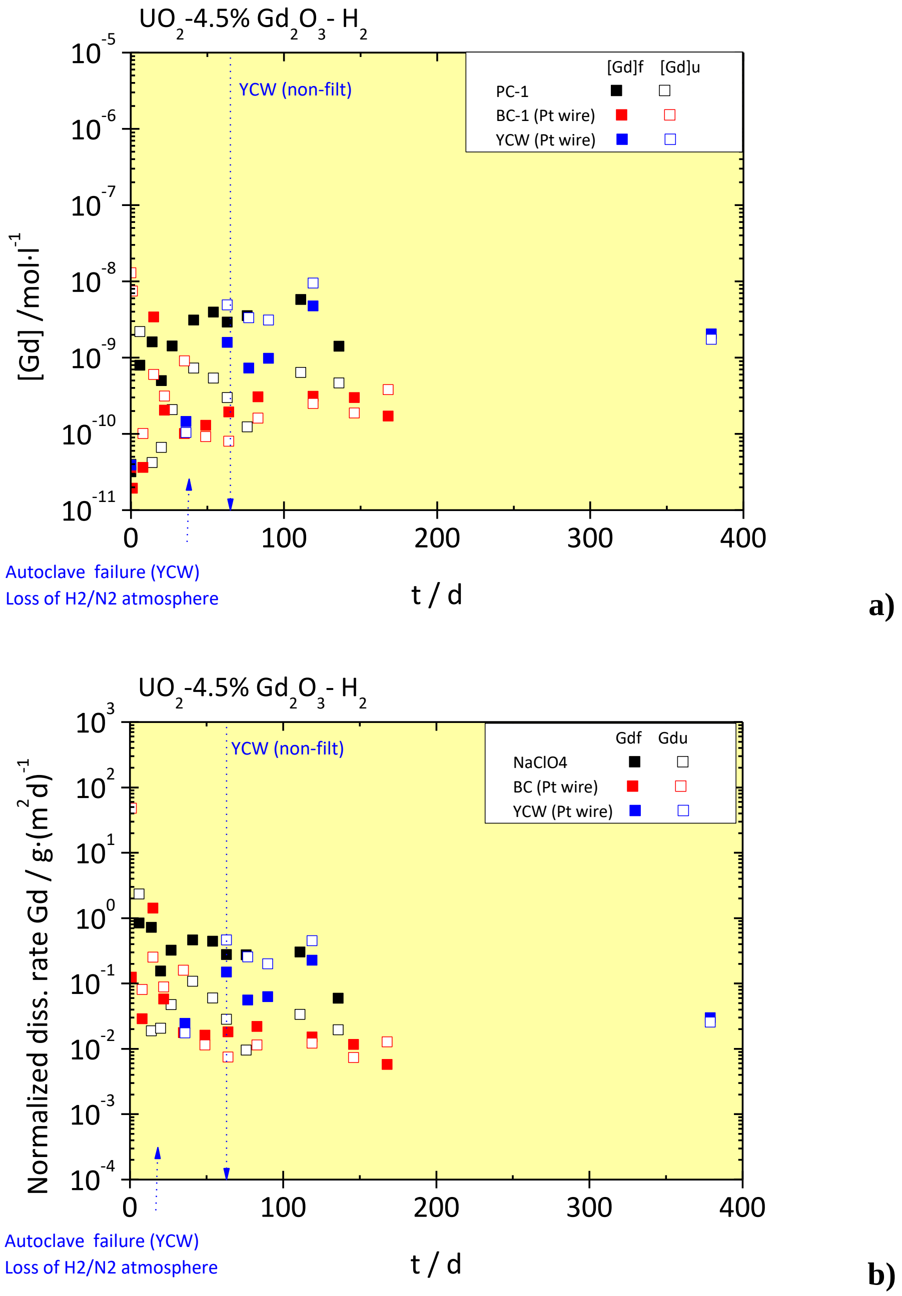

Figure 3.1.4.10: Gd concentration measured (a) and Normalized dissolution rate (b) in the aqueous phase vs time. Experiments carried out with UO_2-4.5 w/o Gd_2O_3 in 0.02M $NaClO_4$ (pH =7.2), 0.019 M $NaHCO_3$ (pH = 8.9) and YCW-6 (pH = 13.5) in autoclave experiments (pH2 = 0.37 ± 1 bar) at 22 ± 3 °C.

The Gd/U ratios in solution indicate a congruent dissolution in PC near to 1 (Figure 3.1.4.11), and below this value in BC and YCW probably due to the concentration values close to the LOQ. Moreover, unlike U, Gd is a non-redox sensitive element and so, its solubility is not controlled by local redox conditions but by chemical reactions involving the chemical nature of solution.

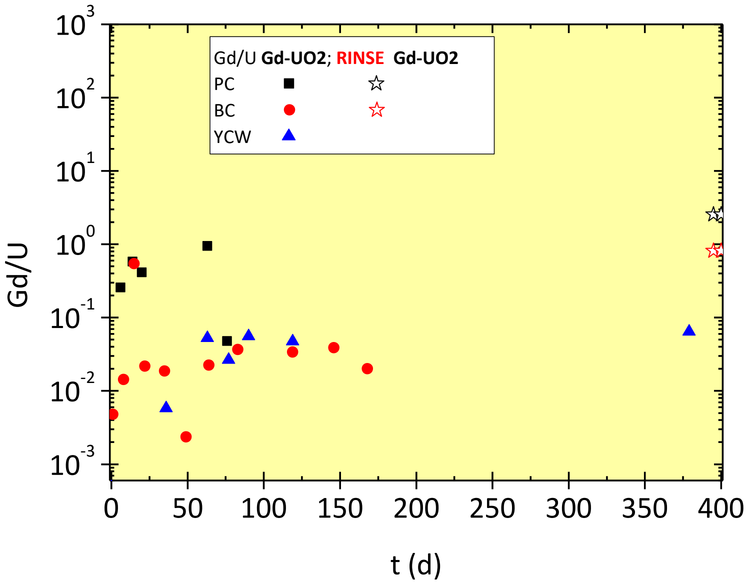

Figure 3.1.4.11: Gd/U concentration ratio in the aqueous phase vs time. Experiments carried out with UO_2-4.5 w/o Gd_2O_3 in 0.02M $NaClO_4$ (pH =7.2), 0.019 M $NaHCO_3$ (pH = 8.9) and YCW-6 (pH = 13.5) in autoclave experiments (pH2 = 0.37 ± 1 bar) at 22 ± 3 °C. Rinse ratio is represented as stars for PC and BC.

Table 3.1.4.1:*Fel! Hittar inte referenskälla.* ***Summary of the initial and final data for pH and redox potential measured in each dissolution experiments.***

	PC (I=0.02M; 22±2°C; pH = 7.2 ± 0.1; Eh = 0.25 ± 0.02 V)			BC (I=0.02M; 23.4±0.5°C; pH = 8.9 ± 0.1; Eh = 0.06 ± 0.03 V)			YCW (I >0.4M; 23.3±0.4°C; pH=13.5±0.1; Eh=-0.09±0.04 V)		
Final values	**pH**	**Eh**	**pe**	**pH**	**Eh**	**pe**	**pH**	**Eh**	**pe**
Blank test	7.02	-0.01	-0.19	9.22	0.11	1.96	13.61	-0.01	-0.10
UO_2-0.06%Cr_2O_3	6.76	-0.02	-0.31	9.25	0.14	2.32	13.54	0.004	0.075
UO_2-0.05%Cr_2O_3-0.02%Al_2O_3	6.98	-0.05	-0.79	9.19	0.10	1.66	13.61	-0.02	-0.39
UO_2-4.5%Gd_2O_3	6.59	-0.02	-0.41	9.27	0.07	1.18	13.60	0.004	0.06

pH and redox evolution

During the experiments, pH measurements were carried out at each sampling time (Table 3.1.4.1). The pH decreases from initially 7.9 down to 6.5 - 7 at the end of experiments in PC. This fact has been previously attributed as a result of the uranium oxide surface buffer capacity by other authors [42]. However, pH increases in BC and remains almost constant in

YCW. The stability of pH values in YCW indicate an unchanging and values are so high that even if slight variations occur this should be difficult to measure.

3.1.4.1 Post-leaching solid characterization

SEM, XRD and Raman measurements on pellets after the dissolution experiments complement the picture of data obtained (Figure 3.1.4.1.1, Figure 3.1.4.1.2, Figure 3.1.4.1.3 for XRD; Table 3.1.4.1.1 and Table 3.1.4.1.4 for SEM and Raman).

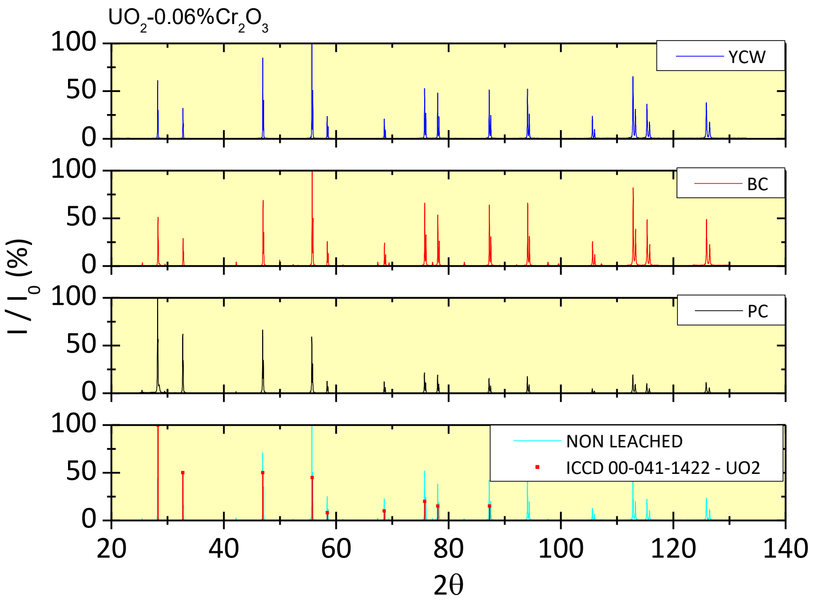

Figure 3.1.4.1.1: Diffraction patterns of post-leached UO2-0.06 w/o Cr2O3 in PC, BC and YCW-6 in autoclave experiments (pH2 = 0.37 ± 1 bar) at 22 ± 3 °C. Rinse ratio is represented as stars for PC and BC.

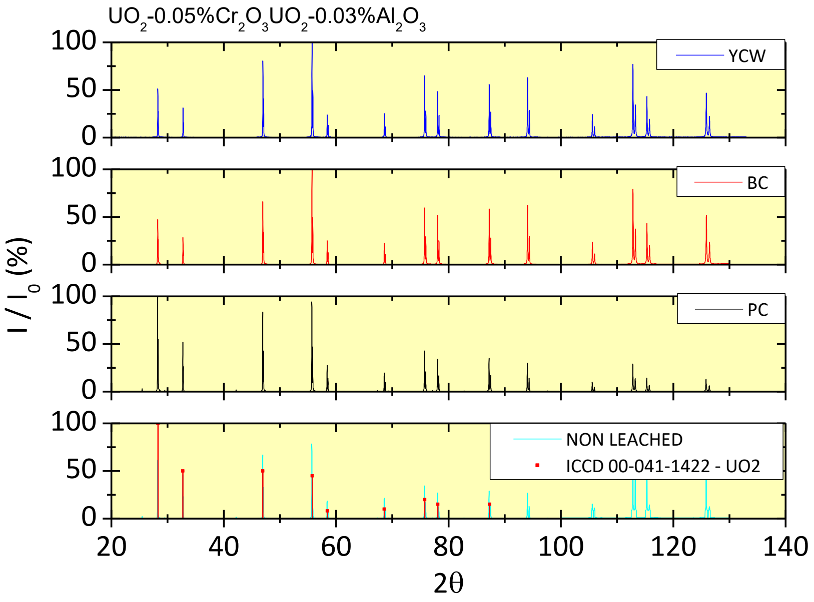

Figure 3.1.4.1.2: Diffraction patterns of post-leached UO_2-0.05 w/o Cr_2O_3-0.02 w/o Al2O3 in PC, BC and YCW-6 in autoclave experiments (pH2 = 0.37 ± 1 bar) at 22 ± 3 °C. Rinse ratio is represented as stars for PC and BC.

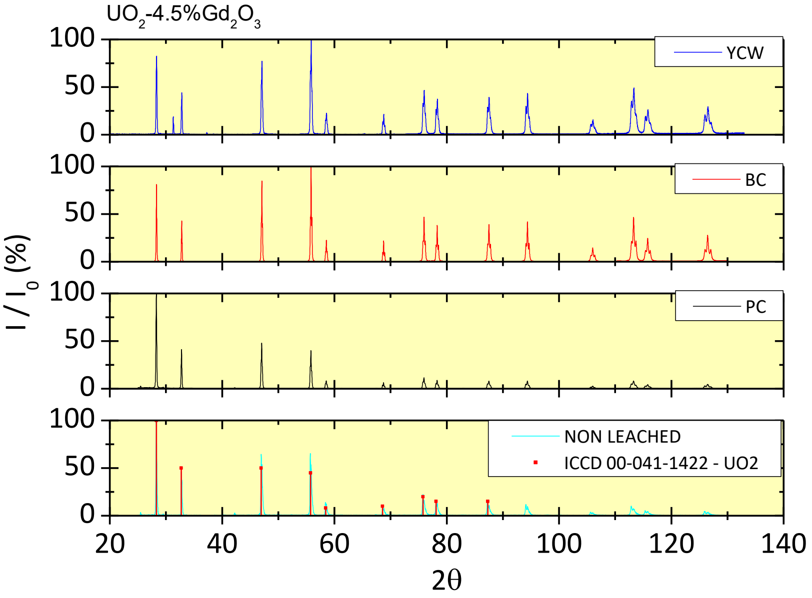

Figure 3.1.4.1.3: Diffraction patterns of post-leached UO2-4.5 w/o Gd_2O_3 in PC, BC and YCW-6 in autoclave experiments (pH2 = 0.37 ± 1 bar) at 22 ± 3 °C. Rinse ratio is represented as stars for PC and BC.

Table 3.1.4.1.1: XRD and SEM micrographs of the leached samples in PC.

PC		
UO_2 -0.06 $^{w}/_{o}$ Cr_2O_3	**UO_2 -0.05 $^{w}/_{o}$ Cr_2O_3 -0.02 $^{w}/_{o}$ Al_2O_3**	**UO_2 -4.5 $^{w}/_{o}$ Gd_2O_3**
Main phases identified/lattice parameter (nm): • ph#1 $(Cr_{0.00061}U_{0.9993})O_2$/ 0.547093(9) • ph#2 $Cr_{0.183}U_{0.817}O_2$/ 0.542284	Main phases identified/lattice parameter (nm): • ph#1 $(Cr_xAl_yU_{0.99x})O_2$/ 0.547126(7) • ph#2 $(Cr_pAl_qU_{0.9xx})O_2$/ 0.541110	Main phases identified/lattice parameter (nm): • ph#1 $(Gd_{0.083}U_{0.953})O_2$/ 0.54689(3) • ph#2 $(Gd_{0.013}U_{0.996})O_2$/ 0.54564(2)
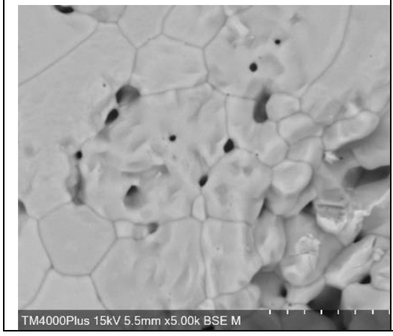	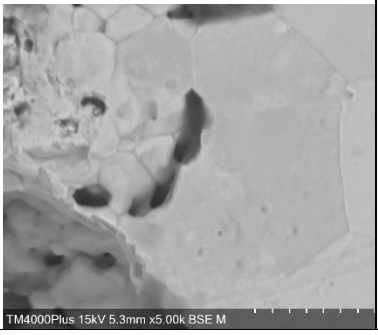	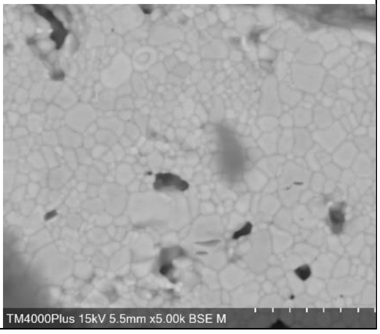

Table 3.1.4.1.2: XRD and SEM micrographs of the leached samples in BC.

BC		
UO_2 -0.06 $^{w}/_{o}$ Cr_2O_3	**UO_2 -0.05 $^{w}/_{o}$ Cr_2O_3 -0.02 $^{w}/_{o}$ Al_2O_3**	**UO_2 -4.5 $^{w}/_{o}$ Gd_2O_3**
Main phases identified/lattice parameter (nm): • 0.5470419(8) Non precipitated phases.	Main phases identified/lattice parameter (nm): • 0.5470803(8) Presence of an amorphous phase around 18.8 (º2θ) well-matched with $Al(OH)_3$ in a proportion bellow 5%.	Main phases identified/lattice parameter (nm): • ph#1 0.546776(3) $U_{1-y}Gd_{0.01875}O_{2-x}$ • ph#2 0.545663(2) $U_{1-z}Gd_{0.083}O_{2-x}$ Slight contribution of precipitated phases compatible with the NaCl.
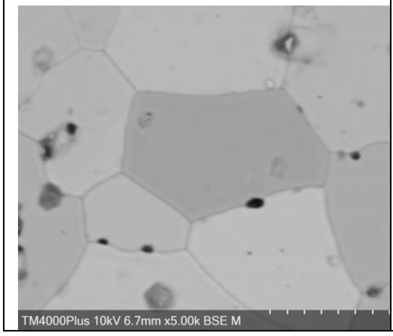	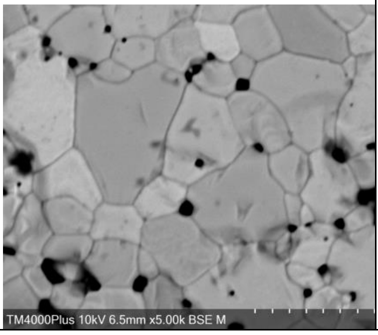	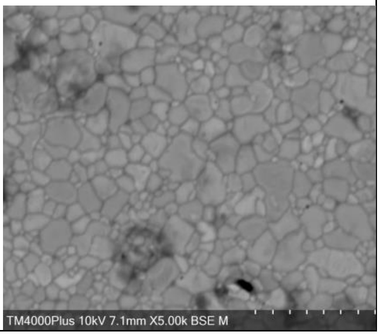

Table 3.1.4.1.3: XRD and SEM micrographs of the leached samples in YCW.

YCW		
UO_2 -0.06 $^{w}/_{o}$ Cr_2O_3	**UO_2 -0.05 $^{w}/_{o}$ Cr_2O_3 -0.02 $^{w}/_{o}$ Al_2O_3**	**UO_2 -4.5 $^{w}/_{o}$ Gd_2O_3**
Main phases identified/lattice parameter (nm): • $(U_{0.998}Cr_{0.002})O_2$ 0.5470608(10) Non precipitated phases.	Main phases identified/lattice parameter (nm): • ph#1 $(Al_xCr_yU_z)O_2$/ 0.5471095(13) Non precipitated phases.	Main phases identified/lattice parameter (nm): • ph#1 $U_{1-y}Gd_{0.016}O_{2-x}$/ 0.54685(2). • ph#2 $U_{1-z}Gd_{0.089}O_{2-x}$/ 0.5459(2). Slight contribution of precipitated phases compatible with $CaCO_3$ and $Ca_2MgSi_2O_7$.
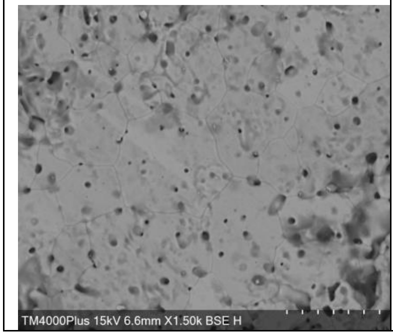	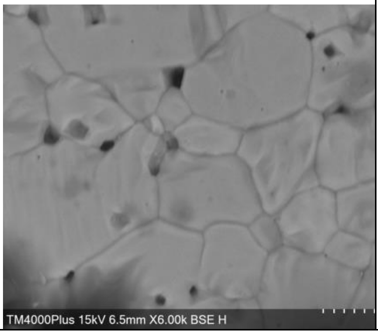	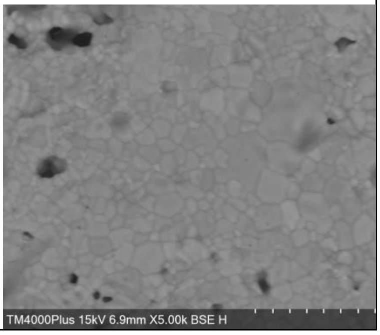

Table 3.1.4.1.4: Raman analysis of leached samples.

PC

Frequencies	**UO_2 -0.06 $^{w}/_{o}$ Cr_2O_3**	**UO_2 -0.05 $^{w}/_{o}$ Cr_2O_3 - 0.02 $^{w}/_{o}$ Al_2O_3**	**UO_2 -4.5 $^{w}/_{o}$ Gd_2O_3**
v T2g (cm^{-1})	445.805 ± 0.77656	445.02 ± 0.82805	447.829 ± 0.99885
v LO (cm^{-1})	571.11 ± 1.68794	569.20111 ± 0.87656	528.543 ± 1.98003
v 2LO (cm^{-1})	1145.11 ± 1.26543	1144.222 ± 0.62794	1146.065 ± 2.15515
Normalized areas	**UO_2 -0.06 $^{w}/_{o}$ Cr_2O_3**	**UO_2 -0.05 $^{w}/_{o}$ Cr_2O_3 - 0.02 $^{w}/_{o}$ Al_2O_3**	**UO_2 -4.5 $^{w}/_{o}$ Gd_2O_3**
Anorm LO	0.09823 ± 0.03372	0.04638 ± 0.03821	4.73507 ± 1.34376
Anorm 2LO	0.90255 ± 0.08895	0.98238 ± 0.16073	0.42133 ± 0.09613

BC

Frequencies	**UO_2 -0.06 $^{w}/_{o}$ Cr_2O_3**	**UO_2 -0.05 $^{w}/_{o}$ Cr_2O_3 - 0.02 $^{w}/_{o}$ Al_2O_3**	**UO_2 -4.5 $^{w}/_{o}$ Gd_2O_3**
v T2g (cm^{-1})	448.343 ± 0.67096	445.70875 ± 0.6132	449.416 ± 0.70668
v LO (cm^{-1})	571.42075 ± 1.15231	569.91525 ± 1.2045	531.3205 ± 0.605
v 2LO (cm^{-1})	1148.36575 ± 0.90427	1145.40567 ± 1.27883	1143.81425 ± 0.90835
Normalized areas	**UO_2 -0.06 $^{w}/_{o}$ Cr_2O_3**	**UO_2 -0.05 $^{w}/_{o}$ Cr_2O_3 - 0.02 $^{w}/_{o}$ Al_2O_3**	**UO_2 -4.5 $^{w}/_{o}$ Gd_2O_3**
Anorm LO	0.17525 ± 0.0551	0.07606 ± 0.01819	4.0707 ± 0.29648
Anorm 2LO	0.92042 ± 0.14947	0.68726 ± 0.04087	0.51742 ± 0.06972

YCW

Frequencies	**UO_2 -0.06 $^{w}/_{o}$ Cr_2O_3**	**UO_2 -0.05 $^{w}/_{o}$ Cr_2O_3 - 0.02 $^{w}/_{o}$ Al_2O_3**	**UO_2 -4.5 $^{w}/_{o}$ Gd_2O_3**
v T2g (cm^{-1})	447.994 ± 0.70668	444.9308 ± 1.50113	447.790 ± 0.70668
v LO (cm^{-1})	570.860 ± 2.78167	566.443 ± 2.82576	531.81867 ± 0.69917
v 2LO (cm^{-1})	1146.27825 ± 2.12505	1143.2265 ± 0.551	1144.98567 ± 0.64201
Normalized areas	**UO_2 -0.06 $^{w}/_{o}$ Cr_2O_3**	**UO_2 -0.05 $^{w}/_{o}$ Cr_2O_3 - 0.02 $^{w}/_{o}$ Al_2O_3**	**UO_2 -4.5 $^{w}/_{o}$ Gd_2O_3**
Anorm LO	0.1116 ± 0.00834	0.08179 ± 0.01391	2.60442 ± 0.26792
Anorm 2LO	0.89894 ± 0.07402	0.88859 ± 0.09731	0.58564 ± 0.11325

The comparison between SEM micrographs of the disc before (Figure 2.4.1.2) and after leaching (Table 3.1.4.1.1, Table 3.1.4.1.2 and Table 3.1.4.1.3) indicates that no precipitation of hydrated phases has occurred. Any trace of solubilized U may presumably remain in solution assisted by complexing anionic agents such us carbonates. This fact, together with the low U concentrations in dissolution measured by ICP-MS, confirms the stability of the UO_2 matrix under these specific conditions. The absence of precipitated, secondary phases containing uranium is also confirmed by XRD results shown in Table 3.1.4.1.1, Table 3.1.4.1.2 and Table 3.1.4.1.3.

In conclusion, leaching fresh doped-UO_2 solid samples in different geochemical environments did not apparently influence the evolution of the microstructure on the fuel surface and on the grain boundaries.

3.1.5 Results from USFD

The $N_L(U)$ at 25 °C decreased with increasing Cr content (Figure 1a). The $N_L(U)$ of undoped UO_2 was also higher than Cr-doped UO_2 at 40 °C (Figure 1b), however, the trend with increasing Cr content was not so clearly defined. This would tend to suggest that the presence of Cr improves the durability of UO_2, at these temperatures. At 60°C, however, the addition of Cr seemed to increase the $N_L(U)$ (Figure 1c) in comparison with the undoped UO_2.

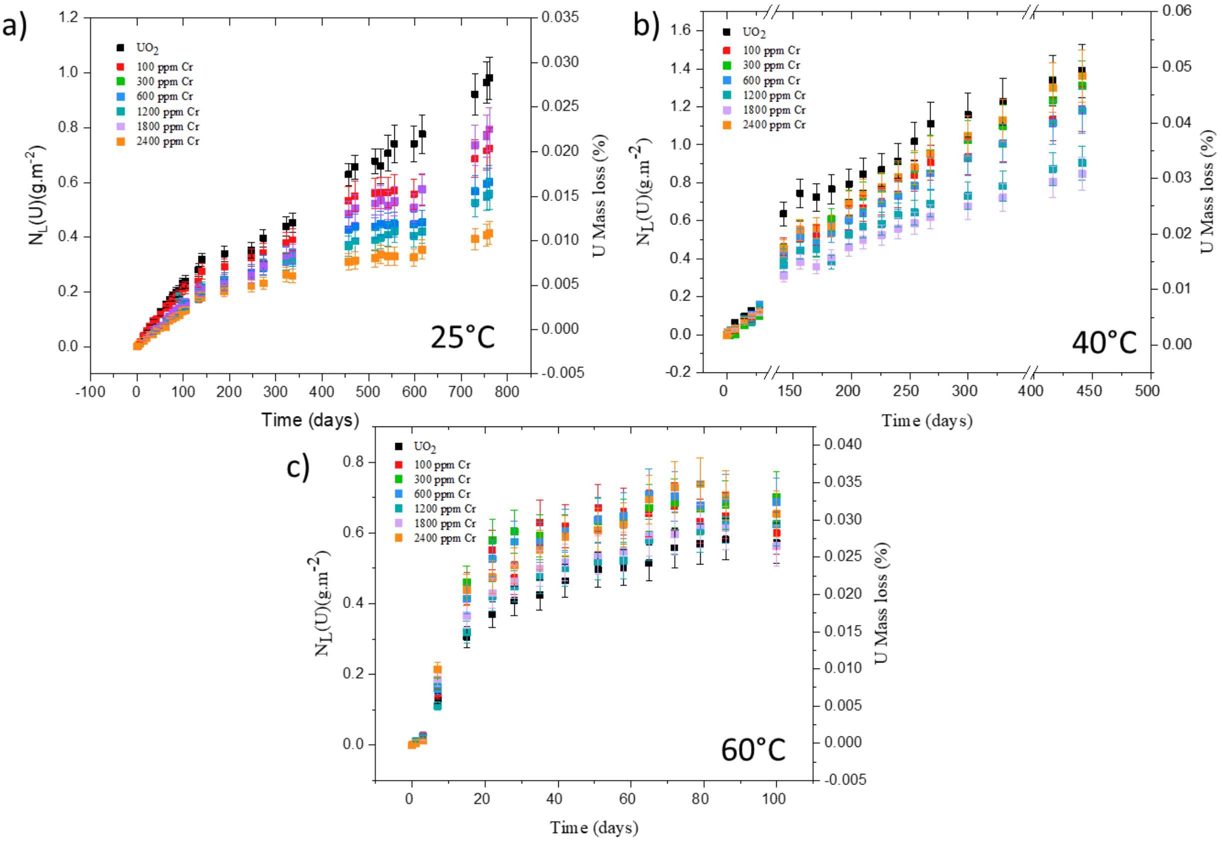

Figure 1. Normalised mass loss of U, $N_L(U)$ (g m^{-2}), of Cr-doped and undoped UO_2 dissolved in 1 mM $NaHCO_3$ + 19 mM NaCl at: (a) 25 °C; (b) 40 °C; and (c) 60 °C.

This behaviour can be further elucidated by comparing the U dissolution rate ($R_L(U)$) of the samples within the three distinct dissolution regimes. A clear reduction in the $R_L(U)$ as the Cr content is increased was observed at 25 °C and 40 °C in both Regime 1 (R1) and Regime 2 (R2) (Figures 2 a-d). Since Cr is the only changing parameter (i.e. there was no increase in grain size with increasing Cr content in our samples, due to the reducing conditions applied during pellet synthesis), any change in dissolution behaviour can be directly related to the chemical influence of Cr in the system. It is hypothesised that this reduction in rate with increasing Cr is a result of galvanic coupling between reduced Cr (as confirmed by Cr K-edge EXAFS analysis performed as part of WP2) present within grain boundaries as precipitates, and UO_2, whereby Cr is preferentially oxidised, giving the liberated electrons to U^{6+} dissolved from the UO_2 surface, reducing it back to U^{4+} and decreasing the amount of U released to solution.

Intriguingly, the opposite behaviour was observed in the 60°C experiment at R1 and R2, where there was an increase in the $R_L(U)$ as a function of Cr content (Figures 2 e-f). We postulate that this is tentative evidence to indicate that the galvanic coupling effect observed at the lower temperatures is outweighed by the kinetic effects of the higher temperature on oxygen diffusion, thus promoting oxidation of the UO_2. Since the U^{5+} and defect content in UO_2 increased with increasing Cr content (as determined by U $M_{4,5}$-edge HERFD XANES and Raman Spectroscopy, performed in WP2), the ability of oxygen to diffuse through the material may also increase, explaining the trend of increasing $R_L(U)$ with increasing Cr content.

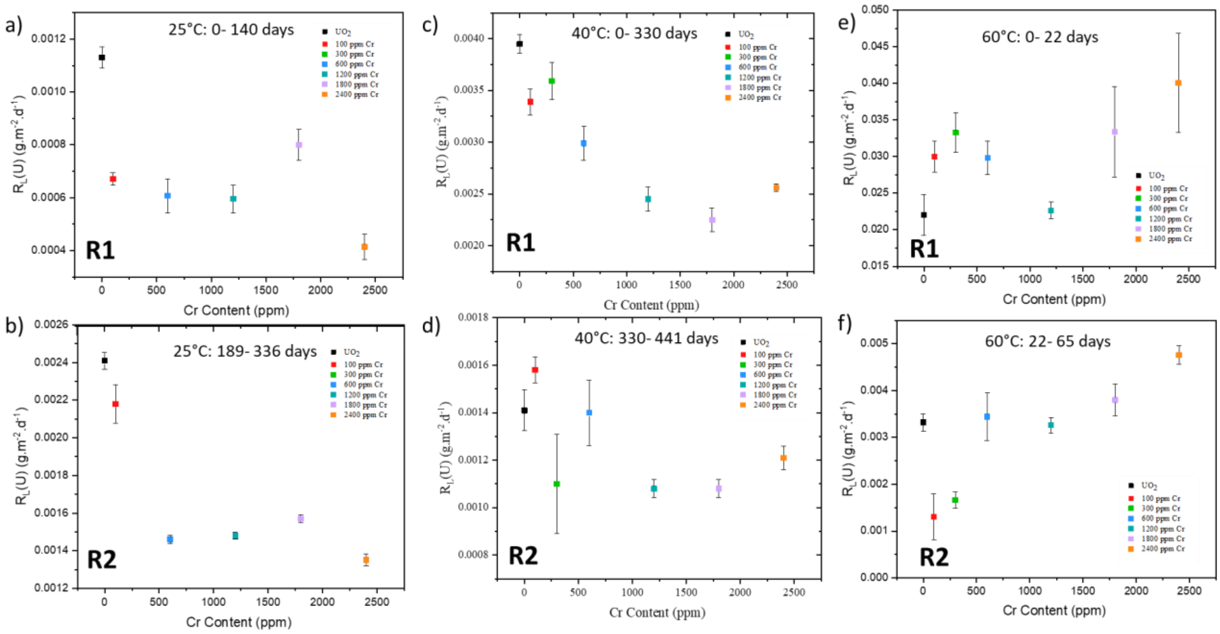

Figure 2. Normalised dissolution rate of U, $R_L(U)$ (g m^{-2} d^{-1}), of Cr-doped and undoped UO_2 dissolved in 1 mM $NaHCO_3$ + 19 mM NaCl at: (a-b) 25 °C; (b-c) 40 °C and; (c-d) 60 °C from rate regimes 1 (R1) and 2 (R2).

Steady-state dissolution, represented by Regime 3 (R3), was reached for all samples in the 25 °C and 60 °C experiments, with U concentrations in the range of 10^{-6} to 10^{-7} mol L^{-1}, depending on the temperature. Within R3, in contrast to the other dissolution regimes, there appeared to be no difference in the $R_L(U)$ a function of Cr content. This is not unexpected, given that under solution saturation conditions; there is no thermodynamic driving force for U dissolution. It could also be possible that the galvanic coupling reaction between Cr and U may have diminished as a function to time (due to oxidation of reduced Cr). Post-dissolution Cr oxidation state measurement would be required to determine whether this is the case or not, and such measurements are not planned as part of the present project. Finally, it is possible that secondary uranium species formed at the surface acted to “block” the reduced Cr particles from the solution and thus reduce the galvanic coupling effect, however, there was no evidence for secondary phase formation except for at 60°C, as exemplified by the negative absolute $R_L(U)$ values and SEM imaging (data not shown).

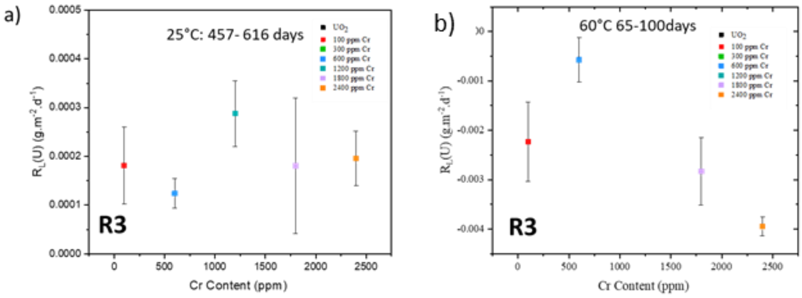

Figure 3. Normalised dissolution rate of U, $R_L(U)$ (g m^{-2} d^{-1}), of Cr-doped and undoped UO_2 dissolved in 1 mM $NaHCO_3$ + 19 mM NaCl, in Regime 3, at: (a) 25 °C and (b) 60 °C.

Evaluation of the activation energy (E_a) for the undoped and Cr-doped UO_2 at 25°C, 40 °C and 60 °C, determined from data acquired in Regime 1 (i.e., in the absence of solution saturation influence), suggest a somewhat different dissolution mechanism for the Cr-doped samples. For example, the E_a obtained for Cr-doped samples was in the range of 57.5 ± 1.9 kJ.mol^{-1} to 61.7 ± 1.9 kJ.mol^{-1}, while that obtained for UO_2 was 30.2 ± 1.4 kJ.mol^{-1}. The higher E_a values obtained for the Cr-doped samples are consistent with dissolution *via* surface controlled reactions, which is in agreement with the hypothesis that galvanic coupling of Cr with U at the sample surface has an influence on the dissolution of Cr-doped UO_2, at least under dilute conditions.

3.2 MOX related model systems

3.2.1 Results from CEA

Leaching behaviour of a homogeneous MOX fuel in a synthetic Callovo-Oxfordian groundwater (COX) and in the presence of a corroded iron foil.

The experiment took place in two stages: a first stage of corrosion of the iron foil in a synthetic COX groundwater (84 days) followed by a leaching experiment of two MOX pellets in the study environment (468 days). This part presents all the results obtained in terms of solution analyses, mass balances and characterization of the leached surfaces. A proposal of mechanisms is also put forward to explain these experimental results which are also the subject of a modeling task in work package 5 of the Disco project.

I) Reminder of the pre-corrosion stage

Iron foils were placed in the autoclave to simulate container corrosion products and to move towards realistic reducing conditions in the absence of the fuel pellet. Such reducing conditions are expected in deep geological disposal. Rolled 99.99% pure iron foils were purchased from Goodfellow. Their size was 2.5 cm by 2.5 cm for a thickness of 125 µm and a weight of around 0.64 g. One iron foil was used for the leaching experiment. Before being set up in the reactor, the foil was rinsed in ethanol and ultrasound-cleaned for 2 minutes.

The iron foil was first pre-corroded in 180 mL of synthetic COX water for around 80-90 days in the absence of the MOX pellets. This first step was intended to ensure the presence of corrosion products on the iron foil surface, to obtain a solution chemistry containing Fe^{2+} ions not initially present in the synthetic COX water, and to have reducing conditions when the MOX pellets were introduced at a later date. The iron foil was slightly curved to enable maximum contact with water, and placed on the platform immediately under the pellet support. Once the leaching reactor had been closed, it was purged with a mixture Ar/CO_2 3000 ppm for 2h30 and then put under a pressure of 3.5 bars. The leaching solution was regularly sampled over 84 days.

II) *Long term leaching experiment with the homogeneous MOX fuel pellets*

After the iron pre-corrosion phase, the reactor was opened to add two homogeneous MOX pellets ($U_{0,73}\ Pu_{0,27}O_2$) with an alpha activity of 2.2×10^9 Bq/g, which were placed on a support above the iron foil. The reactor was then closed again, purged with a mixture of Ar/CO_2 3000 ppm for 30 min, and returned to a pressure of 3.5 bars with the same gas mixture. Samples of the leaching solution were regularly collected over time.

II-1) Solution analysis results

The concentrations of COX water elements were monitored (Ca, K, Mg, Na, Si, Sr, Fe). Most of the element concentrations were found to be constant over the duration of the experiment (including the pre-corrosion phase), except for calcium, strontium, silicon and iron. The evolution of the concentrations of these elements is shown in Figure 3.2.1.1. The calcium and strontium concentrations are decreasing over time (from 330 to 280 mg.L^{-1} for calcium and from 20 to 14 mg.L^{-1} for strontium), probably indicating the precipitation of secondary phases, which will be looked for during the solid analyses.

The iron concentration increases during the pre-corrosion stage until reaching a plateau around 20 mg.L^{-1}, suggesting a thermodynamic equilibrium with a secondary phase (corrosion product). After adding fuel pellets, the increase in iron concentration resumes and seems to reach a second level of around 70 mg.L^{-1}. Over the long term, the concentration of iron in solution gradually decreases. It is possible that these levels and the final decrease are due to the precipitation / dissolution of different iron-based phases, which will be sought during the characterizations of the solid. Anoxic corrosion of metallic iron is clearly the main source of iron into the solution as demonstrated by the presence of H_2 in the gas phase with a content of 13800 ppm after 468 days of leaching.

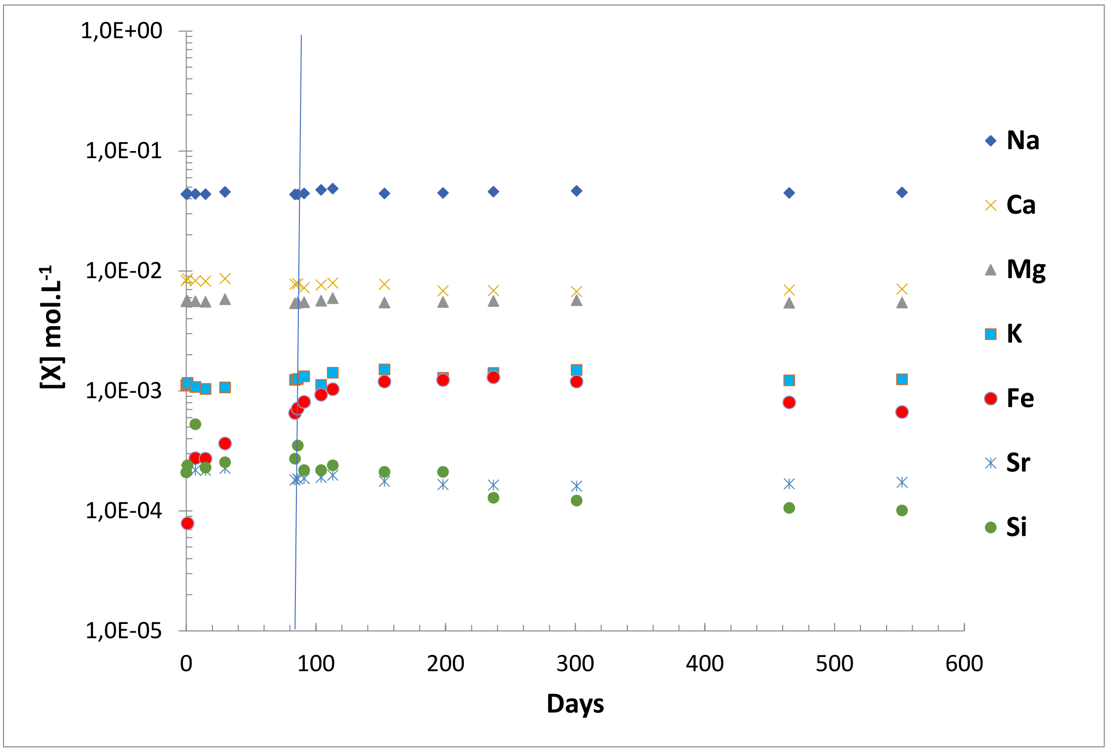

Figure 3.2.1.1: Evolution of the chemistry of synthetic COX groundwater over time (84+468 = 552 days). The vertical bar corresponds to the end of the pre-corrosion stage (84 days) and to the introduction of the MOX pellets into the reactor.

The samplings also allowed monitoring over time of the actinides concentrations and the physico-chemical parameters (Eh and pH). The pH was constant during the experiment, at a value of 8.2 ± 0.2. The redox potential was measured around -0.1 ± 0.03 V / SHE directly in the leachate after opening the reactor at the end of the experiment. The measurements in the intermediate samples were more unstable. The concentrations of H_2O_2 and Pu were below the detection limits of the methods used that is 10^{-7} mol.L^{-1} for H_2O_2 and 5×10^{-10} mol.L^{-1} for Pu.

Concerning the uranium concentrations, the results indicate a significant effect of iron on the oxidative dissolution of this homogeneous MOX fuel. Uranium concentrations are less than 1

$\mu g.L^{-1}$ after few months of leaching (Figure 3.2.1.2). Furthermore, an experiment carried out without iron but with hydrogen contents equivalent to that produced by corrosion of the iron foil did not show inhibition of the dissolution. This experiment, which is not part of this project, shows that under the experimental conditions of our study, iron is the main active redox species.

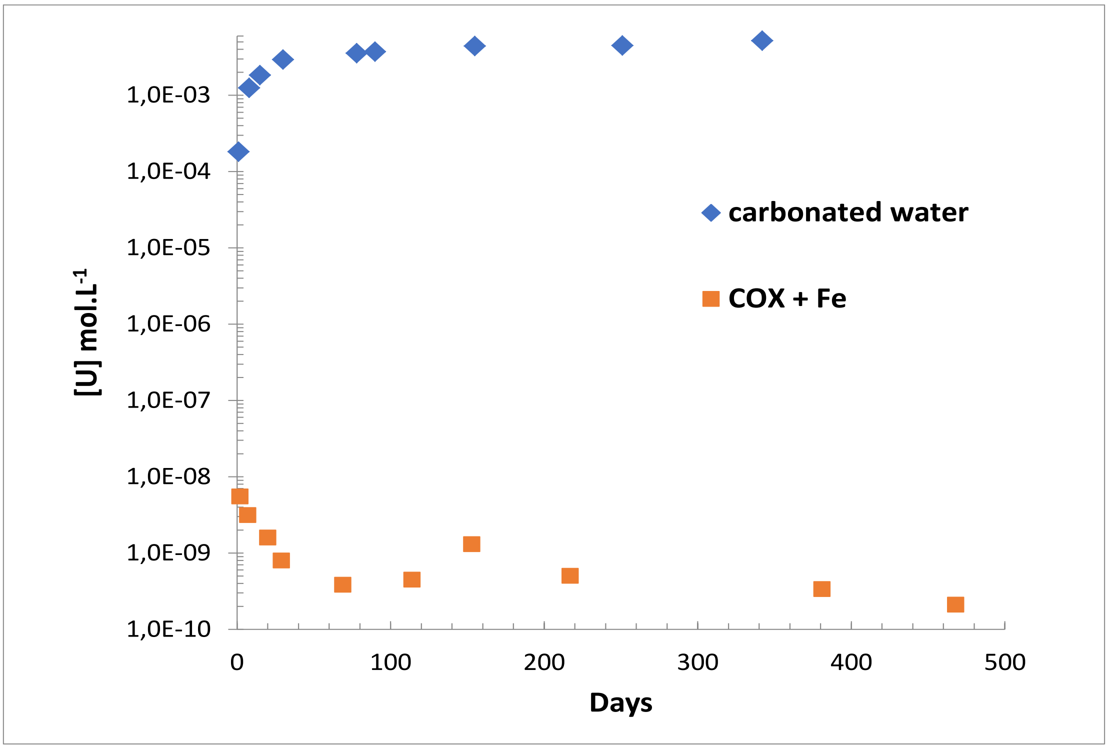

Figure 3.2.1.2: Evolution of uranium concentrations over time (468 days). Carbonated water is a reference to illustrate the major role of iron on the drop in concentrations.

This concentration is in agreement with the solubility of amorphous UO_2: xH_2O, thus indicating a thermodynamic equilibrium and not an oxidative dissolution. The total mass balance of uranium indicates that it is mainly sorbed or precipitated on the TiO_2 liner or on the iron foil, with a very low total released of 0.8 µg.

II-2) Surface characterization

Characterizations of the surface of the MOX pellets and of the iron foil were carried out after the leaching experiment: SEM imaging coupled with elemental analyses (EDS) and Raman spectroscopy. The results of these analyses are presented below, first with the characterizations of a homogeneous MOX pellet, followed by the characterizations of the iron foil.

The pictures obtained by SEM (Figure 3.2.1.3) made it possible to demonstrate massive precipitation on the surface of the MOX fuel pellets. This layer, with a thickness estimated at 26 µm, seems to be made up of a set of interlaced sheets, these sheets themselves being formed of balls. The surface does not seem entirely covered by this precipitate, but it is possible that the handling of the pellet resulted in the partial removal of the deposit.

Elemental analyses (Figure 3.2.1.4) show that this phase is mainly composed of iron and silicon (~ 3%). Uranium and plutonium are sometimes also detected during elemental analyses, which may be due to a contribution from the underlying MOX matrix, or to sorption / coprecipitation mechanisms on iron.

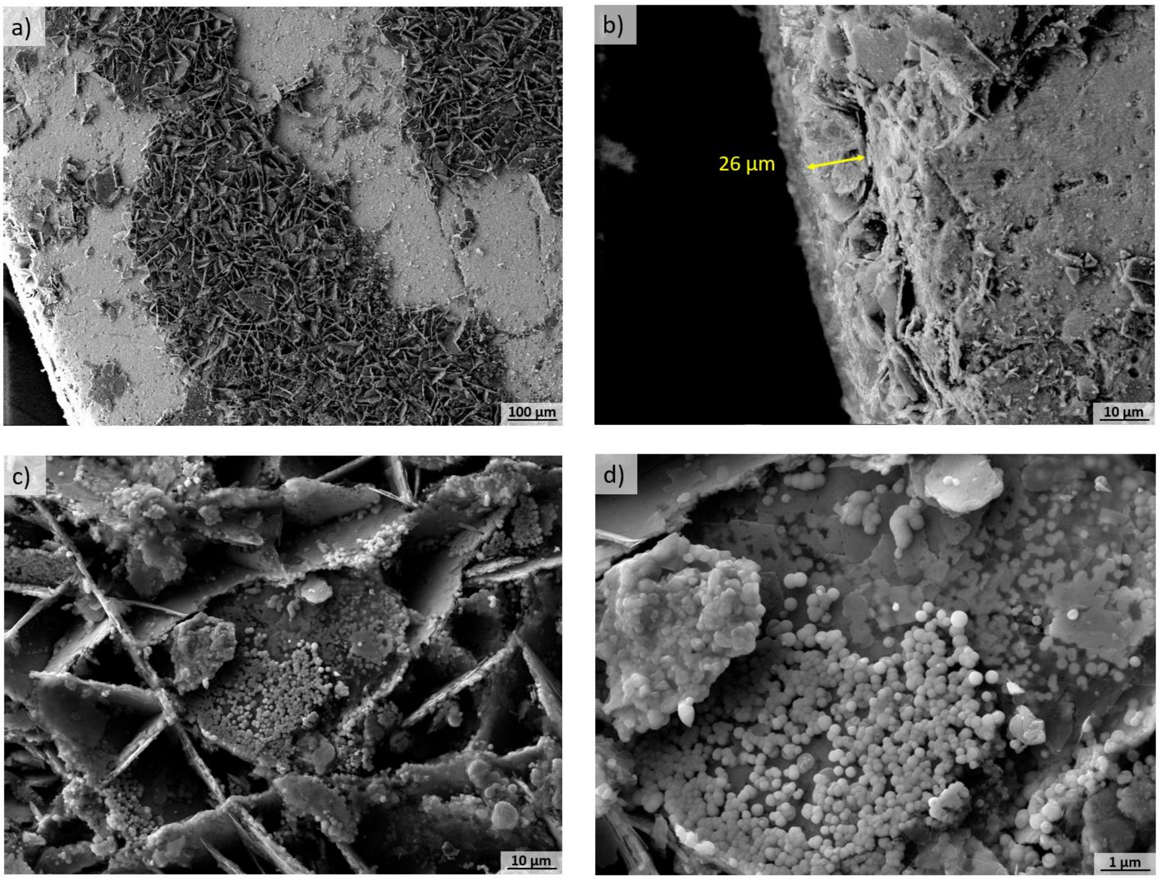

Figure 3.2.1.3: SEM observations of the surface of the MOX pellet after one year of leaching in a synthetic COX groundwater and in the presence of a corroded iron foil.

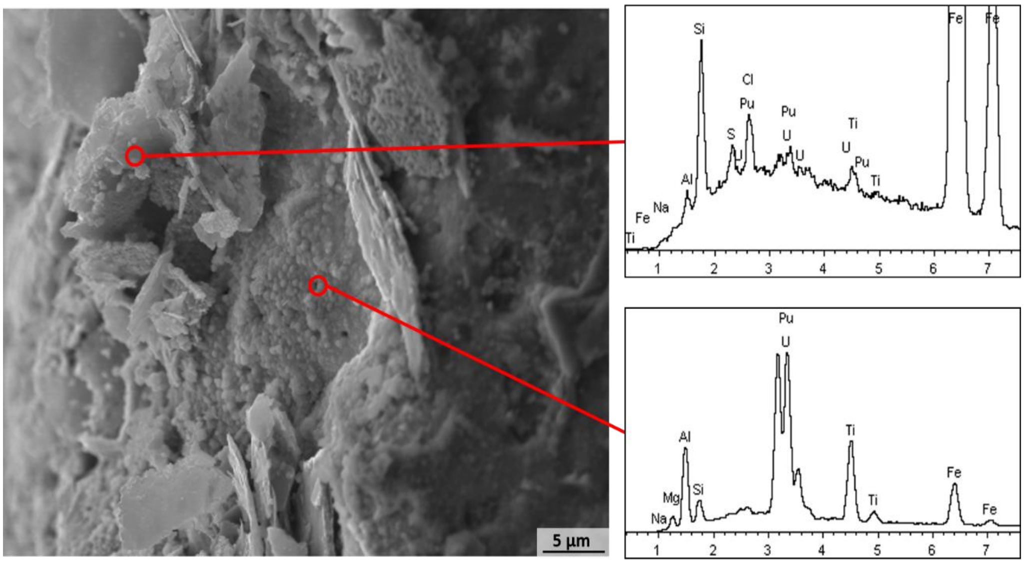

Figure 3.2.1.4: SEM observations and EDS spectrum obtained on the surface of the MOX pellet after one year of leaching. The analysis confirms the presence of iron plates.

In order to determine the nature of the phase observed, analyses by Raman spectroscopy were also carried out. In order not to alter the phase, the first spectra were acquired at low laser power. Subsequently, a study was conducted to choose the optimal working power, that is to say the maximum usable power without altering the sample. Several spectra have therefore been acquired by increasing the power of the beam. At low power (0.12 mW), the spectrum obtained corresponds to that of magnetite (Figure 3.2.1.5).

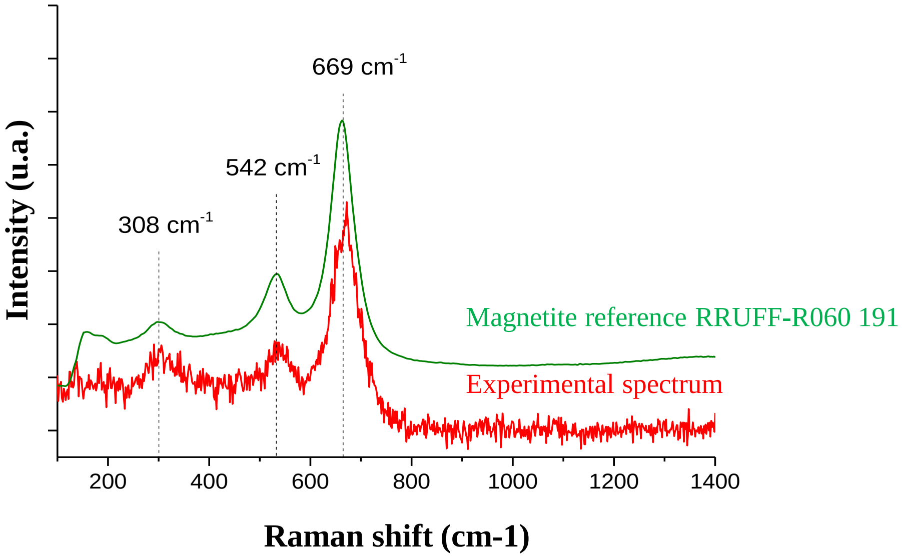

Figure 3.2.1. 5: Raman spectrum of Magnetite obtained on the surface of the MOX fuel pellet.

SEM images of the surface of the iron foil, shown in Figure 3.2.1.6, show a strong precipitation of secondary phases. Two kinds of phases can be observed: needles and balls /

sheets. Elemental analyses show that the needles are mainly composed of calcium with low strontium contents. These results are in agreement with the drop in calcium and strontium concentrations in solution mentioned before. The balls of sheets, on the other hand, are mainly composed of iron.

In order to identify the phases observed, Raman analyses were carried out. The power was initially adjusted to 0.29 mW in order not to alter the phases. Two different spectra have been collected on the surface of the iron blade: the chukanovite spectrum and the aragonite spectrum (Figure 3.2.1.7).

Aragonite corresponds to the needles observed on the surface by SEM. The iron balls correspond to chukanovite, the morphology observed being similar to that observed elsewhere in the literature [43]. Other elements are also present, including sulphur, magnesium, chlorine and silicon, which can promote the precipitation of aragonite and chukanovite at the expense of calcite and siderite.

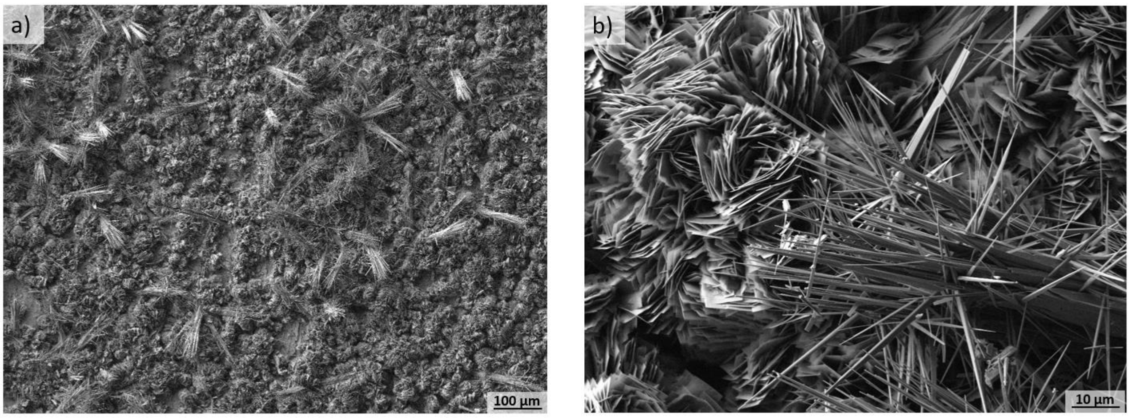

Figure 3.2.1.6: SEM observations of the surface of the iron foil after 552 days of leaching in a synthetic COX groundwater.

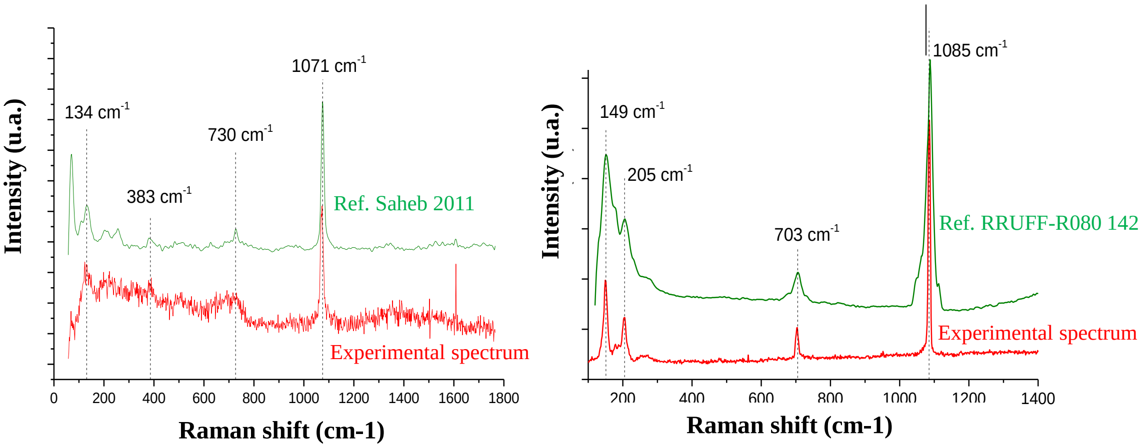

Figure 3.2.1.7: Raman spectra of chukanovite (left) and aragonite (left) obtained on the surface of the iron foil.

Aragonite is a polymorph of calcite and several studies show that it is favoured in environments rich in magnesium, which is the case for COX groundwater. Furthermore, it is interesting to note that Aragonite tends to transform into Calcite under the effect of temperature, thus indicating that Aragonite is metastable and evolves into Calcite.

Similarly, by studying the superposition of Pourbaix diagrams of siderite and chukanovite produced by Azoulay et al. [44] it appears that the stability domain of chukanovite is entirely included in that of Siderite. This indicates that chukanovite is metastable, probably evolving into siderite in the long term.

II-3) Dissolution mechanisms

Fe(II) released in solution by the iron foil anoxic corrosion consumes H_2O_2 produced by alpha-radiolysis of water. This redox reaction occurs where radiolytic H_2O_2 is produced, i.e. on the extreme surface of the MOX pellets. The Fe(III) produced precipitates immediately onto the MOX pellets as magnetite. Thanks to this consumption of H_2O_2, the oxidative dissolution of MOX fuel is strongly inhibited by the presence of metallic iron. It would seem that the location of the redox front on the extreme surface of MOX favours the inhibition of oxidizing dissolution under alpha radiolysis which occurs in the very first microns of the reactional interface. In parallel, a local increase in pH around the iron foil due to its anoxic corrosion enables the precipitation of carbonated secondary phases (aragonite, chukanovite) onto its surface.

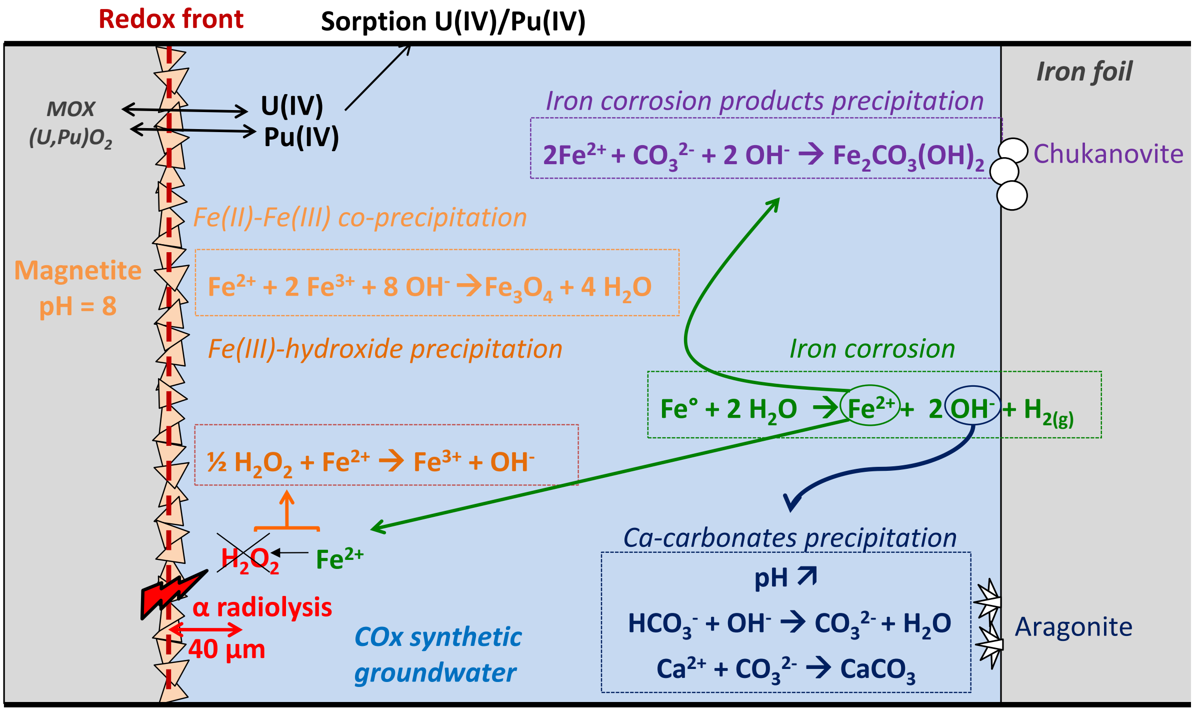

Figure 3.2.1.28: General scheme showing the coupled mechanisms of dissolution of a homogeneous MOX fuel in a synthetic COX groundwater and in the presence of an iron foil.

These mechanisms are very similar to those observed on UOx type fuels. However, in previous work [43], Magnetite had not been observed on the surface of the fuel pellets but rather iron hydroxides like akaganeite. The slightly more basic pH measured for the MOX experiment seems able to explain these differences in the iron-based phases formed. Finally, all of this data is the subject of modeling work in the context of work-package 5.

3.2.2 Results from UCAM

Three blank samples and two homogeneous mixed oxide ($U_{0.75}Th_{0.25}O_2$) pellets were leached for fifteen days. The consumption of H_2O_2 and the concentrations of Th and U in solutions were measured over the duration of the experiment.

(i) Thorium release (NL_{Th}) in $U_{0.75}Th_{0.25}O_2$

Measured Th concentrations as a function of time are shown in Figure 3.2.2.1. No Th could be detected above the LOQ (280 ± 360 = 640 ppt Th).

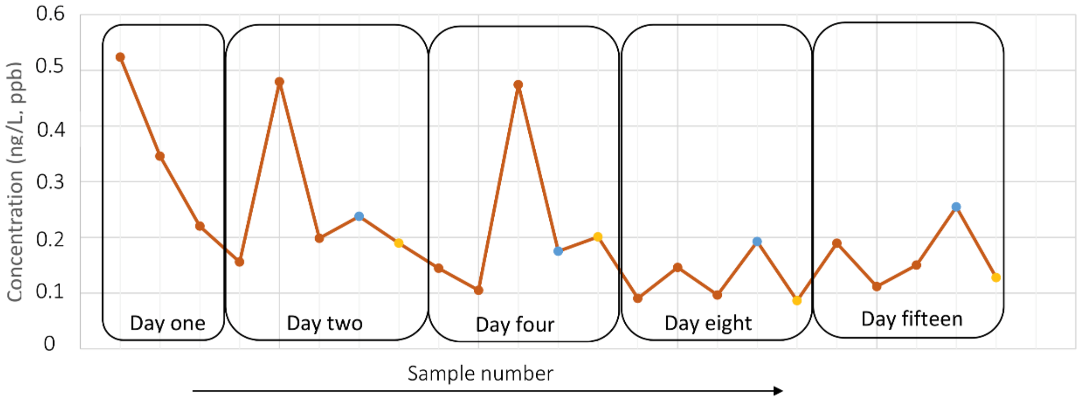

Figure 3.2.2.1: Th concentrations in three blank solutions (brown) and two solutions containing a homogeneous U/Th MOX pellet (yellow and blue).

(ii) Uranium release (NL_U) in $U_{0.75}Th_{0.25}O_2$

Measured U concentrations are shown in Figure 3.2.2.2. The concentration of U increases steadily over the duration of the experiment rising to an average of 371 ppb after 15 days. Despite the strict anoxic atmosphere of the experiment, the carbonate in the COX simulant groundwater maintains the U dissolved by H_2O_2 oxidation in the solution. Filtration of the solutions shows a very small difference in concentration when filtering with 0.45 µm or 0.02 µm filters. Indicating the absence of any significant colloids larger than 20 nm.

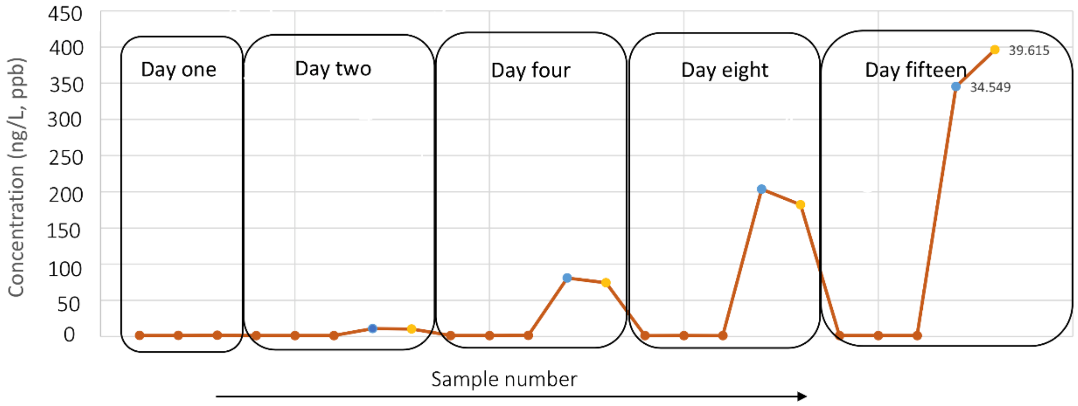

Figure 3.2.2.2: U concentrations in three blank solutions (brown) and two solutions containing a homogeneous U/Th MOX pellet (yellow and blue).

The calculated uranium release for both homogeneous pellets is shown in Figure 3.2.2.3.

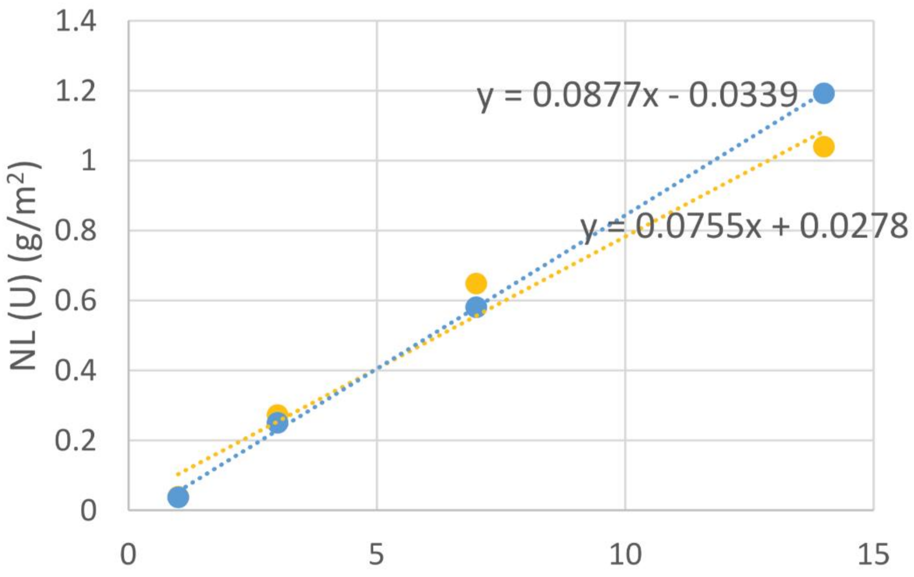

Figure 3.2.2.3: Normalised release of U from the homogeneous mixed oxide pellets. The gradients on the graph correspond to a mean release rate of 4.0 x 10^{-9} mols m^{-2} s^{-1}.

The release rate of U corresponds to 4.0 x 10^{-9} mol m^{-2} s^{-1}. This can be compared to the consumption of H_2O_2, which is 3.1 x 10^{-9} mols l^{-1} s^{-1} when allowance for the H_2O_2 decomposition due to interaction with sample container surface and potentially COX water components, see Figure 3.2.2.4 when pellets were present the H_2O_2 showed an increased consumption of H_2O_2 between 25% and 35%. Similar leaching experiments on endmembers and inhomogeneous U/Th pellets are in train. To this point, the data on U release and H_2O_2 consumption in homogeneous $U_{0.75}Th_{0.25}O_2$ can be compared with the early stages of the homogeneous $U_{0.73}Pu_{0.27}O_2$ dissolution experiments in this project [45].

In that project the U release rate (initial release to compare with the 15 day data here) was 1.4 x 10^{-9} mol m^{-2} s^{-1} and the H_2O_2 consumption was too low to measure (produced by alpha activity at the surface and consumed at the surface). However, mass balance considerations are used to estimate the fraction of oxidative dissolution to be

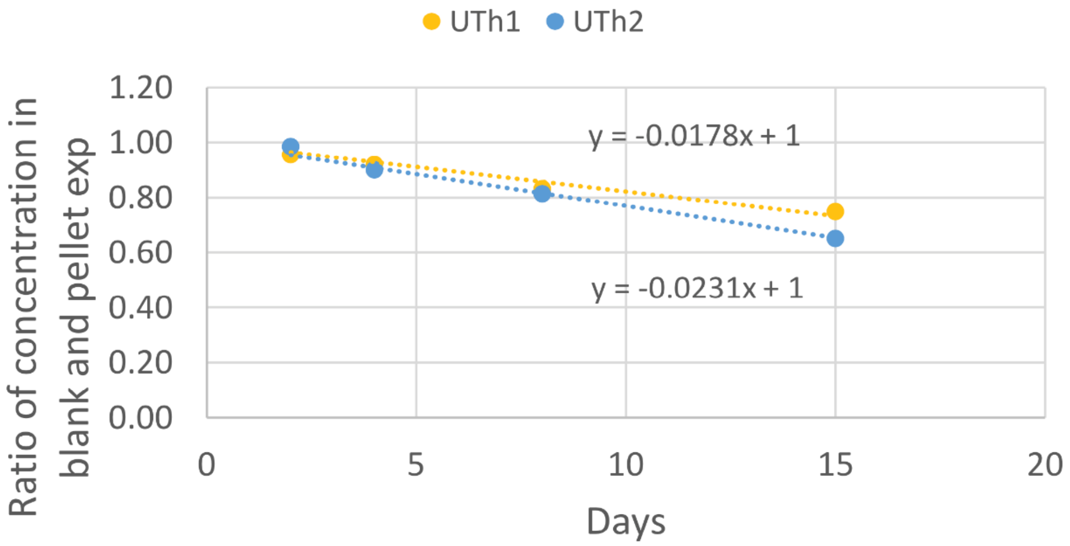

Figure 3.2.2.4: Relative consumption of 1.3 x 10^{-4} M H_2O_2 in COx water solutions with homogeneous U/Th pellets normalised to the underlying consumption of H_2O_2 in containers without pellets.

12.5% in the initial regime. For the similar U/Th pellets this fraction was 5.0%.

The overall process of the interaction of H_2O_2 with the surface of the mixed oxide was proposed**Fel! Bokmärket är inte definierat.** for homogeneous $U_{0.73}Pu_{0.27}O_2$ in equation (2).

$$\frac{d[H_2O_2]}{dt} = \left(k^{prod} - k^{disprop}[H_2O_2] - k_U^{oxid}[H_2O_2]\right)A_v \qquad (2)$$

The relevant parameters for the homogeneous $U_{0.75}Th_{0.25}O_2$ experiments are:

$$\frac{d[H_2O_2]}{dt} = gradient\ of\ [H_2O_2]\ with\ time = 3.1\ \times 10^{-11} mol\ l^{-1} s^{-1}$$

$$k^{prod} = production\ rate\ (zero\ );\ initial\ [H_2O_2] =\ 1.3\ \times 10^{-4}\ mol\ l^{-1}$$

$$k^{disprop}[H_2O_2] = catalytic\ consumption\ \ = 2.95\ \times\ 10^{-11} mol\ l^{-1} s^{-1}$$

$$k_U^{oxid}[H_2O_2] = gradient\ of\ U\ mass\ loss = 4.0\ \times 10^{-9} mol\ m^{-2} s^{-1}$$

$$A_v =\ surface\ area\ of\ pellet\ per\ litre\ of\ solution$$

These parameters provide an alternate system test to compare with homogeneous U/Pu pellets of similar actinide ratios and inhomogeneous U/Th and endmember pellets.

4 Summary of results & specific observations

This report concludes the results of dissolution experiments on Cr/Al/Gd-doped-UO_2-based and MOX model systems performed by DisCo WP4 participants. In particular, this report provides the modellers from WP5 with detailed information from the various groups involved in WP4 on the pellets used in the experiments, the experimental conditions, and the experimental observations in a structured and coherent way by using an electronic exchange format. Thus this deliverable and the electronic data exchange provide a solid basis for future modelling activities within DisCo WP5. The dissolution behaviour of the model systems was studied on pellet samples, which were prepared by the various groups active in WP2 by different approaches. In particular the preparation of the doped UO_2-materials led to a set of samples, which covers broad ranges in terms of dopant levels/composition and microstructure. Since these parameters are not well known for irradiated modern fuel pellets, the approach followed here ensures that the envelope of these parameters in the model systems covers most likely also those in “real” SNF. Moreover, this range of material properties will aid in elucidating effects of microstructure and dopant concentration and speciation on the dissolution behaviour in single-effect and multi-parametric studies. This will further strengthen the complementary approach followed in DisCo of combining leaching studies on SNF with dissolution studies on model materials for unravelling the long-term corrosion behaviour of conventional and modern SNF in a variety of repository-relevant conditions.

4.1 SCK.CEN

Static leaching experiments were performed at SCK CEN with Pu and Cr doped UO_2 in a cementitious water with pH 13.5 and a bicarbonate solution with pH 9 and compared with undoped analogues. Tests were conducted in autoclaves under 10 bar H_2 pressure in presence of Pd/Pt catalyst to scavenge the traces of atmospheric oxygen. In spite of the fact that the outermost layer of the Cr-doped pellets has a relatively small grain size and Cr concentration, the Cr-doping appeared to reduce by a factor 5-6 the U concentrations in solution for UO_2 with and without Pu at pH 13.5, but not or much less at pH 9. For both leaching media, the effect of dissolved H_2 was not sufficient to prevent the short term radiolytical oxidation/dissolution, or to reduce oxidised U(VI) in solution. All uranium concentrations were higher than the solubility of UO_2 in reducing conditions, but the stabilization of the uranium concentrations for the Pu doped UO_2 with time could still be ascribed to the presence of H_2 or to the solution saturation by a U-phase. The Cr doping could favour the H_2 effect at pH 13.5. Complementary surface analysis of the leached surface (e.g. Pu doped samples), modelling calculations and other method to control the redox conditions could be considered in the future to explain the observed Cr effects.

In all systems, the high initial U release suggests the dissolution of a slightly oxidised $UO_{2+x\ \mathrm{layer}}$ in spite of the washing. Possibly some oxidation of the pellet occurred during the transfer from the PE bottle used for the washing to the autoclave, even if the oxygen concentration in the glove box is < 10 ppm. For a given model system (UO_2, Cr-UO_2, Pu-UO_2, Pu-Cr-UO_2), this initial release is not affected by pH, complexing agent (OH^- or CO_3^{2-}) or alpha field. On the other hand, we can clearly distinguish a lowering effect of Cr on the initial U(VI) release in absence of an alpha field at both pHs. A similar dissolution reducing Cr effect appears slightly delayed at pH 13.5 in presence of alpha field, but it is not present at pH 9. These results suggest that at high pH, Cr makes the UO_2 surface more resistant against oxidation, or prevents the release of U(VI) from the surface. For the inactive tests, the measured U concentrations are higher at pH 13.5 than at pH 9 (Figure 2.1.2.2- red and blue symbols). These concentrations remain nevertheless within the UO_2 solubility range [9], except for UO_2 at pH 13.5 showing a higher U concentration [46- 47]. These observations reveal a favoured complexation of U(VI) from the remaining oxidised layer by the hydroxyl ions at high pH compared to hydrogeno-carbonate ions at pH 9.

In presence of an α-field, the measured U concentrations are always higher than the UO_2 solubility range. This is caused by radiolytical oxidation in spite of the H_2 gas. For Pu-Cr-UO_2 at pH 13.5, the concentrations stabilize immediately after the initial release at around 1×10^{-7} mol.L^{-1}, while for Pu-UO_2 a renewed release occurs between 10 and 35 days to reach a U concentration of 5×10^{-7} mol.L^{-1}. This suggests again a stabilising effect of the Cr at high pH. A continuous release is observed also for Pu-UO_2 and Pu-Cr-UO_2 at pH 9, reaching concentrations of about 3×10^{-7} mol.L^{-1} up to 35 days. At this lower pH, the Cr stabilising effect is no so pronounced. After 35 days, no further increase of the U concentration is detected. This suggests that on the short term the dissolved H_2 cannot prevent radiolytical UO_2 oxidation or U(VI) dissolution, or reduce back U(VI) in solution, but after a period of renewed oxidation or release, it could become effective. Another explanation of the flattening of the concentration after 35 days could be the control of U in solution by a U-phase. Such flattening effect was already observed in tests with Pu-doped UO_2 without Cr with a similar alpha activity although no H_2 gas was present [48]. At pH 13.5, the Cr doping could increase the H_2 effect, but whatever the experiment this H_2 effect was not effective enough to reach U concentrations at the level of the UO_2 solubility range.

In spite of the fact that the outermost layer of the Cr-doped pellets has a relatively small grain size and Cr concentration, we thus observe an effect of the Cr doping in certain conditions. Several hypotheses can be proposed to explain these observations:

- The formation of a phase at the UO_2 surface blocking the further dissolution. As revealed by the SEM analyses, no Cr-phase has been observed at the surface of the leached inactive samples, only U_4O_9 is suspected at the surface of the inactive samples leached at pH 9. However, such a phase would not block the U release. We cannot yet conclude for the leached active samples.
- A redox effect of the chromium in the solid due to the presence of oxygen vacancies formed by the presence of Cr in the UO_2 matrix or in solution. Within few months, we can have access to Raman analyses at SCK CEN, which might be helpful to validate this hypothesis [49]

- An enhancement of the catalytic properties of the UO_2 surface by the presence of Cr, increasing the reduction of oxidising species by H_2, even if the reducing effect of the H_2 is much smaller than expected. Even if we have a Cr depletion at the outermost layer of the pellet, the grains are clearly separated and deep grain boundaries are present, making the Cr present deeper in the pellet accessible (see section 3.1.1.6: surface analyses).

Based on our current results, none of these hypotheses can be favoured, but modelling calculations possibly performed by DisCo partners of the WP5 or complementary surface analysis could be considered in a near future to support the data interpretation.

In parallel, these experiments are compared to similar experiments done at VTT- Technical research Centre of Finland with the same materials but using metallic iron to control the redox conditions in place of hydrogen. While at VTT they measured U concentration from 10^{-9} mol.L^{-1} decreasing to 10^{-11} mol.L^{-1} after 180 days with no clear effect of Cr or Pu doping [50], SCK CEN determined concentrations by several order of magnitude higher with a Pu and Cr-doping effect. The results raise the question on the possible role of metallic Fe on the U release. Therefore, additional experiments will be conducted by both institutes outside the EU-Disco programme.

4.2 FZJ

In DisCo deliverable D41 [8,12] a surface passivation effect was reported when repeatedly employing the same pellets in the dissolution tests. The results of these experiments show a decrease of the uranium concentration in the solution from run to run which is independent on the H_2O_2 concentration in the solution used (see Figure 4.2.1). Between each run an extensive washing step of the used pellets in bicarbonate solution was performed.

In Figure 4.2.2 the results of dissolution experiments with Cr-doped pellets for two selected experiments are shown. After a first dissolution step and the complete usage of H_2O_2 a new amount of fresh solution was added to the existing solution. The addition of the fresh solution and therefore new H_2O_2 has nearly no effect on the dissolution of uranium. This is in good agreement with the results from the experiments with pure UO_2 pellets shown in Figure 4.2.1.

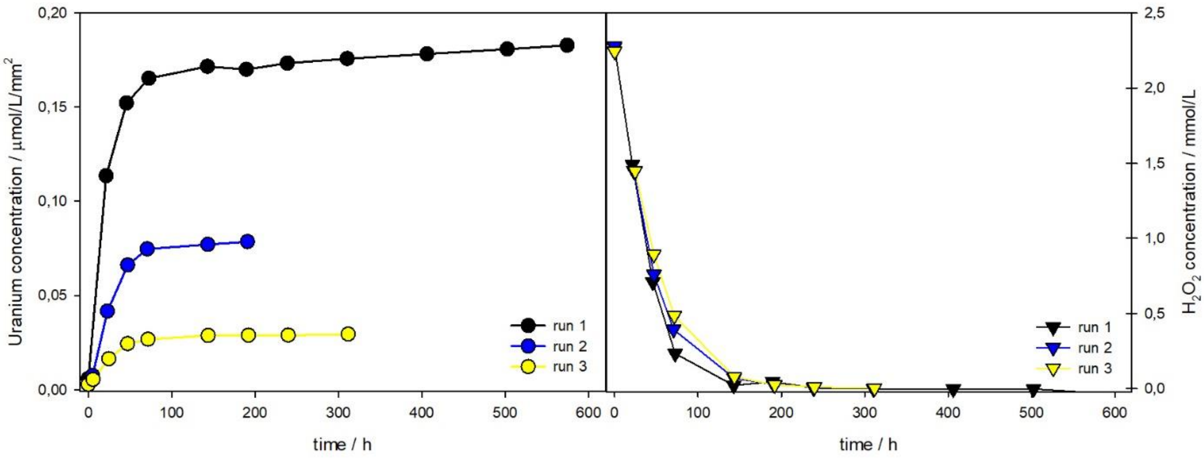

Figure 4.2.1: Concentration of uranium in solution normalised to geometrical surface (left) and H_2O_2 in solution (right) depending on run time for one representative reference sample (pure UO_2). Between each run samples and complete experimental setup was extensively washed with $NaHCO_3$ solution.

XRD and Raman measurements suggest that the formation of a thin layer of a secondary phase or of undissolvable hyperstoichiometric uraniumoxide on the surface of the pellets seems to cause this surface passivation [12]. This observation is supported by the fact that the extensive cleaning step, most likely due to the mechanical abrasion, led to a partial reactivation of the surface in the experiments described above (Figure 4.2.2.1). As result of this observation only pristine pellets were used in the dissolution experiments.

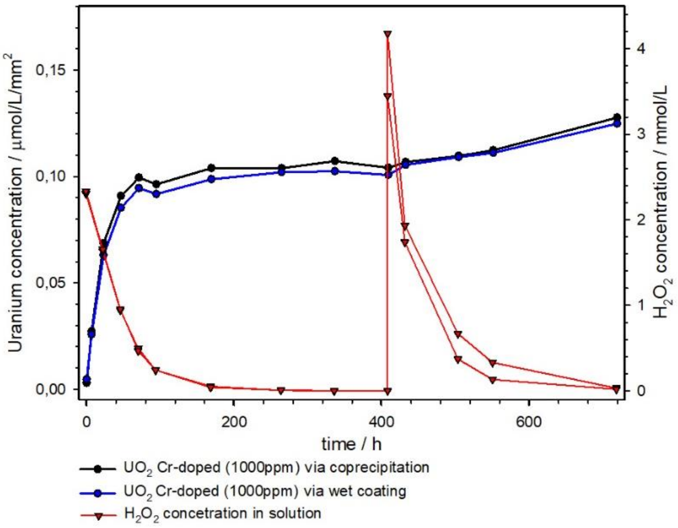

Figure 4.2.2: Concentrations of uranium in solution normalised to geometrical surface and corresponding concentration of H_2O_2 in solution depending on run time for two representative Cr-doped UO_2 samples. Different doping methods were used for the different samples.

4.3 VTT

Investigations of VTT revealed the following specific observations:

- No effect of Cr/Pu doping under anaerobic conditions in the presence iron foil
- Blank experiments and the observed difference between SCK CEN and VTT experiments both indicate a strong role of metallic iron on U behaviour

4.4 CIEMAT

According to the schedule proposed in previous meetings, all the systematic dissolution experiments were carried out and finalized on time. These experiments consisted of testing the impact of water composition on pellet dissolution. Pellets were manufactured and characterized within WP2 of the project.

The main outcomes of the undertaken leaching experiments are:

- There is a higher influence of leachant nature (i.e. pH) on both the concentration of elements in solution and dissolution rates than that of dopants. This is confirmed by comparing results of different doped UO_2 pellets in the same leaching medium.
- This effect of the leachant is specially emphasized in bicarbonate water, where complexing agents could enhance the solubilisation of U(VI) formed on the surface of the pellet as a result of the oxidation of U(IV). This is not happening in PC and YCW, thus demonstrating that the total doping effect on the leaching behaviour seems to be minimal.
- Autoclaves where the experiments have been performed undergo a slight loss of pressure during the duration of the tests.

There are still a number of ongoing activities and "open questions" that have arisen from the interpretation of the results and comparison of data with literature, and may help to draw the complete picture of doping effect on long-term behaviour of "model fuels":

- As pointed out by other authors, EPMA (Electron Probe Micro-Analysis) measurements, would help to understand how much and how is it dopants distributed in doped-UO_2 samples.
- Interpretation of the leached surfaces characterizations and link with modelling (WP5).
- Even though complexing agents inhibit precipitation of U secondary phases, could some of them still be present? Serve as an example the proposed by Yamamura et al [51]: $Na_2U_2O_7 \cdot H_2O$ in equilibrium with $UO_2(OH)_3^-$, $UO_2(OH)_4^{2-}$, and $UO_2(CO_3)_3^{4-}$.
- Is there a possible catalytic activity by H_2 in Cr_2O_3 results, which is improved by the synergic effect of Cr_2O_3 -Al_2O_3 in the oxidative dissolution of U?

4.5 USFD

Three rate regimes were identified for the dissolution of UO_2 and Cr-doped UO_2 at each temperature: Regime 1 (R1), reflecting the initial dissolution rate; Regime 2 (R2), reflecting a period where solution saturation begins to influence the dissolution rate and; Regime 3 (R3), which reflects steady state dissolution, i.e., where the dissolution rate is solubility-limited. An assessment of the activation energy, as a function of Cr content, was determined and compared to that of undoped UO_2 .

The results show that Cr-doping reduces initial dissolution rates at temperatures below 60 °C. This may be an effect of galvanic coupling between the reduced Cr existing in the grain boundaries and the UO_2 matrix, allowing preferential oxidation of Cr. At 60 °C, an opposite effect is seen and Cr-doping appears to enhance the initial dissolution rate. A possible explanation may be that at elevated temperatures, oxygen diffusion is be faster and outweigh any effect of galvanic coupling. After the initial stages, steady state dissolution was found at both 25 °C and 60 °C and no effect of Cr-doping was seen. Hypothetically, the galvanic effect is diminished after time as the Cr is oxidized. Higher activation energies were found for Cr-doped samples compared to the undoped samples, and this is in line with the hypothesis of galvanic coupling reducing the initial rates.

5 Concluding perspective

In conclusion, the bottom-up approach followed helped to understand how the addition of Cr-oxide into the fuel matrix affects SNF dissolution behaviour under repository relevant conditions. The results of the dissolution experiments performed with the model materials obtained by the DisCo partners build the basis for numerical simulations on the dissolution behaviour of modern SNF. The data evaluation indicates that the addition of Cr and the consequential modification of the fuel matrix does not lead to a significant change of the dissolution behaviour of these fuels under repository relevant conditions compared to standard SNF (i.e. dissolution rates agree within an order of magnitude).

These studies have clearly shown how single-effect dissolution studies carried out with systematically produced and carefully characterised UO_2-based model materials can provide additional insights into the behaviour of modern doped LWR-fuels under the post-closure conditions expected in a DGR, complementary to dedicated dissolution experiments with SNF. However, apparently some of the dissolution data and observations are not entirely coherent and further refined data evaluation is recommended.

6 References

[1] Commissariat à l'énergie atomique (CEA) (2009): Nuclear fuels. A Nuclear Energy Division Monograph. Gif-sur-Yvette, 147 pp.

[2] J. Arborelius, K. Backman, L. Hallstadius, M. Limbäck, J. Nilsson, B. Rebensdorff, G. Zhou, K. Kitano, R. Löfström, G. Rönnberg (2006), Journal of Nuclear Science and Technology, 43, 967–976.

[3] A. Massih (2014), Swedish Radiation Safety Authority 2014-21 ISSN 2000-0456, Sweden (2014).

[4] C. Cachoir, K. Lemmens in Scientific Basic for Nuclear Waste Management edited by Oversby and Werme (Mat. Res. Soc. Symp. Proc 807, Kalmar, Sweden 2003) pp 59-64.

[5] R. Delville, K. Vanaken, P. Dries (2020), Specification Sheet doped UO_2 pellet for the Disco project. T-0557, SCK CEN, 2020.

[6] T. Cardinaels, K. Govers, B. Vos, S.Van den Berghe, M.Verwerft, L.de Tollenaere, G. Maier, C. Delafoy (2012), J. Nucl. Mat. 424 252.

[7] ASTM E112-13: Standard Tests Methods for determining average grain size, International, West Conshohocken, PA, ASTM 2013, available at htpp://www.astm.org.

[8] D. Bosbach D., C. Cachoir, E. Myllykylä , C. Jegou , J. Cobos, I. Farnan, C. Corkhill. Deliverable D4.1 of the European DisCo project (2019) available at https://www.disco-h2020.eu/Home/Deliverables.

[9] Neck, V., Kim, J.I., (2001), Radiochimica Acta 89, 1-16.

[10] Bosbach, D., Cachoir, C., Myllykylä, E., Jegou, C., Rodriguez-Villagra, N., Farnan, I, Corkhill, C., 2019. WP4-model materials experiments: Dissolution results for modelling input. Deliverable D4.2 of the European DisCo project.

[11] Ekeroth, E., Jonsson, M., (2003), Journal of Nuclear Materials 322, 242-248.

[12] Maier, A.C., Kegler, P., Klinkenberg, M., Baena, A., Finkeldei, S., Brandt, F., Jonsson, M., (2020), Dalton Transactions 49, 1241-1248.

[13] Zetterström Evins, L., Juhola, P., Vähänen M., 2014, REDUPP Final Report (FP7, agreement no. 269903), Posiva Working Report 2014-12.

[14] Ollila, K., Myllykylä, E., Tanhua-Tyrkkö, M., Lavonen, T. (2013), Journal of Nuclear Materials, 442, 320-325.

[15] I. O. f. Standardization, "ISO 643:2012. "Micrographic determination of the apparent grain size".", ed, 2012.

[16] S. Brunauer, P. Emmet, and E. Teller, J. (1938): Am.Chem. Soc., vol. 60, p. 309.

[17] A. Milena-Pérez, L. J. Bonales, N. Rodríguez-Villagra, S. Fernández, V. G. Baonza, and J. Cobos (2021), Journal of Nuclear Materials, vol. 543, p. 152581, 2021/01/01/ 2021.

[18] A. Massih (2014), Malmö högskola, School of Technology.

[19] L. Bourgeois, P. Dehaudt, C. Lemaignan, and A. Hammou (2010), *Journal of Nuclear Materials,* vol. 297, pp. 313-326.

[20] J. H. Yang, K. S. Kim, I. H. Nam, J. S. Oh, D.-J. Kim, Y. W. Rhee, et al. (2012), Journal of Nuclear Materials, vol. 429, pp. 25-33.

[21] N. Liu, J. Kim, J. Lee, Y.-S. Youn, J.-G. Kim, J.-Y. Kim, et al. (2017), Electrochimica Acta, vol. 247, pp. 496-504.

[22] J. M. Elorrieta, L. J. Bonales, N. Rodriguez-Villagra, V. G. Baonza, and J. Cobos (2016), Physical Chemistry Chemical Physics, vol. 18, pp. 28209-28216.

[23] L. J. B. J.M. Elorrieta, S. Fernández, N. Rodríguez-Villagra, L. Gutiérrez-Nebot, V.G. Baonza, J. Cobos (2018), Journal of Nuclear Materials, vol. 508, pp. 116-122.

[24] J.-C. Brachet, E. Rouesne, J. Ribis, T. Guilbert, S. Urvoy, G. Nony, et al. (2020), *Corrosion Science,* vol. 167, p. 108537, 2020/05/01/ 2020.

[25] V. Peres, L. Favergeon, M. Andrieu, J. C. Palussière, J. Balland, C. Delafoy, et al.(2012), Journal of Nuclear Materials, vol. 423, pp. 93-101.

[26] N. Y. Toker, L. S. Darken, and A. Muan (1991), Metallurgical Transactions B, vol. 22, pp. 225-232.

[27] W. Lian. (2009), "Near-field chemistry of a HLW/SF repository in boom clay – scoping calculations relevant to the supercontainer design.," SCK-CEN2009.

[28] V. Neck, M. Altmaier, T. Ganghänel. C.R. Chimie (2007), 10, 959.

[29] Brown, Basu, Ding, Christensen and DePaolo (2018), PNAS, (2018), 115 (35) 8688-8693.

[30] T. Yajima, Kawamura, Y., Ueta, S.(1995), Mat. Res. Soc. Symp. Proc, vol. 353, p. 1137.

[31] K. Ollila (2008), POSIVA report2008.

[32] K. Ollila and L. Ahonen (1998), POSIVA OY, HELSINKI, FINLAND 1998.

[33] J. Giménez, F. Clarens, I. Casas, M. Rovira, J. de Pablo, and J. Bruno (2005), Journal of Nuclear Materials, vol. 345, pp. 232-238.

[34] S. N. Nguyen, H. C. Weed, H. R. Leider, R. B. Stout (2005), MRS Proceedings, vol. 257, p. 339.

[35] B. Grambow, J. Bruno, L. Duro, J. Merino, A. Tamayo, C. Martin, et al., Final Activity Report: Project MICADO Model for Uncertainty for the mechanism of dissolution of spent fuel in nuclear waste repository, 2010.

[36] N. Unceta, F. Séby, J. Malherbe, and O. F. X. Donard (2010), Analytical and Bioanalytical Chemistry, vol. 397, pp. 1097-1111.

[37] A. D. Apte, V. Tare, and P. Bose (2006), Journal of Hazardous Materials, vol. 128, pp. 164-174.

[38] B. R. Bickmore, K. L. Nagy, A. K. Gray, and A. R. Brinkerhoff (2006), Geochimica et Cosmochimica Acta, vol. 70, pp. 290-305.

[39] Y. Niibori, M. Kunita, O. Tochiyama, and T. Chida (2001), Journal of Nuclear Science and Technology, vol. 37, pp. 349-357.

[40] J.-G. Kim, Y.-K. Ha, S.-D. Park, K.-Y. Jee, W.-H. Kim (2001), Journal of Nuclear Materials, vol. 297, pp. 327-331.

[41] T. A. Olds, S. E. Karcher, K. W. Kriegsman, X. Guo, J. S. McCloy(2020), Journal of Nuclear Materials, vol. 530, p. 151959.

[42] B. Kienzler, V. Metz, L. Duro, and A. Valls (2014), "FIRST-Nuclides (Contract Number: 295722). DELIVERABLE (D-N°:5.4) Final (3rd) Annual Workshop Proceedings," 2014.

[43] M. Odorowski, C. Jegou, L. De Windt, V. Broudic, G.Jouan, S.Peuget, C. Martin (2017), Geochimica et Cosmochimica Acta, 219. 1-21.

[44] I. Azoulay, C. Rémazeilles, Ph. Refait, (2012), Corrosion Science, 58, 229-236.

[45] Kerleguer, V., C. Jegou, L. De Windt, V. Broudic, G. Jouan, S. Miro, F. Tocino C. Martin. (2020), Journal of Nuclear Materials vol. 529. 151920.

[46] T. Mennecart, C. Cachoir, K. Lemmens. J. Radioanal (2015), Nucl. Chem 304 (1), 61.

[47] C. Cachoir, S. Salah, T. Mennecart, K. Lemmens (2016), Procedia Chemistry 21, 306.

[48] C. Cachoir, T. Mennecart. Level 5 Report “Spent fuel Dissolution in Supercontainer conditions” RP.W&D.0060: Programme 2009-2014. SCK CEN report ER-231 (2016).

[49] H. Smith, T. Cordara, R. Mohun, M. Stennett, N. Hyatt and C. Corkhill. Assessment of Cr-doped uranium dioxide materials. Oral presentation at the Pre-final DisCo Meeting April 12th, 2021 (videoconference).

[50] E. Myllykylä. Dissolution of alpha-doped UO_2 with and without Cr in the presence of corroding Fe, in synthetic and natural groundwater. Oral presentation at the Pre-final DisCo Meeting April 12th, 2021 (videoconference).

[51] T. Yamamura, S. Nishikawa, H. Moriyama, A. Kitamura, T. Yamamoto, and A. Fukui (1999), Radiochimica Acta, vol. 83, pp. 139-146.

Acknowledgement

The research leading to these results has received funding from the European Commission Horizon 2020 Research and Training Programme of the European Atomic Energy Community (EURATOM) (H2020-NFRP-2016-2017-1) under grant agreement n° 755443 (DisCo project).